Master's thesis

NTNU
Norwegian University of Science and Technology
Department of Electric Power Engineering

Birger Nordvi

The Future of Fuel Cell Technology in Maritime Applications

Master's thesis in Energy and Environmental Engineering
Supervisor: Trond Toftevaag and Kjetil Uhlen
July 2020

NTNU
Norwegian University of Science and Technology

KONGSBERG

Norwegian University of
Science and Technology

The Future of Fuel Cell Technology in Maritime Applications

Birger Nordvi

Master's Thesis

Norwegian University of Science and Technology
Department of Electric Power Engineering

Submitted: July 2020

Supervisors: Trond Toftevaag and Kjetil Uhlen
Industry Partner: Kongsberg Maritime

KONGSBERG

Abstract

From the industrial age through the age of oil, humankind has created immense advancements in production, technology and quality of life. Unfortunately, the progress has come at the expense of the environment; and the need is greater than ever before for environmentally friendly technology that can lead to an improved balance between the modern society and nature.

Fuel cell technology is a viable and future-oriented solution to providing environmentally friendly electrical power production, both in general and for maritime applications.

In this master's thesis, an expansive theoretical review of fuel cell technology, in terms of the characteristics, possibilities and limitations of various fuel cell types and of potential energy carriers, is presented — both separately and from a broader recommendatory system performance perspective.

Hydrogen is a popular energy carrier for fuel cells, but an analysis of hydrogen energy carriers like Liquid Organic Hydrogen Carriers (LOHCs), metal hydrides, ammonia (NH_3) and methanol (CH_3OH) shows that many of the disadvantages of hydrogen, particularly low volumetric energy density and challenging storage requirements, can be alleviated or avoided by choosing more suitable energy carriers.

A case study of an offshore wind turbine constructing Service Operation Vessel (SOV) is included. The case study is based on computer simulations of a realistic SOV load consumption profile in a hybrid, carbon-neutral, solid oxide fuel cell powered microgrid, with an electric battery functioning as an Auxiliary Electric Storage Component (AESC) for peak shaving and transient load buffering. The simulations indicate the performance and feasibility of deploying fuel cells in microgrids in onshore and maritime applications, and also show the effectiveness of using batteries to compensate for the limited dynamic response capability of fuel cells. The case study is further supplemented with a sensitivity analysis, with respect to fuel cell rated power, to study the effect that fuel cell system sizing has on the electrical power production efficiency, energy carrier consumption, hybrid load sharing and battery system scaling.

Sammendrag

Fra den industrielle revolusjonen til oljealderen har menneskeheten skapt enorme fremskritt innen produksjon, teknologi og livskvalitet. Dessverre har fremgangen kommet på bekostning av miljøet; og behovet er større enn noen gang for miljøvennlig teknologi som kan skape en bedre balanse mellom det moderne samfunnet og naturen.

Brenselcelleteknologi er en gunstig og fremtidsrettet løsning for miljøvennlig elektrisk kraftproduksjon, både generelt og i maritime anvendelser.

I denne masteroppgaven presenteres en bred teoretisk gjennomgang av brenselcelleteknologi, med hensyn til egenskaper, muligheter og begrensninger til ulike brenselcelletyper og potensielle energibærere — både separat og fra et bredere, rådgivende systemperspektiv.

Hydrogen er en populær energibærer for brenselceller, men en analyse av hydrogenbærere som flytende organiske hydrogenbærere (LOHCs), metallhydrider, ammoniakk (NH_3) og metanol (CH_3OH) viser at mange av ulempene med hydrogen, spesielt lav volumetrisk energitetthet og utfordrende lagringskrav, kan begrenses eller unngås ved å velge mer passende energibærere.

En casestudie av et vindturbinkonstruerende offshoreskip av typen Service Operation Vessel (SOV) er inkludert. Casestudien er basert på datamaskinsimuleringer av en realistisk forbruksprofil for en SOV konfigurert med et hybrid, karbonnøytralt og brenselcelledrevet mikrogrid, med et elektrisk batteri som fungerer som avlastninghjelp for brenselcellene. Avlastningen består hovedsaklig i å håndtere lastendringer og topplaster. Simuleringene indikerer ytelsen og gjennomførbarheten av å innlemme brenselceller i mikrogrid på land og i maritime bruksområder. I tillegg vises også effektiviteten av å bruke batterier for å kompensere for den begrensede dynamiske responsevnen som brenselceller — og spesielt høy-temperatur brenselceller — har. Casestudien er i tillegg supplert med en sensitivitetsanalyse, med hensyn til nominell brenselcelleeffekt, for å studere hvilken virkning som dimensjonering av brenselcellesystemet har på effektiviteten til elektrisk kraftproduksjon, energibærerforbruk, hybrid lastdeling mellom brenselceller og batteri, samt skalering av batterisystemet.

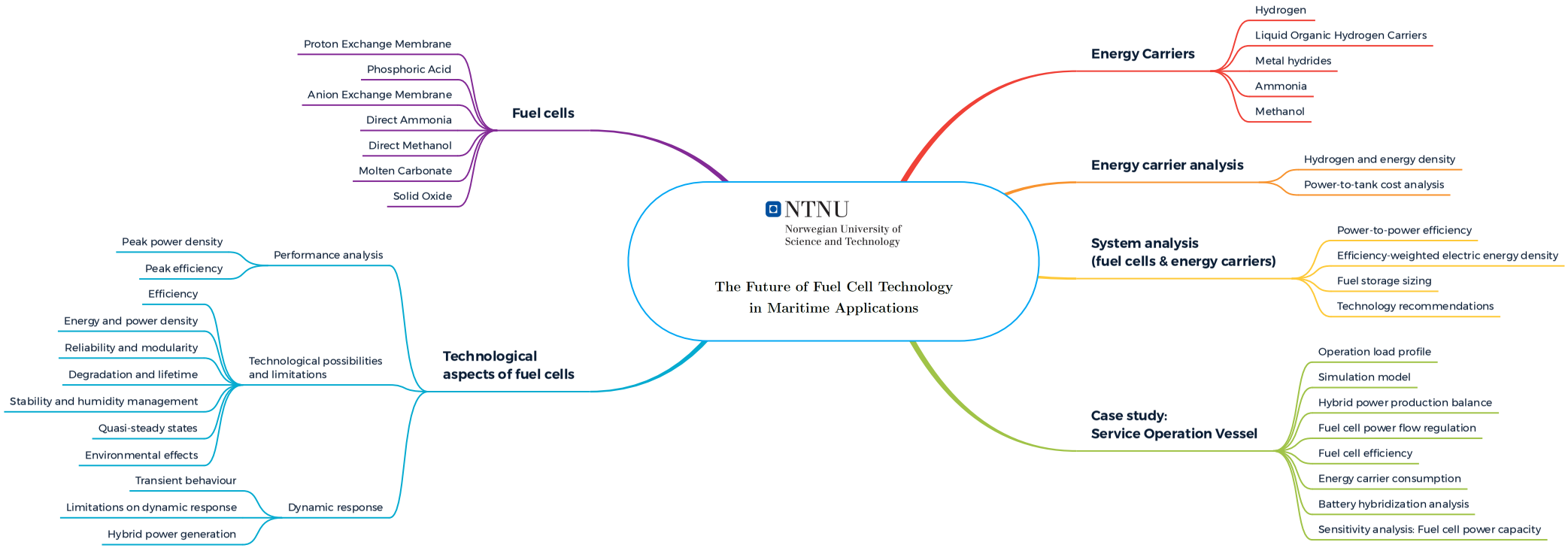
NTNU
Norwegian University of Science and Technology
The Future of Fuel Cell Technology in Maritime Applications
Fuel cells
Proton Exchange Membrane
Phosphoric Acid
Anion Exchange Membrane
Direct Ammonia
Direct Methanol
Molten Carbonate
Solid Oxide
Technological aspects of fuel cells
Performance analysis
Peak power density
Peak efficiency
Technological possibilities and limitations
Efficiency
Energy and power density
Reliability and modularity
Degradation and lifetime
Stability and humidity management
Quasi-steady states
Environmental effects
Dynamic response
Transient behaviour
Limitations on dynamic response
Hybrid power generation
Energy Carriers
Hydrogen
Liquid Organic Hydrogen Carriers
Metal hydrides
Ammonia
Methanol
Energy carrier analysis
Hydrogen and energy density
Power-to-tank cost analysis
System analysis (fuel cells & energy carriers)
Power-to-power efficiency
Efficiency-weighted electric energy density
Fuel storage sizing
Technology recommendations
Case study: Service Operation Vessel
Operation load profile
Simulation model
Hybrid power production balance
Fuel cell power flow regulation
Fuel cell efficiency
Energy carrier consumption
Battery hybridization analysis
Sensitivity analysis: Fuel cell power capacity

Preface

This master's thesis concludes my endeavours at the 5-year integrated Master of Science program Energy and Environmental Engineering at the Norwegian University of Science and Technology (NTNU), and is the continuation and expansion of my review of hydrogen and fuel cell technology that started with a specialisation project at NTNU in 2018.

The hydrogen and fuel cell focus of the project thesis in 2018 was proposed by industry partner Rolls-Royce Marine, which for this master's thesis continued their partnership as Kongsberg Maritime. I decided on the project because I found environmentally friendly fuel cells and energy carriers to be very fascinating technologies with interesting future prospects for renewable energy consumption and, at least for me, a relatively unexplored sphere of the technology realms of electrical engineering.

While the project thesis laid the ground work for an introduction to fuel cells and hydrogen technology, the master's thesis goes broader and deeper into the topics by including more energy carriers to the analysis, reviewing fuel cell types more in-depth, combining these aspects to consider system performances and by performing a more comprehensive and realistic case study of fuel cell performance in an offshore maritime vessel.

The problem description has been developed in close cooperation with the industry to cover the need for information about the applicability of fuel cell technology and carbon-neutral energy carriers in maritime applications.

Acknowledgements

The author would like to thank supervisor, and now docent emeritus, Trond Leiv Toftevaag at the Department of Electric Power Engineering at NTNU for all his valuable help and guidance with both this master's thesis and the preceding project thesis [1].

A thank you also goes to supervisor and professor Kjetil Uhlen at the Department of Electric Power Engineering at NTNU for his assistance with this master's thesis.

This master's thesis has been developed in cooperation with Henrik Alpo Sjöblom, Vidar Smines, Martijn Peter De Jongh, Lars Husdal, Sverre Rye Torben and the rest of the team at industry partner Kongsberg Maritime — former Rolls-Royce Marine and partner for the project thesis. I'm very grateful for all their help and knowledge sharing, and have found Kongsberg Maritime to be a very professional, welcoming, helpful, supportive and reliable partner throughout the evolution of this master's thesis. Kongsberg Maritime has also provided a realistic load profile based on power consumption data from an offshore Service Operation Vessel, and has hence contributed to raising the realism and real-world applicability of the simulations performed for this thesis.

The author would also like to send a warm thank you to Associate Professor Mehdi Zadeh and Assistant Professor Svein Aanond Aanondsen at NTNU's Department of Marine Technology for the hours they so generously spent on introducing an electric engineering student to the world of marine engineering.

Generous support has also been provided for this master's thesis by PhD Candidate Benjamin Lagemann at the Department of Marine Technology at NTNU. Benjamin went out of his way to help on a volunteer basis and for that he deserved a big thank you!

Ludger Blum at Forschungszentrum Jülich and Mark Selby at Ceres Power Limited have both supported this thesis by providing valuable experimental fuel cell data, for which the author is very thankful.

A long, but wonderful and life-changing journey at the Master of Science program Energy and Environmental Engineering at the Norwegian University of Science and Technology in Trondheim is concluded with this master's thesis. My sincere appreciation goes to all my friends and fellow students that shared this journey with me.

And, of course, a big thank you to my parents for all their love and support.

Acronyms

AC Alternating Current

AEMFC Anion Exchange Membrane Fuel Cell

CAPEX Capital Expenditure

CHP Combined Heat and Power

DAFC Direct Ammonia Fuel Cell

DC Direct Current

DIR Direct Internal Reforming

DMFC Direct Methanol Fuel Cell

IIR Indirect Internal Reforming

LOHC Liquid Organic Hydrogen Carrier

MCFC Molten Carbonate Fuel Cell

OPEX Operating Expenditure

PAFC Phosphoric Acid Fuel Cell

PEMFC Proton Exchange Membrane Fuel Cell

SOC State of Charge

SOV Service Operation Vessel

VSC Voltage Source Converter

Glossary

anion An atom or molecule with more electrons than protons, and thus a net negative charge.

anode An electrode where current enters into an electric circuit. Essential part of fuel cells and batteries. Forms a closed electric circuit together with the cathode and electrolyte.

catalyst Catalysts are materials that improve chemical reactions — with respect to factors like reaction temperature, energy requirements and reaction rates — by providing an alternative chemical reaction pathway for the reactants without the catalyst being expended in the process.

cathode An electrode where current exits from an electric circuit. Essential part of fuel cells and batteries. Forms a closed electric circuit together with the anode and electrolyte.

cation An atom or molecule with less electrons than protons, and thus a net positive charge.

closed circuit A complete electrical connection, in which electric current flows or circulates.

DC bus A DC bus is a common DC network connection point for two or more DC components.

DC-AC converter A power electronics converter that bridges a DC network with an AC network. Can potentially control voltage levels, power flow, frequency, phase, etc.

DC-DC converter A power electronics converter that bridges two DC busses/-components with different voltage levels. Can also control the power flow.

dynamic response How a (sub-)system or component reacts to or handles transient loads.

efficiency The efficiency of a component, system or process is the amount of output (for instance electric energy) divided by the amount of input.

electrocatalyst A catalyst that participates in electrochemical reactions.

electrolysis A production technique used to produce hydrogen and oxygen from water.

electrolyte An electrically conduction solution in which cations, anions and electrons can be transported.

energy carrier A gas, liquid or solid used for storing or transporting energy.

gravimetric density The amount of something per weight unit.

heterogeneous catalyst A heterogeneous catalyst is a solid catalyst where the reaction occurs at the catalyst surface and the catalyst and the reactants are in different phases

hybrid power generation The power production by different power production components such as fuel cells, batteries, capacitors, diesel generations, etc. in a system. See power-to-tank efficiency and tank-to-power efficiency.

hydride A compound of hydrogen with a metal.

hydrogen carrier A gas, liquid or solid used for storing or transporting hydrogen.

hydrogen purification The process of removing impurities from hydrogen; to produce hydrogen of high purity.

ion An atom or molecule with a net positive charge. See anion and cation.

LC-filter A filter combined of inductor(s) and capacitor(s) to alter characteristics of signals. Used to make smoother sinusoidal AC output from power electronics converters.

load (electric) The electric power consumption by an electric component or (sub-)system.

load profile A measurement or graph of the load consumption as a function of time.

load sharing How a hybrid power generation system shares the power production between components/systems.

membrane A selective barrier which allows only some things such as certain molecules or ions to pass through.

PI controller A Proportional and Integral controller. Alternatively a PID controller, which also has a Derivative part. Used for controlling systems and components by minimising the difference between a desired state and the actual state.

power capacity See rated power.

power electronics The application of electronics to control the conversion of electric power. Often used to change between voltage levels, control the flow of electric power or to bridge AC and DC networks.

power-to-power efficiency The total efficiency of the processes involved in producing an energy carrier with electric power and later producing electric power from the energy carrier. See power-to-tank efficiency and tank-to-power efficiency.

power-to-tank efficiency The total efficiency of the processes involved in producing an energy carrier ready for storage.

rated power The highest power input or output of a particular equipment.

reformer A system performing reforming.

reforming A processing technique in which the molecular structure of a chemical compound is altered. For instance used to extract hydrogen from hydrogen carriers.

State of Charge The amount of electric energy stored in a battery as a percentage of maximum capacity.

steady state A state, of a system or process, that is static and non-transient with respect to time.

synthesis Essentially the reverse of reforming. A processing technique in which atoms or molecules are combined. For instance used to produce hydrogen carriers.

tank-to-power efficiency The total efficiency of the processes involved in producing electric power from an energy carrier.

transient load A change in the load. Usually focuses on the dynamic consequences the change itself has on power production and other system components.

volumetric density The amount of something per volume unit.

Contents

1 Introduction

1.1 Objective

The main objective of this report is to give an expansive technological overview of fuel cell technology and relevant energy carriers for fuel cells, both in general and for maritime applications in particular.

1.2 Problem description

- Assessment of hydrogen and alternative hydrogen-based fuels (such as ammonia, liquid organic hydrogen carriers and synthetic methanol), and their production and handling.
- Assessment of relevant fuel cells for the above-mentioned alternative hydrogen-based fuels and comment on operating characteristics and other differences.
- Make recommendations for good combinations of fuel cells and energy carriers.
- Modelling (establishment of simulation model) of one or more fuel cell systems in combination with a battery and conducting analyses based on a realistic load profile for offshore vessels.

1.3 Deliverables

- Review of fuel cell technologies and important fuel cell characteristics.
- Fuel cell performance analysis: peak power density; peak efficiency; and potential for higher system efficiency.
- Assessment of technical possibilities and limitations of fuel cells.
- Analysis of dynamic response and transient load following capabilities of fuel cells, and factors limiting the dynamic response.
- Recommendations for hybridisation of fuel cells with electric storage components.
- Expansive review of energy carriers for fuel cells: hydrogen (H_2); Liquid Organic Hydrogen Carriers (LOHCs); metal hydrides; ammonia (NH_3); and methanol (CH_3OH).
- Comparison of storage requirements and volumetric energy density for energy carriers.
- Source-to-tank cost analysis for hydrogen, ammonia and methanol.

- System analysis of fuel cells and energy carriers, with respect to:
  - Total electric power-to-tank, tank-to-power and power-to-power efficiency;
  - Total electric energy density;
  - Energy carrier storage tank sizing;
  - Technology selection recommendations for fuel cell and energy carrier combinations.
- Case study of fuel cell performance on board a Service Operation Vessel (SOV) based on a realistic load profile, and including:
  - Presentation of load profile;
  - Establishment and description of simulation model;
  - Result presentation and discussion for: power balance; hybrid load sharing and transient load buffering; battery system performance and sizing; fuel cell power flow regulation.
- Extended SOV case study with sensitivity analysis for fuel cell power capacity, with respect to:
  - Absolute and relative fuel cell power production;
  - Instantaneous and average fuel cell efficiency;
  - Energy consumption;
  - Battery State of Charge (SOC) and battery system scaling.

1.4 Limitations

One of the main challenges of this thesis has been to procure reliable data for the properties (efficiency, durability, etc.) of all the different fuel cell types, reforming processes and, to a more limited extent, the different energy carriers. Most of the desired data has been obtained, but some of the data gathering efforts have been without result.

Another limitation of this report is that the technical fuel cell properties are based mostly on fuel cell data from research literature and not on commercial solutions. The fuel cell data and analyses presented in this thesis are therefore more representative of recent technological developments in the research sphere, rather than representing the state of commercially available fuel cells.

While maritime applications are the target of the technological fuel cell review, only a Solid Oxide Fuel Cell system on board a Service Operation Vessel has been simulated as a case study. The only CAPEX/OPEX (capital and operational expenditure) analysis of this report is a limited fuel cost analysis of hydrogen, ammonia and methanol.

Even though this report covers many types of fuel cells and energy carriers, it should not be taken as an exhaustive list of such. For instance ethanol, while having an impressive energy density, has not been expressively evaluated in this thesis as the production of ethanol requires fermentation and therefore competes directly with agricultural food production.

The case study computer simulations have only been performed for a solid oxide fuel cell.

1.5 Software

Microsoft Excel has been used to structure and calculate various data for fuel cells and energy carriers. All of the case study simulations have been performed in Simulink. MATLAB has been used extensively to process data from Simulink-simulations and generate most of the graphs created for this report. Microsoft Visio has been used to illustrate the regenerative nature of Liquid Organic Hydrogen Carriers. Xmind 2020 has been used to create the mind map-based illustrations and the technology selection matrix. Python has been used to automate retrieval, archiving and citation exportation of research literature. LaTeX has been used to generate this report.

2 Fuel Cell Technologies

2.1 Proton Exchange Membrane Fuel Cell (PEMFC)

The Proton Exchange Membrane Fuel Cell is also known under the name Polymer Electrolyte Membrane Fuel Cell.

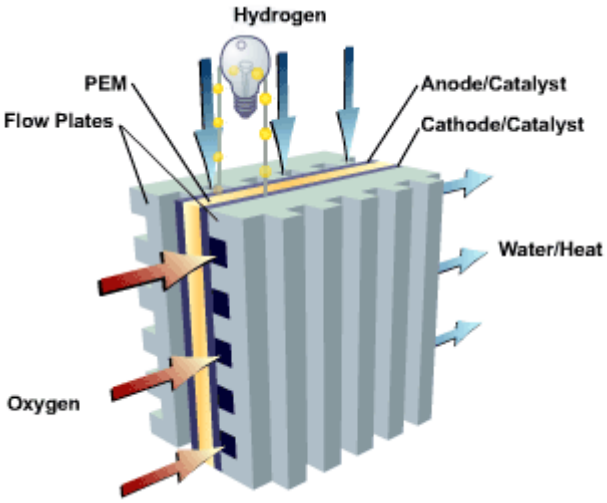

Figure 1: The physical cell structure of a PEM Fuel Cell with the anode and cathode separated by a proton conducting membrane. Source: [2]

2.1.1 Thermal properties

The Proton Exchange Membrane Fuel Cell exists as both a low temperature (LT-PEMFC) and a high temperature fuel cell (HT-PEMFC). The low-temperature version has an operational temperature in the range of 60 °C to 85 °C. The temperature range is a consequence of a complicated water management balance that seeks to maintain a wet membrane while keeping the gas-diffusion pores of the membrane dry. [3, 4]

The membrane needs to be kept in a hydrated condition since water functions as a charge carrier for proton conductivity through the membrane from the hydrogen to the oxygen side of the fuel cell. If the membrane becomes dehydrated, the power delivery capacity of the cell decreases and cell resistance increases. Conversely, excessive cell hydration leads to flooding and reduced oxygen diffusion, so a humidity balance is essential. [4]

The relatively low temperature of PEMFCs, compared to other fuel cells, imposes to a little degree limitations on thermal inertia and promotes a relatively short start-up duration of approximately two minutes, as well as relatively fast

transient performance. However, good kinetic reactions require heat, so there is always a delicate balance between the physical properties. [3]

High-temperature PEMFCs can produce electric power at operating temperatures from 120 °C and up to 200 °C. Various performance improvements are gained by an elevated operating temperature, including reduced carbon poisoning susceptibility of the catalysts, lower material costs, increased heat utilisation, reaction rates and mechanical strength. [4]

HT-PEMFCs also do not need a water management system since no liquid water will be present in the stack with operating temperatures above 100 °C. This enables simplified operation and lower operational costs. Nonetheless, a good heat management system is still needed to remove excess heat and for maximising performance, efficiency and durability of high temperature fuel cells. The elevated heat level, compared to a low-temperature PEMFC, allows for more efficient heat extraction from the fuel cell stack and higher entropy of the heat for reusability purposes in Combined Heat and Power (CHP) applications or for fuel reforming processes. [4, 5]

As mentioned, high-temperature PEM fuel cells have many advantages compared with low-temperature fuel cells, nevertheless, high temperature cells are still being developed and "[...] the number of publications on the HT-PEMFC system is still limited" [4, p. 9297].

The HT-PEMFC is also known as a Phosphoric Acid Fuel Cell (PAFC), and will be discussed in more detail starting on page 9, while also being compared further with the LT-PEMFC in the following sub-sections.

2.1.2 Electrochemistry and catalyst properties

The low-temperature nature of Proton Exchange Membrane Fuel Cells requires an expensive platinum catalyst in order to achieve a sufficiently high electrochemical reaction rate, and consequently a high power density and good transient performance. Furthermore, the combination of a low-temperature fuel cell and a platinum catalyst also has the important disadvantage that the catalyst is very susceptible to carbon poisoning by means of catalyst surface adsorption, which degrades and deactivates the catalyst surface even for very low carbon concentrations. The LT-PEMFC therefore requires fuel of high purity and with very low concentrations, less than 10 ppm (parts per million), of carbon (C) and carbon monoxide (CO). [3, 4, 6]

High-temperature fuel cells, on the other hand, have a higher carbon and carbon monoxide tolerance and are hence more suited than LT-PEMFCs for simple reforming of hydrogen carrying fuels, for instance methanol with steam reforming [4]. Reforming, in the context of fuel cells, is a process where a hydrogen carrier is heated to several hundred degrees Celsius in the presence of a catalyst in order to extract hydrogen from a chemical compound consisting

of hydrogen and other atoms. The topic of reforming will be expanded upon in the sections 2.7.6, 5.4.5 and 5.5.5. The reason for the higher carbon tolerance of HT-PEMFCs is that the adsorption of carbon monoxide at the surface of platinum catalysts and electrodes is reduced with higher temperatures. A High Temperature PEMFC can tolerate carbon monoxide (CO) concentrations up to around 3% to 5%, which is equivalent to 30,000 ppm to 50,000 ppm. [3, 4, 5, 6, 7, 8]

2.1.3 Compatible energy carriers

The Proton Exchange Membrane Fuel Cell is fueled by high-purity Hydrogen (H_2) gas, either directly from a hydrogen source or by means of extraction and purification of hydrogen from hydrogen carrier compounds using reforming and purification processes [4].

Possible hydrogen carriers include

- Liquid Organic Hydrogen Carriers (LOHCs) (section 5.2)
- Metal hydrides (section 5.3)
- Ammonia (NH_3) (section 5.4)
- Methanol (CH_3OH) (section 5.5)
- natural gas
- gasification of coal

For any of these fuels to be used as hydrogen sources for PEMFCs, the hydrogen purity must be within acceptable nitrogen and carbon monoxide limits, as "[...] the LT-PEMFC requires pure hydrogen (99.999%) to operate [...]" [4, p. 9294].

Energy sources for the PEMFC and other fuel cells will be extensively discussed in chapter 5, starting on page 49.

2.1.4 Efficiency

The efficiency of Proton Exchange Membrane Fuel Cells is in the range of 40% to 60% [3, 4], with commercial solutions promising peak system efficiencies of 57% to 58% [10, 11] and a maximum power efficiency of 45% [11].

Figure 2 shows the efficiency for both a 93 kW fuel cell stack and system [9]. It is clear from the graph that increasing net power production correlates with decreasing stack efficiency. On the other hand, at very low power, system losses become dominant and drastically reduce the system efficiency.

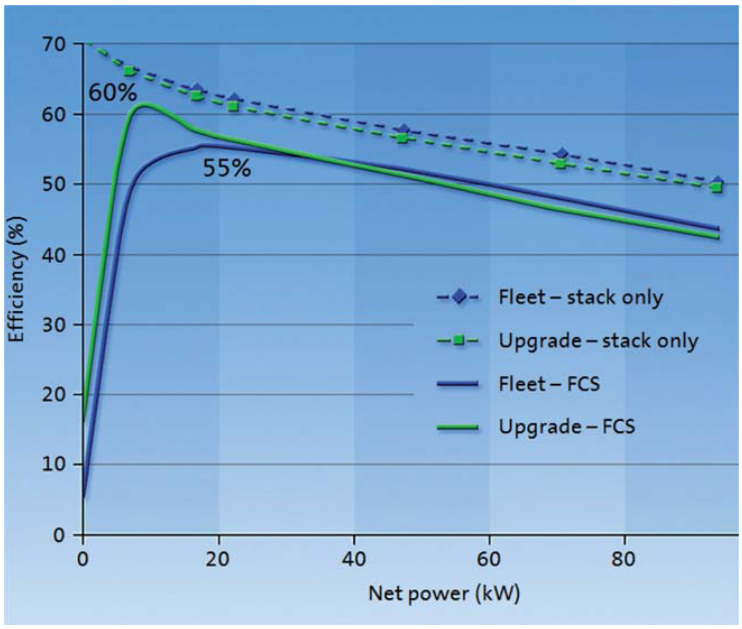

Figure 2: Efficiency graph for a standalone PEM fuel cell stack and a complete PEM Fuel Cell System (FCS). Source: [9]

2.1.5 Power density

"The peak power density [of a fuel cell] is a good indicator of overall cell performance" [13, p. 574] and the power density of PEMFCs have been reported to be as high as 1,750 mW/cm^2 [12], as can be seen in fig. 3.

A commercial fuel cell producer reports that a 100 kW PEMFC has a volume of 276 litres and weighs 170 kg [11], resulting in a volumetric and gravimetric power density of 362 W/litre (362 kW/m^3) and 588 W/kg.

2.1.6 Durability

Proton Exchange Membrane Fuel Cells have lifetime reported to be 10,000 hours [12], 20,000 hours [10, 11] or 30,000 hours [14], depending on the source, however the actual lifetime will vary greatly depending on the applied load profile of the cell stacks. Relatively fast or high frequency load changes, for instance in automobile applications, can reduce the lifetime to around 2,500 to 3,000 hours [14].

> "Although the loss of efficiency during the fuel cell lifetime is unavoidable, its rate can be minimised through an understanding of the degradation and failure mechanisms. This will allow increasing the fuel cell durability and reliability and achieving the desire[d] targets for each application" [15, p. 144].

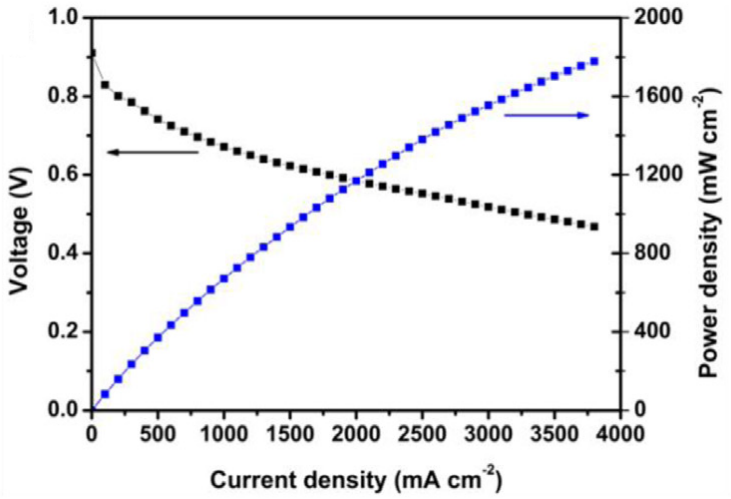

Figure 3: Power density (right y-axis) for a Proton Exchange Membrane Fuel Cell operating on pure hydrogen at 90 °C. Source: [12]

The durability and lifetime of fuel cells will be discussed in more detail in chapter 3 and 4, starting on page 37.

2.2 Phosphoric Acid Fuel Cell (PAFC/HT-PEMFC)

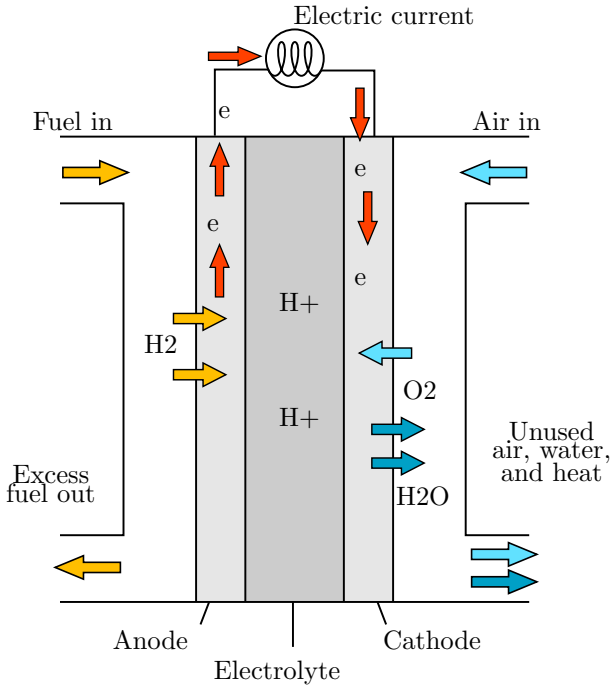

Figure 4: The internal structure and reactant flows of a Phosphoric Acid Fuel Cell. Sources: [16, 17]

2.2.1 Thermochemical properties

The Phosphoric Acid Fuel Cell (PAFC), also known as a HT-PEMFC, operates at temperatures in the range of 140 °C to 220 °C and is in many ways comparable with the Low Temperature Proton Exchange Membrane Fuel Cell (PEMFC). The PAFC has, however, a liquid phosphoric acid (H_3PO_4) electrolyte for the charge carrier transportation of hydrogen ions (H^+) from the anode to the cathode electrode. This type of electrolyte gives some extra challenges for operation and system start-up since phosphoric acid is in a solid state up to a temperature of 42 °C. The electrolyte is further contained in a Teflon-bonded silicon carbide matrix. [3, 18, 19, 20]

The anode, cathode and net cell reaction of the Phosphoric Acid Fuel Cell is presented in equation eqs. (1) to (3), respectively. [19, 20]

$$\text{Anode: } 2\,H_2 \longrightarrow 4\,H^+ + 4\,e^- \tag{1}$$

$$\text{Cathode: } O_2 + 4\,H^+ + 4\,e^- \longrightarrow 2\,H_2O \tag{2}$$

$$\text{Net cell reaction: } 2\,H_2 + O_2 \longrightarrow 2\,H_2O \tag{3}$$

The PAFC is at low-temperature operation susceptible to carbon and carbon monoxide (CO) poisoning/absorption of the platinum catalyst surface. However, the temperature of the Phosphoric Acid Fuel Cell is high enough (>140 °C) for CO to desorb by a reverse catalyst reaction, which is not possible in a Low-Temperature PEMFC (LT-PEMFC) due to the boiling point of water. [8, 19]

At 200 °C, the Phosphoric Acid Fuel Cell, with platinum catalyst, has a CO tolerance of 3%, or 30,000 ppm. In addition, the fuel cell performance has been shown to be unaffected by CO concentrations of 1.0% when operating at 210 °C. [6, 7, 8]

2.2.2 Compatible energy carriers

The literature on the feasibility of using steam reforming of energy carriers like methanol is not entirely coherent. Different views are presented below.

One source concludes that the PAFC is very susceptible to methanol, ammonia and nitrogen contamination in reformed fuel gas [21]. Therefore, the quality demands on the reforming and purification process is high to produce high-purity hydrogen.

In case of catalyst contamination, the cell voltage will drop and may stay reduced for an hour for methanol contamination and may take over 600 hours to recover for ammonia contamination [21].

Other sources find that a PAFC/HT-PEMFC can successfully be incorporated with a methanol reformer, because the CO-concentration of the reformate gas is below 0.2% [7] or around 1% [8], depending on sources, and well within a tolerance limit of 3%, as mentioned above. In these studies, the CO-amount only slightly decreased the fuel cell performance and the conclusion is that "[t]he high CO tolerance makes it possible to use the [methanol] reformate gas directly from the reformer without further CO removal" [7, p. 397]. [3, 6, 7, 8]

One can therefore conclude that the PAFC's resistance against carbon poisoning means that this type of fuel cell is tolerant to steam reformed carbon-containing fuels like Methanol (CH_3OH), if first reformed to be within acceptable CO limits, likewise for Hydrogen (H_2), Liquid Organic Hydrogen Carriers (LOHCs) and Metal hydrides. [6, 7, 8, 19, 22, 23]

It is also worth noticing that since "[...] a reformer is a consumer of heat and water and a fuel cell stack is a producer of heat and water, integration of the stack and the reformer is expected to improve the system performance" [7, p. 397].

2.2.3 Efficiency

The electrical efficiency of Phosphoric Acid Fuel Cells is between 40% and 50%. For Combined Heat and Power (CHP) applications, the system efficiency is just about 85% or 90%, depending on the sources. [19, 22, 24]

2.2.4 Power density

Phosphoric Acid Fuel Cells usually operate with a voltage level between 600 mV to 800 mV, and a current level in the order of 100 mA/cm^2 to 400 mA/cm^2, giving a power density in the range of 60 mW/cm^2 to 320 mW/cm^2 [20]. Another publication found a maximum power density of 560 mW/cm^2 for a specific set of cathode material compound and electrolyte matrix [25]. And fueled with pure hydrogen and oxygen, a high-performance PAFC achieved a peak power density of 614 mW/cm^2 [23].

PAFCs are not as powerful as other fuel cell types, given the same volume and weight. The cell stacks are therefore often large, heavy and expensive [22], but have the advantage of being a relatively low-temperature fuel cell that tolerates carbon-containing fuels.

2.2.5 Technological maturity

"The PAFC is considered the 'first generation' of modern fuel cells. It is one of the most mature cell types and the first to be used commercially" [22]. Commercially, Phosphoric Acid Fuel Cells have been available for decades and systems with at least 11 MW have been tested. [19]

2.2.6 Durability

The Phosphoric Acid Fuel Cell are very durable. Already in 1998, a commercial PAFC with a rated power output of 100 kW exceeded 40,000 hours of operation time, with less than 10% drop in the voltage level for a steady power production of at least 99 kW. [20]

2.3 Anion Exchange Membrane Fuel Cell (AEMFC)

This fuel cell is a type of Alkaline Fuel Cell (AFC), but with a polymer membrane, and is also known as

- Alkaline Anion Exchange Membrane Fuel Cell (AAEMFC)
- Alkaline Membrane Fuel Cells (AMFCs)
- Alkaline Polymer Electrolyte Fuel Cells (APEFCs)
- Polymer Electrolyte Alkaline Fuel Cells (PEAFCs)
- Hydroxide Exchange Membrane Fuel Cells (HEMFCs)
- Solid Alkaline Fuel Cells (SAFCs).

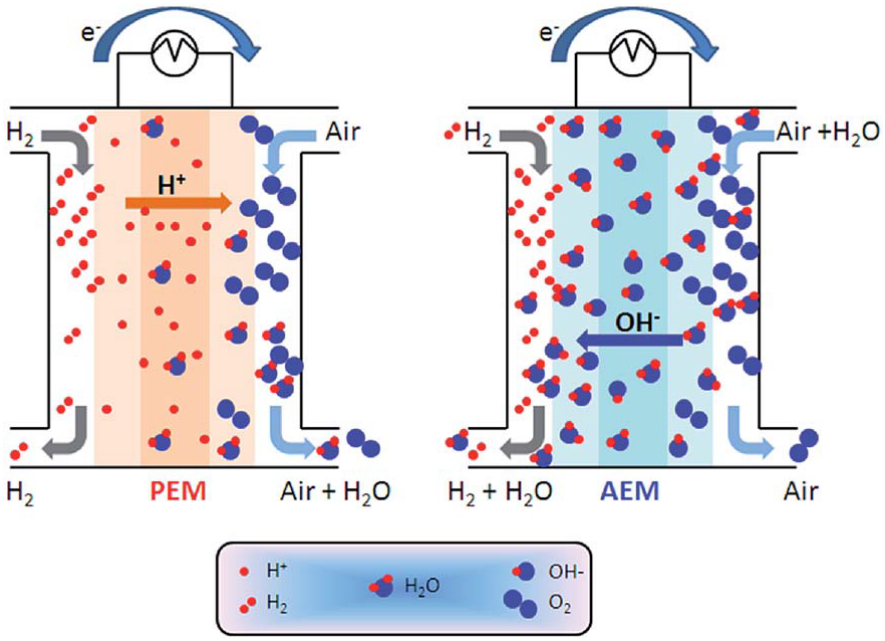

Figure 5: Schematic comparison of the two fuel cells Proton Exchange Membrane Fuel Cell (PEMFC, left side) and Anion Exchange Membrane Fuel Cell (AEMFC, right side). Source: [26]

2.3.1 Thermochemical properties

Technically, the Anion Exchange Membrane Fuel Cell (AEMFC) is very similar to the Proton Exchange Membrane Fuel Cell (PEMFC). The main difference is that the PEMFC has an acidic membrane that exchanges protons (positively charged ions) from the anode to the cathode, while the AEMFC has an alkaline

membrane that exchanges anions (negatively charged ions) from the cathode to the anode. The effect is still the same: an electric circuit is established to produce electric power. [27]

The AEMFC is a low-temperature fuel cell operating at around 60 °C to 80 °C, but can also run at temperatures as low as 30 °C. Higher temperatures are advantageous for performance and reduced CO-poisoning. [28]

The anions in an AEMFC can be alkaline (OH^-, ${CO_3}^{2-}$ and ${HCO_3}^-$) or non-alkaline (Cl^-) [26, 27]. For simplicity, this thesis will not review the different electrolyte compounds, but focus on hydroxides (OH^-) as the principle example — partly because hydroxide is the most common anion species [27].

Hydrogen react with hydroxide at the anode of the Anion Exchange Membrane Fuel Cell, forming water and releasing two electrons per molecule of hydrogen, as shown in eq. (4) [27].

$$2\,OH^- + H_2 \longrightarrow 2\,H_2O + 2\,e^- \tag{4}$$

The electrons transported through an electric load from the anode react with water and oxygen at the cathode to form hydroxide (OH^-), which then diffuses through the membrane to the anode side of the fuel cell electrolyte. The anode and cathode together form an electrode pair. The equation for the chemical cathode reaction is presented in eq. (5). [27]

$$\frac{1}{2}\,O_2 + H_2O + 2\,e^- \longrightarrow 2\,OH^- \tag{5}$$

Unlike the PEMFC, an Anion Exchange Membrane Fuel Cell requires water to be supplied to the cathode side, together with air, and the water will be expelled from the anode side, together with hydrogen. The Proton Exchange Membrane Fuel Cell also produces water, but rather at the cathode side where it mixes with air. Figure 5 gives an overview of the reactant flows, as well as a comparison with the PEMFC.

2.3.2 Advantages of using an alkaline electrolyte

The use of an alkaline pH cell environment in Alkaline Exchange Membrane Fuel Cells provide several possible advantages over the acidic PEMFCs, including [27]:

(a) The AEMFC can be made without expensive platinum (Pt) catalysts, due to enhanced oxygen reduction catalysis;

(b) Wider range of stable stack and cell materials for the fuel cell;

(c) The AEMFC is not limited to pure hydrogen, but can utilise other types of energy carriers.

2.3.3 Compatible energy carriers

In addition to Hydrogen (H_2), Anion Exchange Membrane Fuel Cells have been reported to run on Methanol (CH_3OH), ethanol, ethylene glycol, glycerol and other alcohols.

Contrary to PEMFCs, which deteriorate significantly for Ammonia (NH_3) concentrations as low as 1 ppm, AEMFCs are compatible with nitrogen-containing fuels because of their alkaline nature and can be fueled with ammonia. [27]

The cost of using other energy carriers than hydrogen is a loss of performance in the form of power density. More about this in section 2.3.5.

2.3.4 Efficiency

Alkaline fuel cells can reach efficiencies of 70% and above, and have therefore been the preferred choice for NASA to power the Space Shuttle Orbiter [29]. The different types of alkaline fuel cells, with their different membranes and configurations, may have different efficiencies.

2.3.5 Power density

The peak power density of Anion Exchange Membrane Fuel Cells have exceeded 1000 mW/cm^2 and can be as high as 1400 mW/cm^2, as observable in fig. 6. However, most of these experiments use pure hydrogen and oxygen. The performance improvements over the years are mainly caused by the evolution of anion exchange membranes with higher anion conductivity. [27, 28, 30]

Despite the possibility of constructing AEMFCs without platinum catalysts, platinum is still the preferred choice for high performance. By 2017, platinum-free catalysts reportedly only produce peak power densities of up to 500 mW/cm^2. [27]

Power density of liquid hydrogen-carriers

The peak power densities of hydrogen-carrier fuels such as methanol, ethanol (C_2H_5OH) and hydrazine ($(NH_2)_2$) is in the order of 130, 180 and 450 mW/cm^2, respectively. Although these densities are relatively high in comparison to many fuel cells, the peak power densities are much lower than for pure hydrogen-utilising Anion Exchange Membrane Fuel Cells. [27]

2.3.6 Carbon tolerance

Carbon and carbon-containing chemical compounds like CO and CO_2 react with platinum-catalysts and impair their performance. Platinum-containing AEMFCs therefore are susceptible to carbon poisoning. Research has been conducted to reduce this problem, and have discovered that cell current densities above 1 A/cm^2 effectively diminish the impact of CO_2. This approach opens

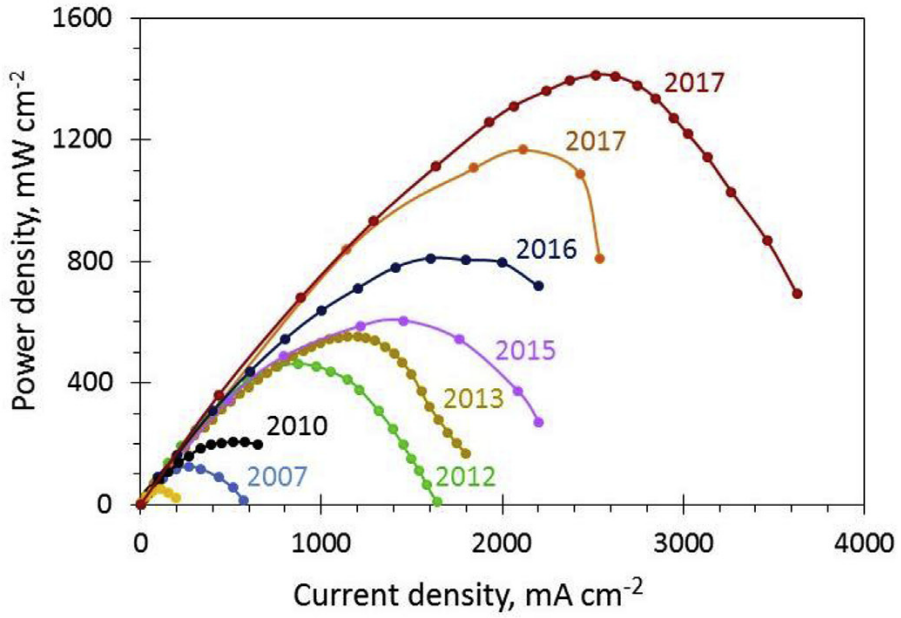

Figure 6: Power density development of Anion Exchange Membrane Fuel Cells reported in literature during the years 2006 to 2017. Source: [27]

up for the possibility of using ambient air instead of pure oxygen for the cells. [27]

2.3.7 Technological maturity

The Anion Exchange Membrane Fuel Cells "[..] have recently gained significant interest and are a current focus in the fuel cell research community" [27, p. 158]. Figure 7 shows the exponential development of the yearly number of research articles published on AEMFCs.

2.3.8 Durability

Despite the high number of research articles on H_2-AEMFCs, the durability of these cells is very low, for an otherwise well-performing fuel cell type. "The overwhelming majority of the studies report performance stability lower than 300 h" [27, p. 167]. It appear that until further progress is made, the cell life of AEMFCs have an upper bound of 1000 hours. [27]

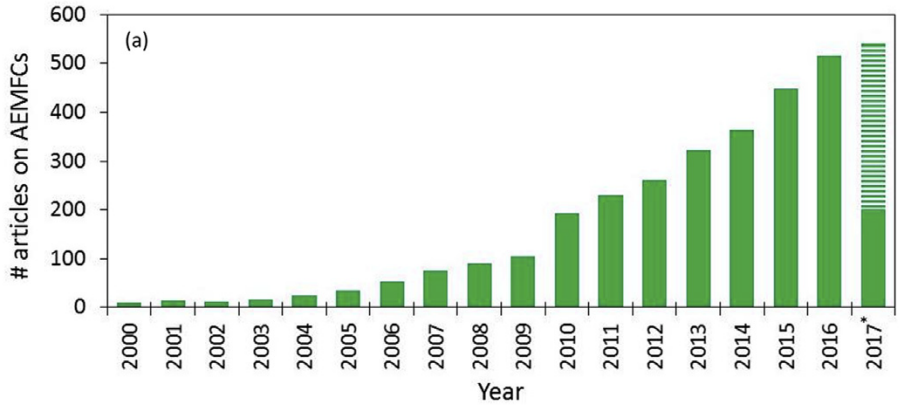

Figure 7: Development of the yearly number of research articles published on Anion Exchange Membrane Fuel Cell (AEMFC). The number for 2017 is an estimate based on the first months of that year. Source: [27]

2.4 Direct Ammonia Fuel Cell (DAFC)

2.4.1 Thermochemical properties

The Direct Ammonia Fuel Cell (DAFC) exists as both a Low- (LT-DAFC) and a High-Temperature fuel cell (HT-DAFC). The low-temperature variants has a operational temperature of 20 °C to 120 °C, while the high-temperature versions operate at temperatures in the range of 500 °C to 1000 °C. [31, 32]

The DAFC internally reforms Ammonia (NH_3) to nitrogen (N_2) and Hydrogen (H_2) at the anode, whereby the hydrogen oxidises and donates electrons to the anode. The electrolyte membrane rejects the flux of electrons, effectively forcing the hydrogen-donated electrons through an external electric circuit over to the cathode side. At the cathode side the electrons react with oxygen and reduce oxygen molecules (O_2) to oxygen ions (O^{2-}). Simultaneously, hydrogen diffuses through the membrane from the anode to the cathode side and reacts with the oxygen ions to form water (H_2O) — similarly to for instance a Proton Exchange Membrane Fuel Cell (PEMFC). Equations (6) and (7) show the chemical reactions at the anode and the cathode side, respectively. [32]

$$2\,NH_3 \longrightarrow N_2 + 3\,H_2 \tag{6a}$$
$$3\,H_2 \longrightarrow 6\,H^+ + 6\,e^- \tag{6b}$$

$$\frac{3}{2}\,O_2 + 6\,e^- \longrightarrow 3\,O_2^- \tag{7a}$$
$$6\,H^+ + 3\,O_2^- \longrightarrow 3\,H_2O \tag{7b}$$

2.4.2 Cooling effect

The Direct Ammonia Fuel Cell can provide a cooling effect, which occurs when ammonia is extracted from the storage tank. The extraction reduces the temperature of the tank because of the pressure drop that occurs when the content is reduced, and because of evaporation of ammonia from liquid to gas state. The temperature drop can then be exploited by a cooling coil which effectively heats up the remaining stored ammonia and stabilises the temperature in the tank. [32]

2.4.3 Compatible energy carriers

Direct Ammonia Fuel Cells can utilise ammonia directly as a fuel with internal fuel cell reforming, or reformed externally to nitrogen and hydrogen before hydrogen is fed directly to the cells. This means that DAFCs can run on pure hydrogen fuel as well, regardless of being extracted from ammonia or not. [13]

2.4.4 Efficiency

A solid electrolyte High-Temperature Direct Ammonia Fuel Cell can achieve stack efficiencies up to 55%. The total system efficiency is significantly lower, around 40%, but can be increased to 44% by utilising the possible cooling effect of ammonia. The system efficiency can further be increased to 46% by thermally decomposing ammonia to hydrogen in a reforming process external to the fuel cells. This also requires utilisation of the cooling effect and the work made available by nitrogen expansion. [32]

Another report finds energy efficiencies for Low-Temperature DAFCs ranging from $52.5\% \pm 1.6$ to $66.8\% \pm 2$, depending on humidifier temperature, and exergy efficiencies between $49.2\% \pm 1.6$ and $62.6\% \pm 2$ [33].

2.4.5 Power density

The effectiveness of DAFCs is sensitive to temperature variations at the anode and in the electrolyte. For instance a temperature drop of 100 °C results in a 66% reduction in power density. It is therefore important to properly regulate the fuel cell system temperature to ensure optimal operational conditions. [32]

The Peak Power Density (PPD) of Low-Temperature Direct Ammonia Fuel Cells reported in research literature span from 0.64 mW/cm^2 to 135 mW/cm^2, with an outlier at 420 mW/cm^2 for a 100 °C Low-Temperature DAFC reported in 2018 [31, 33, 34].

Peak power densities up to 1190 mW/cm^2 have been reported for High-Temperature DAFCs with a solid oxide electrolyte. This type of DAFC is essentially the versatile Solid Oxide Fuel Cell (SOFC) supplied with Ammonia (NH_3).

2.4.6 Technological maturity

Even though the history of Direct Ammonia Fuel Cells span back many decades, "[s]ubstantial improvements in performance are still needed for DAFCs to become a practical power source for transportation applications" [31, p. 2481], because so far "[...] ammonia fuel cells have attracted limited research effort" [31, p. 2475].

2.5 Direct Methanol Fuel Cell (DMFC)

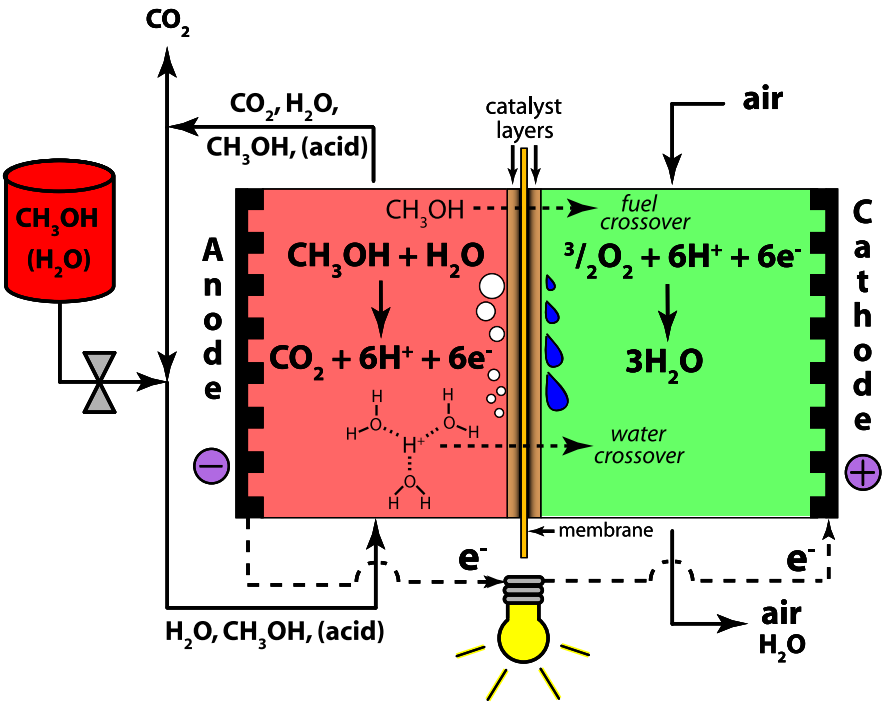

Figure 8: Chemical reactant flows of a Direct Methanol Fuel Cell. Source: [35]

2.5.1 Thermochemical properties

The Direct Methanol Fuel Cells are in many ways similar to the Proton Exchange Membrane Fuel Cell (PEMFC), but fueled with Methanol (CH_3OH) rather than Hydrogen (H_2) [36, 37]. The operating temperature of DMFCs are in the range of 60 °C to 260 °C [37, 38, 39], which is quite low compared to high-temperature fuel cells than can reach 1000 °C, such as the Solid Oxide Fuel Cell (SOFC).

At the anode, methanol reacts with water and is oxidised to carbon dioxide (CO_2) and hydrogen ions (H^+) as shown in eq. (8).

$$CH_3OH + H_2O \longrightarrow CO_2 + 6\,H^+ + 6\,e^- \tag{8}$$

The electrons at the anode are transported through an electric circuit, producing electric power, until they reach the cathode where they reduce oxygen, which then reacts with hydrogen ions to form water (H_2O) as in eq. (9).

$$\frac{3}{2}\,O_2 + 6\,H^+ + 6\,e^- \longrightarrow 3\,H_2O \tag{9}$$

The overall net cell reaction is then the consumption of methanol and oxygen with the end-products carbon dioxide and water as shown in eq. (10) and fig. 8. [36, 37, 40]

$$CH_3OH + \frac{3}{2}O_2 \longrightarrow CO_2 + 2\,H_2O \tag{10}$$

The low-temperature nature of Direct Methanol Fuel Cells requires a very expensive platinum (Pt) electrocatalyst to ensure sufficient reaction rate. DMFCs also have a problem with unwanted methanol crossover, where methanol reacts directly with oxygen at the cathode without producing electric energy for external use. [37, 41]

Nonetheless, a typical Direct Methanol Fuel Cell "[...] is compact in design, needs no compressor or humidification, and feeds directly off methanol in liquid form" [40, p. 716] and "[...] can be made smaller and less costly" [40, p. 716] compared to other fuel cell types.

2.5.2 Compatible energy carriers

The Direct Methanol Fuel Cell can be directly fed with liquid Methanol (CH_3OH), which allows for quick refueling [40].

2.5.3 Efficiency

The efficiency of Direct Methanol Fuel Cells is quite poor [3] and has been reported to be in the order of 25% for long-term tests and up to 35% for short-term tests [40].

There exist certain challenges with efficiency and power for methanol when supplied to a direct methanol fuel cell (DMFC). DMFCs have challenges with respect to membrane cross-over, heat and water management in addition to lower efficiency compared with hydrogen fuel. Approximately "[o]nly 30% of methanol energy can be utilised with current direct methanol fuel cell technology, rest is wasted in cross-over and heat". [42, p. 2]

Membrane cross-over is problematic because it allows the methanol fuel to react directly with oxygen on the cathode side of the fuel cell, which in effect reduces the cell voltage and cell kinetics (cell reaction rate). Mixing methanol with water also reduces the cell current output, which also limits the performance output of the cell. [42]

2.5.4 Power density

The fact that six electrons are released for every reacting molecule of methanol means that the Direct Methanol Fuel Cell has a very high energy density in theory [37, 41]. The actual power densities reported in science literature are

however in the magnitude of 20 mW/cm^2 to 80 mW/cm^2 [38, 43, 44], which is very low compared to other fuel cell technologies.

The low power density of DMFCs in practice is attributed to slow kinetics of the methanol oxidation reaction, which correlates with the low temperature of the cells. "Increasing the temperature can [therefore] effectively increase the methanol oxidation kinetics [...]" [39, p. 1] and reduce undesirable methanol crossover. [39]

The potential for performance improvements has been measured to be 50 mW/cm^2 per 100 °C increment for temperatures below 205 °C, and 208 mW/cm^2 per 100 °C increment for temperatures above 205 °C. The limit of 205 °C is considered a transition temperature where higher performance gains above this temperature limit is considered to be caused by enhanced kinetics and reaction rates of methanol oxidation. [39]

Using the knowledge of increased performance at elevated temperatures, a peak power density of 236 mW/cm^2 has been reported for a Direct Methanol Fuel Cell operating at a temperature of 260 °C.

2.5.5 Technological maturity and durability

An important challenge for the implementation of Direct Methanol Fuel Cells is high degradation rates and a limited number of known cases that have reported a durability longer than 2000 h without a performance drop of 20% or more. In addition, "[t]he majority of literature data on long-term operation of DMFC is obtained for the lab-scale tests reported by academic research groups, while little information is available from the fuel cell industry" [41, p. 225]. There are, nonetheless, some reports of durability up to 20,000 h. [39, 41]

The durability of fuel cells is heavily influenced by the number of start-stop cycles and the dynamic load profile [41], and will be further discussed in the chapters Technical Possibilities and Limitations of Fuel Cells (page 37) and Dynamic Response of Fuel Cells (page 43).

Some measures to improve performance and extend the durability of DMFCs are air breaks and load cycling. The air breaks helps to recover the catalyst back to its metallic state, while the load cycling method copes with the problem of water buildup around the cathode by removing the load demand on the cell for 30 seconds every 30 minutes. [41]

2.6 Molten Carbonate Fuel Cell (MCFC)

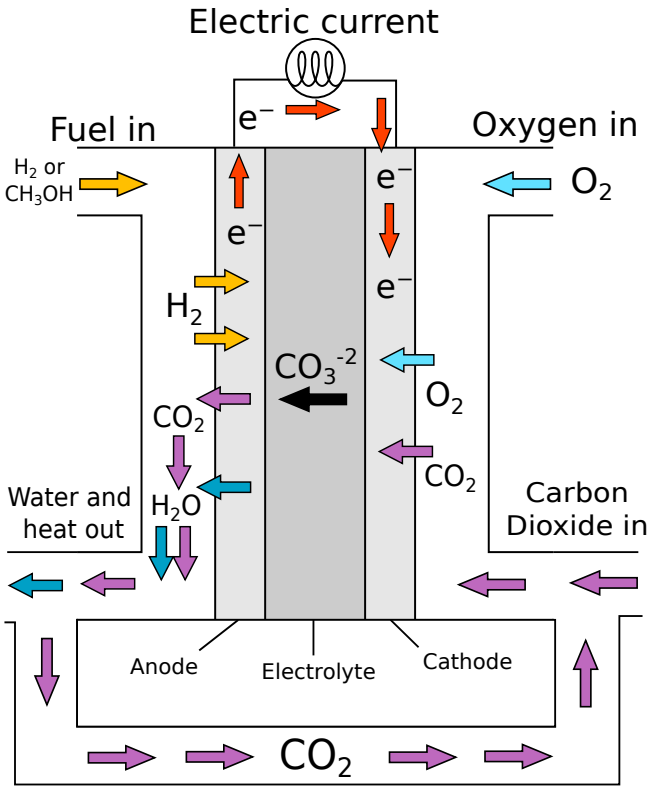

Figure 9: The internal structure and reactant flows of a Molten Carbonate Fuel Cell. Rework of [16] based on [17].

2.6.1 Thermochemical properties

The Molten Carbonate Fuel Cell (MCFC) is an alkali-carbonate, high-temperature fuel cell with an operating temperature between 600 °C and 650 °C. "Both [the] anode and the cathode are nickel-based whereas the electrolyte consists of harmless salts of lithium, potassium and sodium carbonates in molten state and are suspended in a porous ceramic matrix" [45, p. 40].

In contrast to, for instance, the Proton Exchange Membrane Fuel Cell (PEMFC), the Molten Carbonate Fuel Cell does not use hydrogen ions (H^+) to transport charge between the electrons and through the electrolyte to form an electric circuit. Instead carbon trioxide (CO_3^{2+}) ions, also known as carbonate, transport the charge in the molten carbonate electrolyte from the cathode to the anode. In this way, CO_2 is actually a necessary closed-loop reagent and its extraction at the anode outlet, as shown in fig. 9, makes CO_2-separation and capture a potential feature of the MCFC. [45]

At the anode of the Molten Carbonate Fuel Cell, hydrogen and carbonate react and oxidise to form water, carbon dioxide and electrons as shown in eq. (11) [45].

$$H_2 + CO_3^{2-} \longrightarrow H_2O + CO_2 + 2\,e^- \tag{11}$$

At the cathode, the electrons arrive from the anode, through an electric circuit where electric power is extracted, and reduce oxygen and carbon dioxide to carbonate ions as chemically described in eq. (12) [45].

$$\frac{1}{2}\,O_2 + CO_2 + 2\,e^- \longrightarrow CO_3^{2-} \tag{12}$$

The reactions at the anode and the cathode combined produce the net reactions as presented in eq. (13). Both the chemical equation and fig. 9 show that CO_2 is released at the anode outlet and to some extent also at the cathode outlet. [45]

$$H_2 + \frac{1}{2}\,O_2 + CO_2(\text{cathode}) \longrightarrow H_2O + CO_2(\text{anode}) \tag{13}$$

2.6.2 Compatible energy carriers

The MCFC can utilise Hydrogen (H_2) as well as hydrocarbon fuels like Methanol (CH_3OH), methane and ethanol due to the high temperature and nickel anode which ensures outstanding conditions for internal reforming of the hydrocarbons to hydrogen. External steam reforming of hydrocarbons to hydrogen is also possible, but is more costly and increases system complexity. [46, 46]

The first step of a hydrocarbon reforming process is to convert the hydrocarbon compound and water to hydrogen (H_2) and carbon monoxide (CO). The second step is then the reaction of the carbon monoxide and water to carbon dioxide (CO_2). [45]

Ammonia (NH_3) is not an appropriate fuel for Molten Carbonate Fuel Cells, unless first reformed to be below the ammonia tolerance limit of the cells. This is because nitrogen compounds (NH_3, HCN and N_2) react with the electrolyte via NO_x. The ammonia tolerance limit in MCFCs is 1% to 3% (10,000 to 30,000 ppm), volumetric. [45, 46]

2.6.3 CO_2-capture capability

The ability of Molten Carbonate Fuel Cells to separate CO_2 make them a possible approach to CO_2-emission reductions. For instance a MCFC can be combined with an Internal Combustion Engine (ICE) to significantly reduce the engine's carbon emissions. A similar approach can also be used for other carbon combustion processes like gas turbines, coal-fired power plants and Combined

Heat and Power (CHP) systems, with CO_2-reductions in the range of 61% to 80% and little to negligible loss of electrical efficiency. [45]

2.6.4 Efficiency

The high-temperature of operation for Molten Carbonate Fuel Cells makes is possible for an overall thermal efficiency of 90%, of which up to 49% is electric power. The efficiency of the MCFC is also relatively load- and scale-independent and the fuel cell stacks can be scaled from kW to MW applications. [45]

2.6.5 Power density

A typical MCFC produce around 100 mA/cm^2 to 200 mA/cm^2 at a voltage of 750 mV/cell to 900 mV/cell [45]. A conversion to watts gives power density in the cells in the range of 75 mW/cm^2 to 180 mW/cm^2, which is quite poor compared to other fuel cells.

2.6.6 Durability

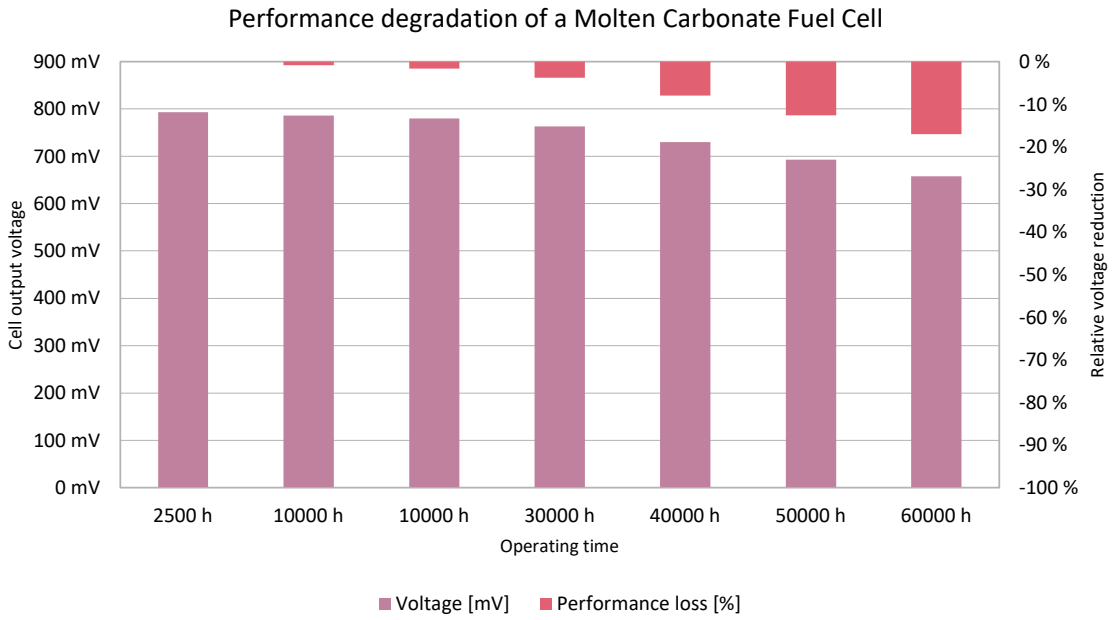

Figure 10: Time-dependent performance degradation in terms of output voltage loss, in absolute and relative numbers, of a Molten Carbonate Fuel Cell operating at 600 °C. Based on experimental data from [47].

Fuel cell stacks generally degrade in performance rather than fail. The same holds true for Molten Carbonate Fuel Cells. [3, 47]

A research team in Japan have conducted a set of long-term durability and performance tests of MCFCs and observed lifetimes up to 66,000 hours (7.5 years) for a MCFC operating at 600 °C, and a lifetime up to 33,000 hours (3.75 years) when the operating temperature was 650 °C. Clearly the fuel cell temperature has a great impact on durability. During the continuous tests, the performance and the voltage degraded progressively as shown in fig. 10. The degradation is mainly attributed to increased internal resistance and increase of cathode oxygen reactions. Even after 60,000 hours the output voltage level was still 83% of the initial level. [47]

2.7 Solid Oxide Fuel Cell (SOFC)

2.7.1 Thermochemical properties

Solid Oxide Fuel Cells operate at very high temperatures, between 500 °C and 1000 °C [3], which leads to a set of distinct advantages and disadvantages. It takes a long time to properly heat the cells to their operating temperature, and the initialisation time of a Solid Oxide Fuel Cell stack is therefore very long compared to low-temperature fuel cell types. [48]

Starting up a SOFC stack takes up to two hours before reaching an internal steady-state temperature distribution, and shutting it down requires around 1.5 hours [49].

The thermodynamic properties of this fuel cell type also imposes limitations on load transient following capability and dynamic response [48], which will be discussed further in section 2.7.2.

2.7.2 Dynamic Response

"The dynamic response of the SOFC model is mainly dominated by the double-layer charging effect [...] and the thermodynamic property of the fuel cell" [48, p. 894].

The double-layer charging effect (internal capacitance)

The double-layer charging effect means that the fuel cell has an inherent capacitance enabling the cells to respond immediately to changes in load. However, despite the fact that the capacitance is in the order of several Farads, the time constant of the cells is small ($\approx 10^{-2}$ s) and therefore the capacitance of the cells will only have a significant effect on the dynamic response in a very small time span of 10^{-3} to 10^{-1} seconds. [48]

Thermodynamic limitations

The thermodynamics of a high-temperature fuel cell like the SOFC is of high importance as "[...] fuel cell life time decreases by rapid thermal change[s]" [50, p. 1] and fuel cells therefore "[...] cannot respond to the electrical load transients as fast as desired" [51, p. 864]. The slow thermodynamic response of the cells "[...] is mainly due to their slow internal electrochemical and thermodynamic responses" [51, p. 864], which cause harmful and life shortening "[...] low-reactant condition[s] inside the fuel cells [...]" [51, p. 864].

The limited adaptability of the SOFCs to fast changing load demands therefore makes it important to control the operation temperature by only slowly changing the power output of the cells [50]. Faster load changes can be buffered by combining fuel cells with highly dynamic energy storage systems, like batteries or super capacitors, in a hybrid power generation setup. In this type of hybrid configuration, the batteries will handle power ripples (ie. high-speed

load oscillations) and the transient loads (ie. changes in power consumption), while the power output of the fuel cell stack will change slowly or even be in steady-state, depending on the load profile. [51]

Load is an expression for the total electric energy or power consumption by one or more electrical components, like for instance motors, lighting, heating and electronics.

The relationship between load transients and cell durability is a very important aspect for Solid Oxide Fuel Cells as a "[...] sensitivity analysis shows that the lifetime of the stack is the most impacting uncertain parameter, followed by fuel prices and by the investment cost of the SOFC stack" [52, p. 1].

Experimental data show that a load change from 50% to 100% of power density for a SOFC entails a relaxation time of 2000 seconds ($0.\bar{5}$ hours) [49]. The relaxation time is "[...] defined as the time the cell voltage needs to recover from an instant output current change to 90% of its new steady state value [...]" [49, p. 815]. Consequently, it can be assumed that a load change from 0% to 100% of rated fuel cell power is best applied during a time duration of at least one hour (3600 seconds) to minimise thermal stresses than can degrade the lifetime of high-temperature fuel cells like the Solid Oxide Fuel Cell.

2.7.3 Efficiency

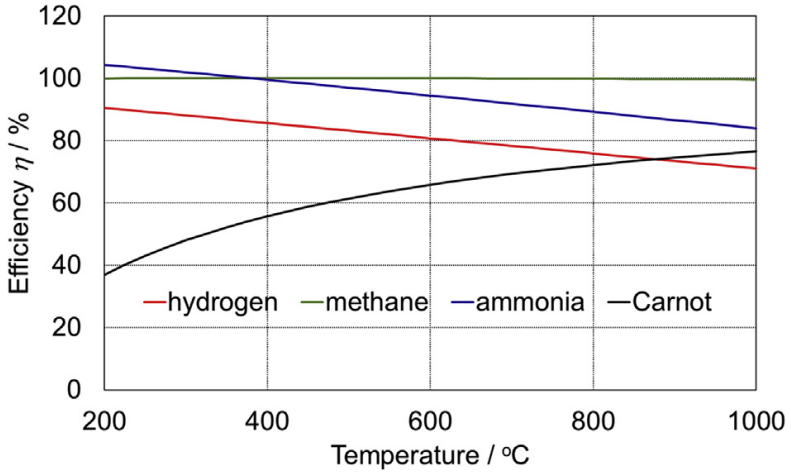

Figure 11: Theoretical efficiencies as a function of temperature for SOFC using Lower Heating Value (LHV) of Hydrogen (H_2), methane or Ammonia (NH_3) as fuels. The efficiency for the Carnot process assumes 25 °C inlet/cold temperature. Source: [53]

Based on data from research literature, a Solid Oxide Fuel Cell stack can reach an electric production efficiency of around 65%. The high temperature nature of SOFC means that the SOFC system efficiency can be further improved

up to 88% (combined heat and electrical) or over 70% (electrical) of Lower Heating Value by utilising the heat or exhaust gasses produced from the stack in a Combined Heat and Power (CHP), Combined Cooling, Heat and Power (CCHP) solution or with a gas or steam turbine. A possible combination of a SOFC stack with a gas turbine is presented in fig. 12. [3, 48, 54, 55]

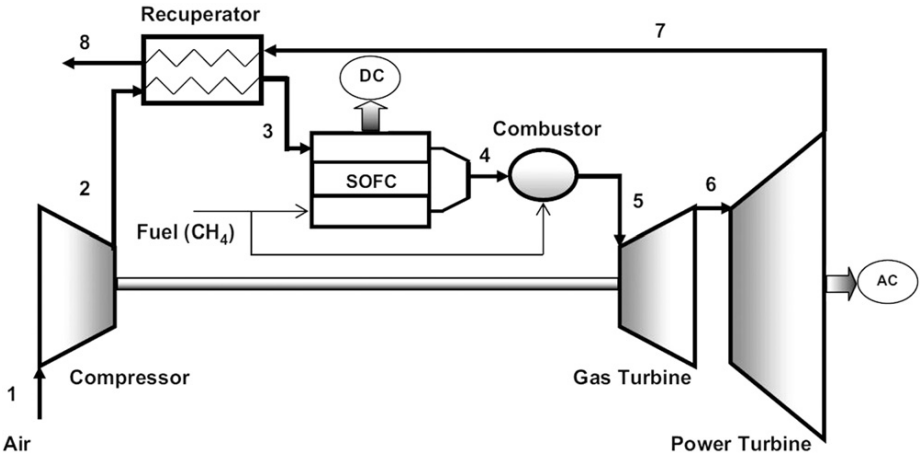

Figure 12: Schematic diagram of a combined SOFC and gas turbine system for high efficiency power generation. The fuel type is not limited to CH_4. Source: [54]

One commercial SOFC producer claims to "[...] have achieved a [world record] in primary energy conversion efficiency to electricity of 74%" [56] at peak efficiency, while also maintaining an electric efficiency "[...] consistently over 60 per cent [...]" [57] for the full span of power production.

The system efficiency profile of an experimental SOFC stack can be observed in figure fig. 17 on page 33, and can be seen to have an efficiency that decreases with increasing power output. In contrast to this, SOFC efficiency profiles provided by the commercial SOFC-producer Ceres Power in the UK (fig. 13) and Forschungszentrum Jülich in Germany (fig. 14) show system efficiencies that peak at mid-range power output levels and decrease significantly at lower production levels and to a lesser degree at higher power levels.

According to Ceres Power, the efficiency profile in fig. 13 is typical for 10 kW, and larger, SOFC systems. For systems with a rated power in the range of 100 kW to 10 MW, the efficiency profile would be similar to the one in fig. 13, but perhaps a bit "flatter" in the sense that 65%+ efficiencies would reside over a winder range of the power curve.

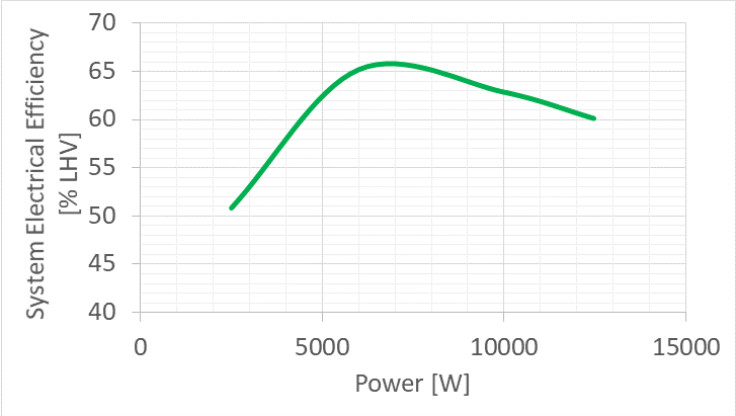

Figure 13: System efficiency with respect to Lower Heating Value (LHV) as a function of power output for a 10 kW SOFC system with some "overrun" capabilities. Kindly provided by Ceres Power.

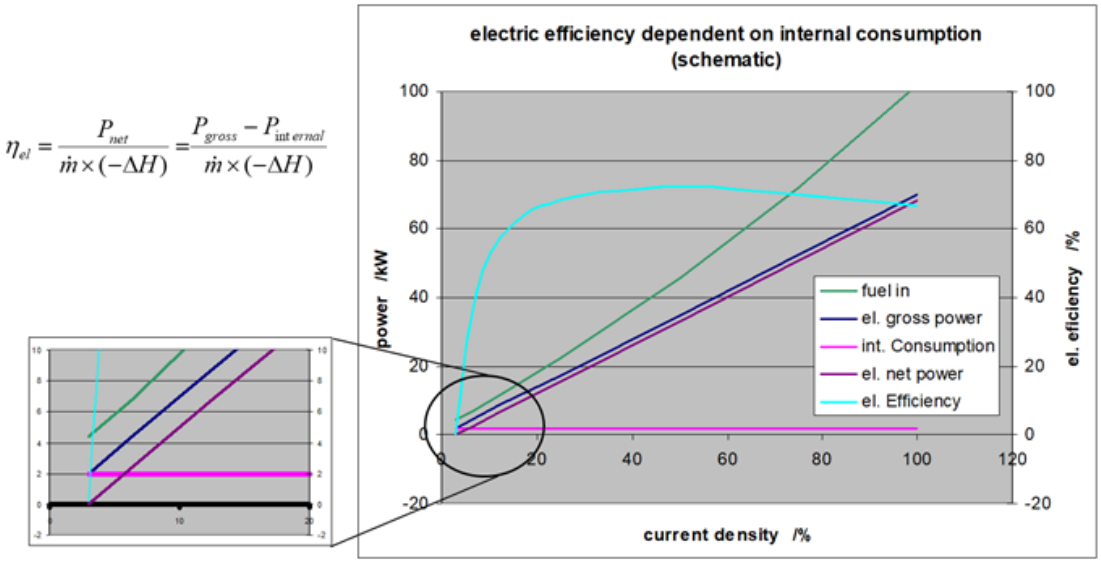

Figure 14: Electrical efficiency (cyan colour, right y-axis) of a SOFC system as a function of current density/net power output. Kindly provided by Forschungszentrum Jülich.

2.7.4 Power density

The peak power density of an ammonia-fed Solid Oxide Fuel Cell is highly dependent on the fuel cell temperature. Increasing the operating temperature by 200 °C "[...] increases the peak power density by nearly three to four times [...]" [13, p. 568]. The high performance at higher temperatures can be ascribed to the incomplete fuel decomposition that occurs at lower temperatures. [13]

A Solid Oxide Fuel Cell based on an oxygen anion conducting electrolyte (SOFC-O) can achieve a maximum peak power density of 1190 mW/cm^2 at a temperature of 650 °C when energised by ammonia fuel. For operating temperatures of 600 °C and 550 °C, the peak power density was reduced to 434 mW/cm^2 and 167 mW/cm^2, respectively. Fuel cell operation temperature management is therefore very important for the performance of Solid Oxide Fuel Cells. [13]

The power density of SOFC-O can be increased significantly to 1872 mW/cm^2 if fuel with pure hydrogen [13]. However, another article point out that "[...] the ammonia fueled SOFC is more efficient than an equivalent hydrogen fueled one, due to the cooling effect of internal reactions that reduces ancillar[y] energy consumptions related to cathode air flow" [58, p. 13583]. Hence, from a performance perspective the power density and efficiency of Solid Oxide Fuel Cells are not perfectly aligned when comparing ammonia and hydrogen as potential fuels.

SOFCs based on a proton conducting electrolyte (SOFC-H) only reach a power density of 390 mW/cm^2, despite an operating temperature as high as 750 °C. [13]

A novel bilayer Solid Oxide Fuel Cell has experimentally been demonstrated to yield a power density of 2100 mW/cm^2 [59], which is extremely high.

2.7.5 Technological maturity

From fig. 16, it can be seen that thousands of research articles on SOFCs have been published during the last two decades. SOFCs are therefore a heavily researched fuel cell technology [59]. And because of its high efficiency and fuel flexibility, the Solid Oxide Fuel Cell is the most widely developed high-temperature fuel cell technology [60].

2.7.6 Compatible energy carriers; Internal and external fuel reforming

Cracking and reforming is a chemical "[...] processing technique by which the molecular structure of a hydrocarbon is rearranged to alter its properties" [61].

Carbon-containing fuels

SOFCs can consume Hydrogen (H_2) and carbon monoxide (CO) directly. For

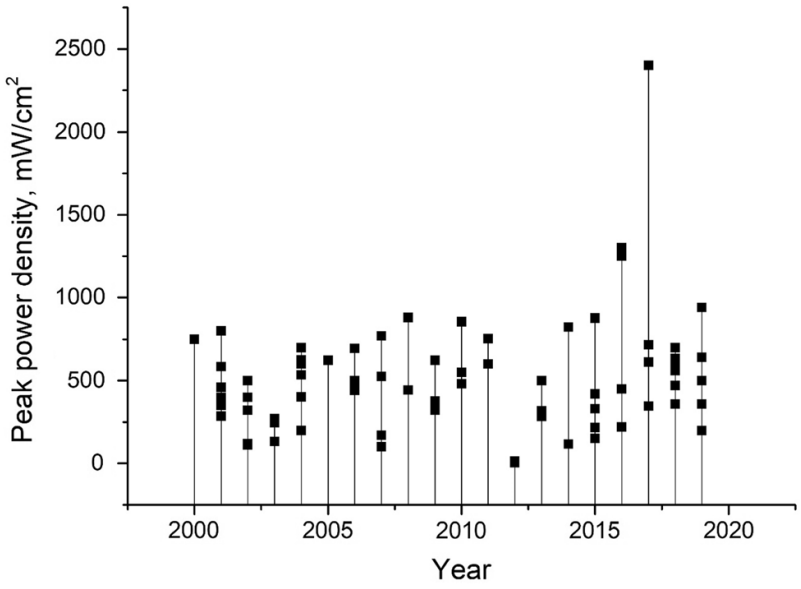

Figure 15: Historical power density development of oxygen-conducting (O^{2-}) Solid Oxide Fuel Cells. Source: [59]

other fuels, such as methane, Methanol (CH_3OH) and ethanol (C_2H_5OH), reforming of the chemical compounds to hydrogen and carbon monoxide is necessary for the utilisation of the fuels in the fuel cell. The reforming can either be performed in a reformer separately from the fuel cell stack in what is called Indirect Internal Reforming operation (IIR-SOFC) or by Direct Internal Reforming (DIR-SOFC), in which the fuels are reformed inside the fuel cell stack at the anode and then directly consumed for electricity production in the cell. [5, 54]

Even though IIR happens outside the fuel cells, a close thermal contact between the reformer and the anode side of the SOFCs exists for good heat transfer between the components and to allow for autothermal operation, in which the process is perpetuated by its own heat production [5, 62].

Direct internal reforming does require "[...] an anode material that has good catalytic reforming and electrochemical reactivities" [5, p. 943], such as a cost effective Nickel/YSZ-catalyst, but DIR-SOFC has the advantage "[...] that the hydrogen consumption by the electrochemical reaction could directly promote the reforming or conversion of hydrocarbons at the anode side. Therefore, DIR-SOFC results in high conversion and high efficiency" [5, p. 943] and allows for Methanol (CH_3OH) and other carbon-containing energy carriers to be used directly as fuels, "[...] with fuel pretreatment inside the SOFC anode" [53, p. 18382].

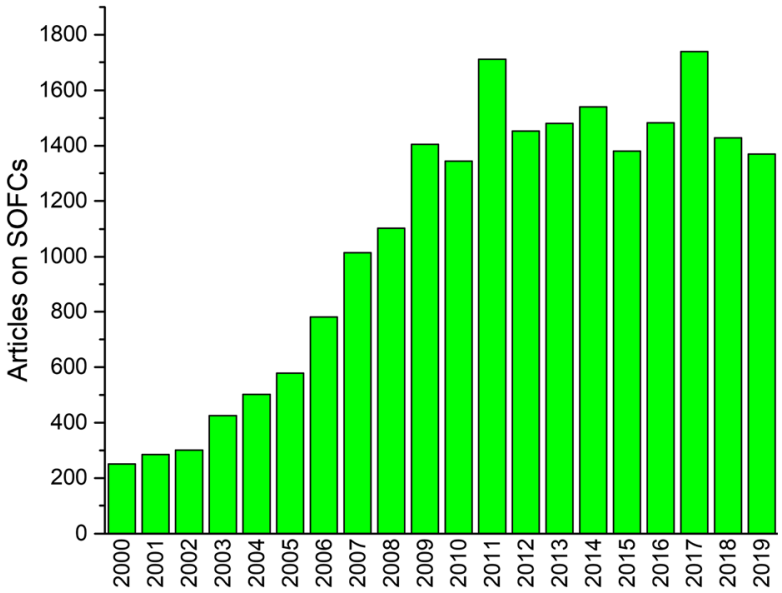

Figure 16: Yearly published research articles on Solid Oxide Fuel Cells between 2000 and 2020. Source: [59]

Ammonia

Commercial SOFCs often have a nickel-based anode. This type of anode excels as a catalyst for chemical ammonia decomposition. Consequently, ammonia can be internally reformed to hydrogen and nitrogen in a Solid Oxide Fuel Cell, after which the hydrogen is immediately available to react electrochemically to produce electric power. [53, 58]

> "In addition, such reaction is endothermal and keeps the cell at a lower temperature than with pure hydrogen. This is very interesting at system level, because all endothermal reactions take part of the heat generated by the cell that should, otherwise, be collected by the cathode air stream. Such stream has to be heated and pressurized to get into the cell with relevant losses in terms of exergy efficiency and any reduction of the temperature in the fuel cell is beneficial. The use of ammonia [therefore] permits a smaller air flow rate with reduced consumption of electricity in the blower." [58, p. 13584]

Internal reforming of ammonia has in experiments shown a 22% increase of system efficiency compared with external reforming where a gaseous mixture of both hydrogen and nitrogen is fed to the fuel cell. This effect is largely due to a reduction in cathode air flow to the cells. [58]

Figure 17 shows the system efficiency for a Solid Oxide Fuel Cell with respect to internal reforming ("NH3") and external reforming ("H2N2"). "Uf" refers

to the fuel utilisation rate, where 0.8 means that 80% of the fuel is combusted in the fuel cell. The figure also gives a good indication of the system efficiency profile for a SOFC with respect to the power output.

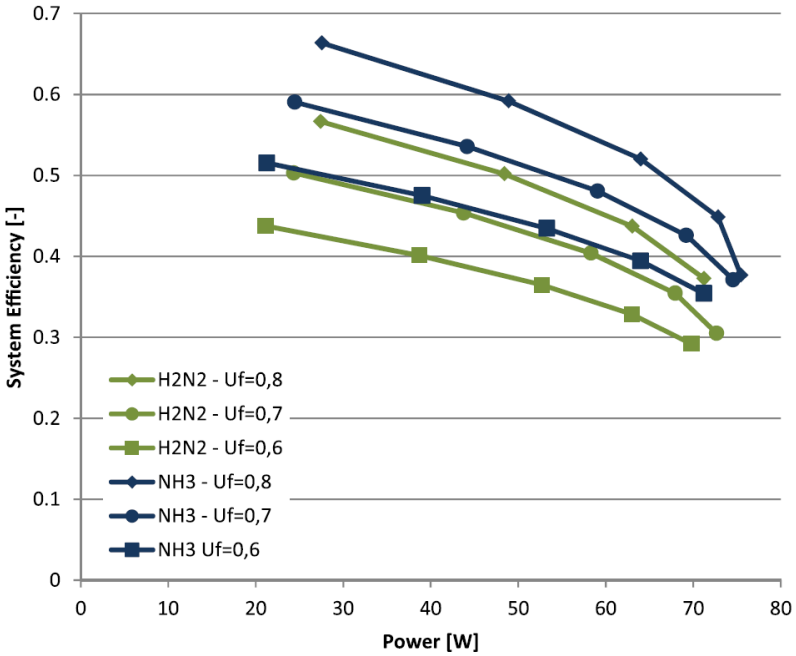

Figure 17: Comparison of system efficiency for internal ("NH3") and external reforming ("H2N2") of ammonia in an experimental Solid Oxide Fuel Cell. "Uf" is the fuel utilisation rate. Source: [58]

2.7.7 Durability

Solid Oxide Fuel Cells have reportedly achieved lifetimes in the range of 30,000 hours to 70,000 hours [36].

2.8 Fuel Cell Performance Analysis

The different fuel cells all have their specific conglomerate of advantages and disadvantages. In this section these cells and their features are analysed and compared to give an overview of key fuel cell performance characteristics.

Take note that many of the values like peak power density and peak efficiency for the fuel cells are for optimal conditions in research literature and does not necessarily represent the values of commercially available solutions at optimal nor sub-optimal conditions. The performance of fuel cells depend heavily on the specific construction of the cells, catalyst properties, fuel characteristics, combined heat and power (CHP) applications, reforming, load percentage, age of the cells and more.

The importance of each performance parameter will depend in a large degree on the specific use case, an will be contingent on whether a particular system design is mainly, for instance, volume, cost, efficiency or safety dependent.

2.8.1 Peak power density

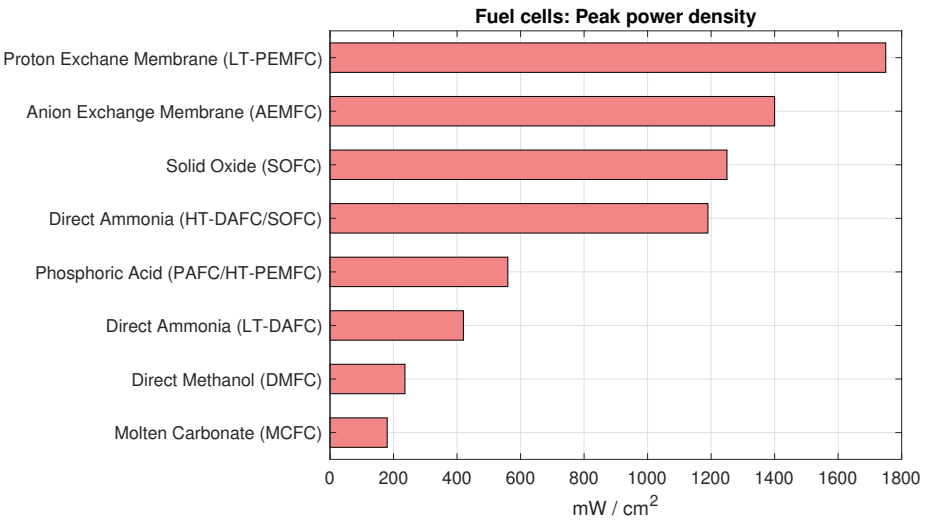

Figure 18: Overview of peak power density of selected fuel cells.

The peak power density of a fuel cell is the amount of electric power that can be produced per fuel cell membrane area, and does not take into account auxiliary systems like fuel reforming and delivery systems, tank capacity cooling/heating systems, etc. Nonetheless, the power density gives a good indication of fuel cell performance and may be used to rule out particularly underperforming systems not viable for specific system design requirements.

Figure 18 shows the different peak performance values for the respective fuel cells. As can be seen from the figure, the peak power densities varies

greatly from 180 mW/cm^2 for the Molten Carbonate Fuel Cell (MCFC) and 236 mW/cm^2 for the Direct Methanol Fuel Cell (DMFC) to 1750 mW/cm^2 for the high-performing, low-temperature Proton Exchange Membrane Fuel Cell (PEMFC), which is closely followed by the Anion Exchange Membrane Fuel Cell (AEMFC) (1400 mW/cm^2) and the high-temperature Solid Oxide Fuel Cell (SOFC) (1250 mW/cm^2). If fueled by pure hydrogen, the SOFC can reach peak power densities as high as 1872 mW/cm^2, replacing the LT-PEMFC for pole position. The Direct Ammonia Fuel Cell (DAFC), with a peak power density of 1190 mW/cm^2, is essentially a SOFC running on ammonia, and this explains the closeness in power density of these fuel cells.

At mid-range densities of 420 to 560 mW/cm^2 are the Direct Ammonia Fuel Cell (DAFC) and the Phosphoric Acid Fuel Cell (PAFC/HT-PEMFC), which both all relatively low-temperature fuel cells.

2.8.2 Peak efficiency

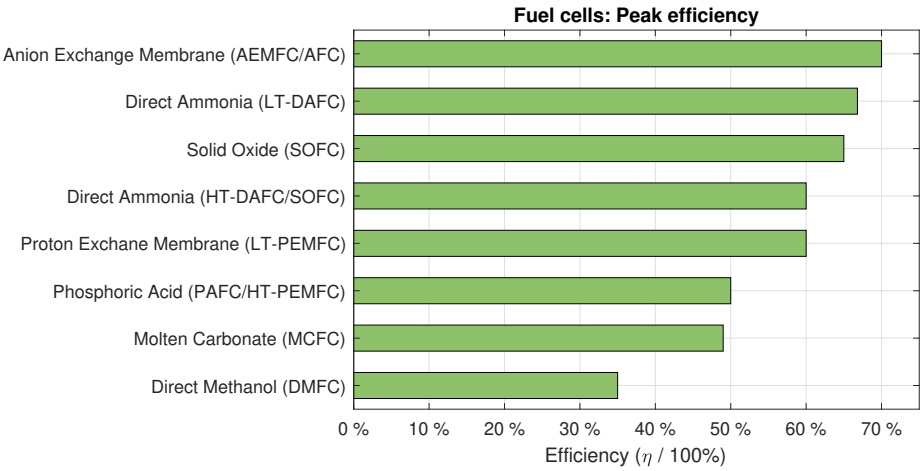

Figure 19: Overview of peak efficiency for fuel cells.

With the exception of the Direct Methanol Fuel Cell (DMFC), all the fuel cells discussed so far have a peak efficiency that lies between 49% and 70%. The top-performing cells are the Anion Exchange Membrane Fuel Cell (AEMFC)/AFC, the low-/high-temperature versions of the Direct Ammonia Fuel Cell (DAFC), the Solid Oxide Fuel Cell (SOFC) and the Proton Exchange Membrane Fuel Cell (PEMFC) with peak efficiencies (η) of 70%, 67%/55%, 65% and 60%, respectively.

Efficiency data for AEMFC was not found specifically, but this type of fuel cell is a sub-group of Alkaline Fuel Cell (AFC), which have efficiencies of 70% and this value has therefore been used as basis for the AEMFC. The AEMFC is nonetheless plagued with short lifetimes (see section 2.3.8), so this is currently

of less importance.

It is a little bit of a stretch to call the HT-DAFC an independent fuel cell type, since it is actually a SOFC fueled with ammonia. Nonetheless, this combination does perform very well, and it can be concluded that the Anion Exchange, the Low-Temperature Proton Exchange Membrane and the Solid Oxide Fuel Cell are very high-performing fuel cells with regard to both power density and efficiency.

The LT-DAFC does perform very well in terms of fuel efficiency, but it is not one of the best fuel cells when considering Peak power density.

The Direct Methanol Fuel Cell (DMFC) and Phosphoric Acid Fuel Cell (PAFC/HT-PEMFC) have peak efficiencies somewhat below the top-tier cells, with mid-range efficiencies equal to 55% and 50%, respectively.

Maximising the system efficiency

The total fuel cell efficiency can be improved considerably by configuring fuel cells as part of a Combined Heat and Power (CHP) system, in which both heat and electricity is produced. At least for the PEMFC, SOFC, PAFC and MCFC the total system efficiency can be in the range from 85% to 90% [24]. The rationale behind the high efficiency of CHP systems is that all fuel cells, as a result of the electricity production, have heat production that can be considered losses if not utilised through any productive means.

3 Technical Possibilities and Limitations of Fuel Cells

Copyright notice
The state of art and related work were reviewed, and an identification of the relevant background material was carried out in the project [1] preceding this thesis. No relevant new material was found during the work on the thesis. The presentation from the project report is included below, with minor edits, for the complete remainder of this chapter.

3.1 Efficiency

3.1.1 Comparison with conventional diesel generators and motors

Fuel cells have a higher efficiency than conventional diesel generators due to the fact that fuel cells can convert chemical energy directly into electricity. Comparatively, diesel generators convert chemical energy into electricity through thermal and mechanical energy, adding additional conversion losses. [3]

State-of-the-art diesel generators have a peak efficiency of around 45%, and a part load efficiency in the range of 20% to 40%, with lower efficiency at lower loads. For electricity generation the low part load efficiency is a result of high mechanical losses that doesn't linearly follow the electric load. In a fuel cell the losses increase linearly with the load for most of the load range. This means that fuel cell systems generally have very good part load characteristics and achieve peak efficiency at low loads. [3]

A typical fuel cell efficiency curve with respect to power output can be seen in figure 20.

3.1.2 Increasing the efficiency

There exist several ways of increasing the efficiency of a fuel cell system. The waste heat from a fuel cell can be converted to electric power by integrating a bottoming cycle into the system. Additionally, any unused fuel that is extracted from the fuel cell can be used to raise the temperatures of the exhaust gasses even further by burning the fuel in a catalytic converter. This will increase both the efficiency and the generated electric power of the bottoming cycle. If a gas turbine is integrated with the fuel cell, then the energy use for the air flow in the cathode can also be improved, and a total system efficiency up to 70% is possible. [3]

Since fuel cells usually have a higher efficiency at lower loads, the operational efficiency of the whole system can be improved by oversizing its capacity. The downside of this is of course increased investment costs and space requirements.

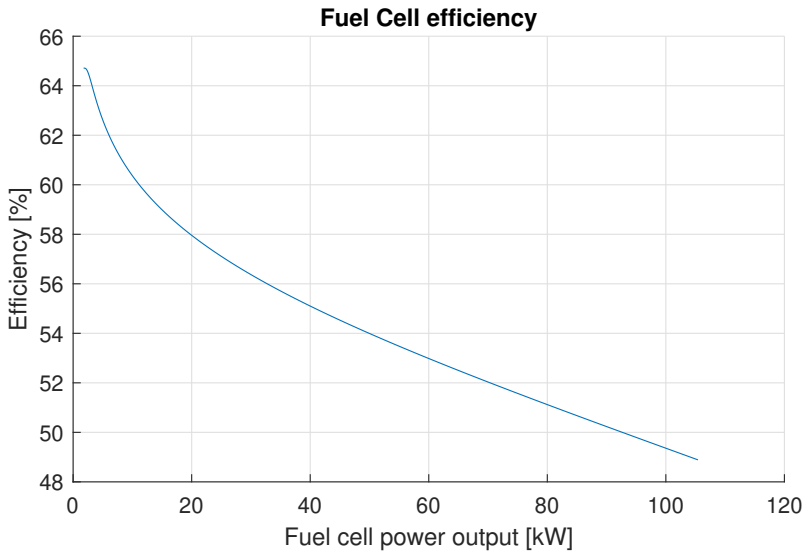

Figure 20: Efficiency curve for a 100 kW PEM fuel cell stack.

3.2 Energy and power density

3.2.1 Scalability of energy and power capacity

In a fuel cell the substances involved in the redox reaction at the electrodes are continuously delivered externally into the cells. This allows for separate dimensioning of both the power and the energy capacity of fuel cell systems to suit the requirements of the individual systems.

3.2.2 Fuel cell power densities

The volumetric and gravimetric power densities for SOFC systems are reported to be in the range of 8 W/l to 60 W/l and 20 W/kg to 230 W/kg, respectively. For PEMFC systems the densities are even higher - especially when fueled by pure hydrogen so that a fuel reformer is not needed. [3]

A diesel drive system has roughly the same gravimetric power density (specific power) as a SOFC system, but when it comes to volumetric power density a SOFC system is outperformed by diesel systems, for which the energy density values generally are in the range of 20 W/l to 70 W/l. [63]

3.3 Reliability and modularity

"Fuel cell systems have few mechanical parts and tend to degrade rather than fail, which results in a high availability" [3, p. 357].

Fuel cells also have high modularity which allows for redundancy and increased reliability through distributed electricity production [3]. If there for

instance is a fire in a ship compartment that incapacitates a fuel cell stack or part of the electricity infrastructure, then fuel cell modules placed in other parts of the ship can continue to deliver electric power and ensure continued functionality of critical systems.

The modularity of fuel cell systems also allows for an extra degree of freedom when designing the ship layout [3].

It is important that a fuel cell is fed with sufficient amounts of reactants as "[s]tarvation, which describes the operating conditions of fuel cells in sub-stoichiometric fuel or oxidant feeding, is a potential cause of fuel cell failure" [14, p. 70]. This topic will be discussed more comprehensively in section 4.2 on limitations of dynamic response.

3.4 Durability

The lifetime of fuel cells has greatly increased the last years due to technology improvements. A 250 kW molten carbonate fuel cell developed in Germany "[...] worked for more than 30 000 h" [36, p. 2865] and a combined heat and power solid oxide fuel cell "[...] achieved a lifetime of 30 000 h, and up to 70 000 h in laboratory testing" [36, p. 2865].

Under steady-state operation the lifetime of a proton exchange membrane fuel cell can be up to 26 300 h, or even more than 30 000 h if used as a fixed power source. Comparatively a PEM fuel cell used in an automotive vehicle, with a high degree of load changes, gives a lifetime of around 2 500 to 3 000 h. [14] The reduces lifetime comes from the fact that "[...] fuel cell lifetime heavily depends on driving cycle" [14, p. 62].

3.5 Degradation and lifetime

A fuel cell is a complex system with a multitude of parts and processes that affect its performance, degradation and lifetime.

While a fuel cell has a higher efficiency at lower loads and currents, a low current can cause corrosion of the platinum catalyst layer and thus reduce the fuel cell's performance and voltage level [14].

Gas starvation may occur if the pressure difference between the anode and the cathode is not properly controlled, during low humidity, if the stack reaches a high temperature or if there is insufficient amount of reaction gas. Further, the Membrane Electrode Assembly (MEA) may be permanently degraded or damaged as a result of repeated hydration and dehydration. [14]

The lifetime of a fuel cell is also negatively affected with every start-stop cycle, during idling, high power output and load changing. Figure 21 shows the relative effect of these factors and makes it clear that start-stop cycles and load changing conditions contribute together to almost 90% of the performance

degradation in a PEM fuel cell. [14]

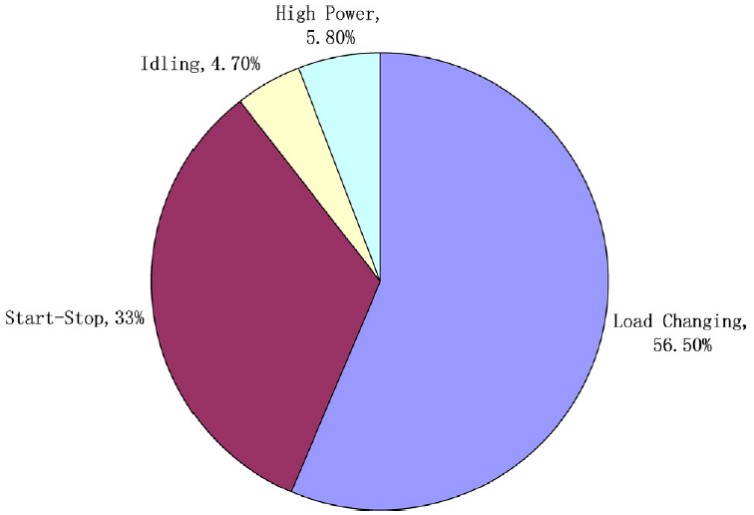

Figure 21: Attribution of degradation rates in fuel cells from different operational factors. Source: [14]

Section 4.2 on page 44 provides a detailed investigation into the degrading aspects of a fuel cell resulting from dynamic response situations.

3.6 Stability and membrane water management

The stability and performance of a proton exchange membrane fuel cell (PEMFC) depends in a large degree on humidification and the water management of the membrane inside the cell. The membrane needs to be sufficiently humidified to allow for the ion transport between the anode and cathode sides. An inadequately humidified membrane will result in a low proton (H^+) conductivity and a limited power output from the cell. It is also important to ensure that the electrodes are not flooded with water. Water condensation limits the electric power output of the fuel cell as the gas transport to the catalysts and the membrane is impeded by water droplets, causing the fuel cell to operate irregularly and degrades the catalyst. [14, 64]

The membrane water activity changes dynamically depending on the water production and removal in the cell, where power output of the cell, fuel cell temperature and fuel flows are important factors. The amount of water generated relates proportionally to the current density. With large current densities, substantial amounts of liquid water is generated inside the fuel cell as a product of the redox reactions. If this is followed by a sudden reduction in the load, the flow of gas to and from the cell is reduced and the existing water content of the gas condenses to liquid water. Similarly, a large load increment will boost

the gas flow rates, thereby increasing the water transport from the cell with an increased risk of dehydration. [14, 64]

Water management is a key issue when it comes to performance and lifetime extension of a fuel cell. The degradation of both the catalysts and the membrane are both significantly affected by poor water management. [14]

A PEMFC effectively loses most of its ability to deliver electric power if the water content of the membrane becomes too low. In this state the fuel cell is practically in an extinguished state with a steady state current density of $\sim$0.1 mA/cm^2 - much lower than a production state of $\sim$125 mA/cm^2. The PEM fuel cell can dry to an extinguished state if operating at high temperatures in open-circuit conditions where inadequate water production takes place. [64]

Dehydration is an important cause of "[...] mechanical stress in the membrane that leads to failures (tearing and cracking), and accelerates the chemical degradation of PEM fuel cells" [14, p. 64].

3.7 Quasi-steady states

There exist a total "[...] of 5 steady states in PEM fuel cells, and the occurrence of autonomous oscillations with extremely long periods $\sim$10000 s" [64, p. 1744]. The autonomous change from one steady state to another occurs after an altered balance between water production and removal in response to a load change. Eventually an equilibrium between the water flows take place and a new steady state takes effect. [64]

The different steady states effectuate on different time scales due to different processes: less than 1 s, around 100 s and greater than 1000 s. The short response is the immediate result of a load change and the intermediate response is assumed to be a result of water diffusion in the cell. The long time span response is a result of adsorption and desorption of water in the membrane, changes of mechanical tension in the membrane and related to how the membrane functions as a water reservoir. [64, 65]

3.8 Environmental effects

A hydrogen fuel cell has effectively zero emission of greenhouse gasses as the only chemical product is pure water (H_2O). Fuel cells can also run on hydrocarbons, and do this at a much higher efficiency than diesel generators and motors. Either way, the use of fuel cell technology instead of conventional combustion engines can significantly reduce the emission of greenhouse gasses like carbon dioxide (CO_2), nitrogen oxides (NO_x) and sulphur oxides (SO_x) to the environment. [3]

This is an important consideration for the global shipping industry which contributes to an estimated 3–5% of the global emission of carbon dioxide and more than 5% of the sulphur oxide emissions, and faces strict current and future

emission regulations. [3]

The actual environmental effects of hydrogen fuel cells depend on the production chain of the cells as well as how the hydrogen is produced and transported.

4 Dynamic Response of Fuel Cells

Copyright notice
The state of art and related work were reviewed, and an identification of the relevant background material was carried out in the project [1] preceding this thesis. No relevant new material was found during the work on the thesis. The presentation from the project report is included below, with minor edits, for the complete remainder of this chapter.

The "[...] dynamic response of the PEM fuel cell is a very complex process; affected by its structure, operational modes and many other factors" [14, p. 68]. Altering some of the parameters of the fuel cell will also change the behaviour and dynamic response significantly. A change in the external load or in the operational parameters of the fuel cell induces transient phenomena and fluctuations in the system, which in turn affects parameters such as gas flows, temperatures, temperature gradients, pressure and relative humidity and condensation. [14]

4.1 Transient behaviour of fuel cells

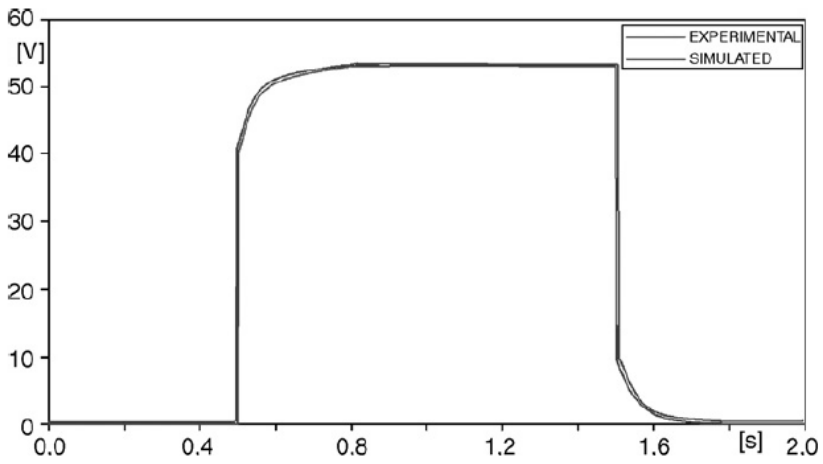

Figure 22: Characteristic voltage response of a fuel cell stack during connection and disconnection of an ohmic load. At 0.5 seconds a load is connected to the fuel cell stack. At 1.5 seconds the load is disconnected from the stack. Source: [66]

Fuel cells can potentially respond very quickly to large load power changes, especially when a maximisation of lifetime is of less importance. To be precise,

a fuel cell can respond as fast as the load it is connected to given that the cell is supplied with a surplus of reactant gasses [67].

While a fuel cell potentially can change the power output almost instantaneously under ideal conditions due to the existence of an electrochemical double layer [65], the voltage response is of a more transient character.

Experiments by H. Weydahl et al. [67] show that the voltage in a fuel cell during a sudden load step has a transient response lasting from 1.6 milliseconds to 0.38 seconds depending on the size of the load change. For transients where the final voltage is below approximately 0.65 V per cell, then a second voltage transient appeared, which reached steady state in less than 2 seconds.

Lazarou et al. [66] conducted transient response experiments on a 1.2 kW PEM fuel cell stack. The stack had an open circuit voltage of 43 V_{DC} (DC voltage), and a voltage of 26 V_{DC} at a rated current of 46 A. A typical voltage response profile for load step changes is shown in figure 22. The average time span the fuel cell stack used to stabilise the output voltage after either connection or disconnection of different ohmic load sizes is shown in figure 23. From this figure it can be seen that the transient voltage response time of the PEMFC is less than 0.34 seconds for a large load increase and less than 0.43 seconds for a large decrease of load size.

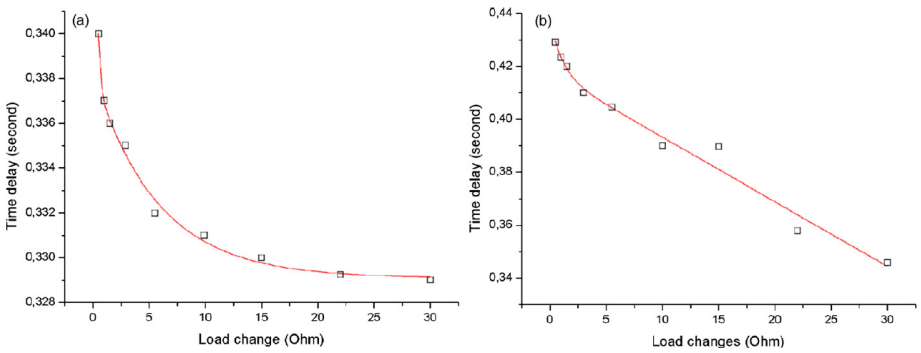

Figure 23: Average time duration for voltage level to reach steady state for a PEMFC stack, with respect to size of load change in ohm, when (a) connecting a load and (b) disconnecting a load. Source: [66]

4.2 Limitations on dynamic response

Under optimal conditions, and without considering lifetime degradation, a fuel cell can respond very fast to changing load conditions. There are, however, other considerations that should be made than what is strictly technically possible. One such very important limitation is how dynamic response and load cycling degrade the fuel cell performance and lifetime [14, 66].

The three most influential transient processes affecting the dynamic response capability of a proton exchange membrane fuel cell is (i) the transport of reactant gas in the fuel cell, (ii) hydration and dehydration of the membrane and (iii) the development and discharging of the fuel cell charge double layer [66].

Improper water management and insufficient reactant flow tends to occur during quick load changes because of slow fuel cell response, all contributing to reduced cell performance and lifetime [14, 64].

Suddenly applying or increasing a load to the fuel cell reduces the output voltage of the cell. A bigger increase of the load causes a bigger and longer lasting voltage drop until the system stabilises at a new steady state, as can be seen in figure 24. The larger the voltage pulse amplitude, the larger the stress on the fuel cell. [14]

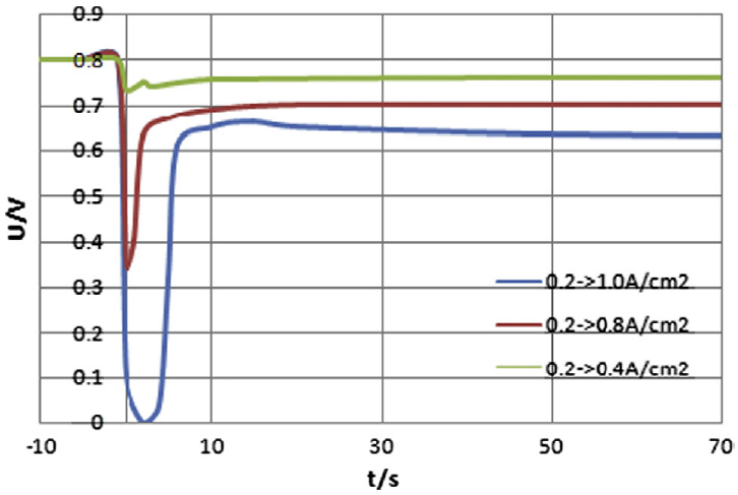

Figure 24: The dynamic response of a fuel cell after a sudden addition of different sized loads. Source: [14]

The voltage drop is not only related to the load increase, but also how fast the load is being applied. When the fuel cell has less time to adapt to a load change, then the voltage drop amplitude increases. Similarly a slower load change allows for the fuel cell to more smoothly adapt to the new operation point, as it is presented in figure 25. Reducing the loading speed, and inversely extending the loading time duration, will increase the lifetime of the fuel cell and is therefore an important consideration when evaluating the dynamic performance of fuel cell systems. [14]

The energy delivered from a fuel cell is extracted from the eletrochemical reactions of the fuel gasses. During an increase in the load and power output of a fuel cell more reaction gas is required. If the speed of the current change is significantly faster than the change of the gas flow rate, then the voltage will

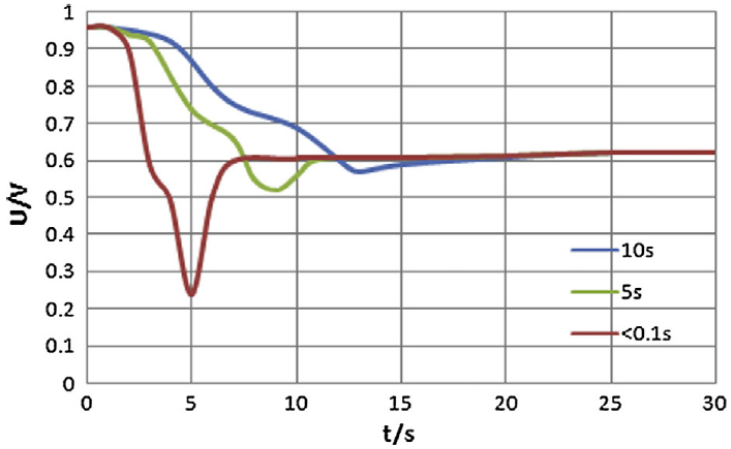

Figure 25: Dynamic response of a fuel cell depending on the loading speed. Source: [14]

drop due to insufficient amounts of reactants at the fuel cell electrodes. The consequence is gas starvation in the cell that causes a voltage drop, carbon corrosion of the membrane electrode assembly and degradation of the fuel cell performance. The voltage drop effect can be mitigated by reducing the load change speed to compensate for the inertia of the reactant gas flow and compressors. Alternatively, the gas stoichiometric ratio can be increased to ensure that there is a surplus of fuel, functioning as a dynamic response buffer, to handle higher load change speeds. The effect on the dynamic voltage response of increasing the stoichiometric ratio is presented in figure 26. [14]

An often used method to reduce the problem of oxygen starvation of fuel cells is to supply sufficient air to the cells before a load change. Such an approach does come at the cost of increased parasitic power in the fuel cell and a decrease of the total system efficiency as more power is needed to drive the air compressor. To avoid oxygen starvation during loading transients it is recommended to pre-supply the fuel cells with an air stoichiometry of 1.5. [14]

Oxygen starvation during load transients can also be handled by pre-setting the operation point of the air compressor before a load change on the fuel cell, assuming there is sufficient time to ramp up the air compressor before the fuel cell load change.

In an article concerning transient behaviour experiments on a PEM fuel cell stack [68], a large step increase in the output current and power of the stack resulted in a voltage undershoot behaviour due to the anode side of the membrane temporarily drying out. Experiments showed that the redistribution of water content in the fuel cell membrane to the anode side was in the order of 8 to 29 seconds. By taking into account the diffusion coefficient of water, the

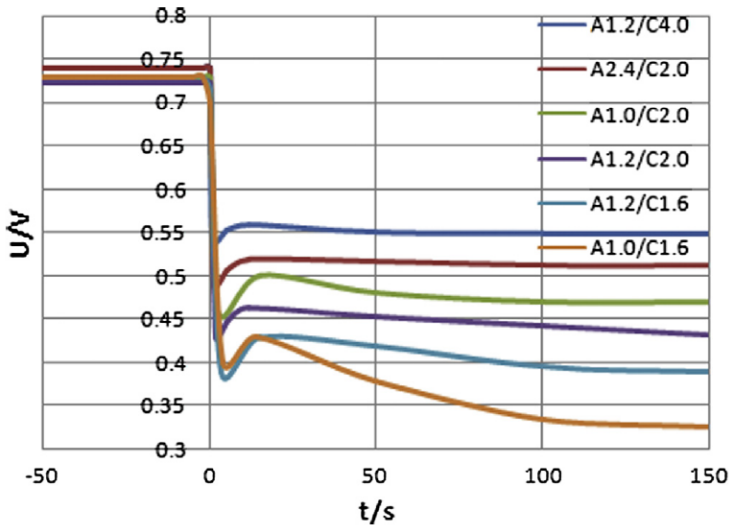

Figure 26: Sensitivity of dynamic response of a fuel cell to different stoichiometric ratios of reactants at the anode (A) and the cathode (C). Source: [14]

time delay was calculated to be approximately 22.4 seconds. A different study performed by Loo et al. [69], quantified numerically the response time of the humidity redistribution in the membrane to be 50 seconds.

Given the data presented so far in this section, it is recommended to limit the dynamic response of a fuel cell stack during a large load change to a minimum of 25 to 60 seconds in order to maximise the durability and performance of the stack. In other words the change of power output per time interval of the stack should be limited to $\Delta P_{FC,max}$ as shown in equation 14:

$$\Delta P_{FC,max} = \frac{P_{FC,max}}{t_{lt,min}} \tag{14}$$

where $P_{FC,max}$ is the nominal power capacity if the FC stack and $t_{lt,min}$ is the minimum loading time of a minimum of 25 or preferably 60 seconds. This gives a maximum loading speed of 4 kW/s and 1.67 kW/s, respectively, for a 100 kW fuel cell stack with a minimum loading time of 25 and 60 seconds.

For applications where a faster dynamic response is required, the fuel cell stack can be combined with diesel generators or highly dynamic energy storage components such as batteries, supercapacitors or flywheels.

4.3 Hybrid power generation

In addition to the long start-up times, high temperature fuel cells are restricted to slow load changes. Both effects are a result of the temperature gradient limitations of the materials in the fuel cell. To compensate for these limitations

of high temperature fuel cells, one or more diesel or gas combustion engines with short start-up times and swift response to load changes can be added in a hybrid power generation system. Such systems have the advantage of increased efficiency, but comes at the cost of increased system complexity. [3]

The slow response of a fuel cell is only partly solved by a hybrid configuration since "[...] the slowest component may restrict the overall system dynamics. For example, fast transients in turbomachinery may induce unacceptable operational conditions on the SOFC stack" [3, p. 356].

4.4 Hybridisation with electric storage components

If the transient behaviour of fuel cells is not satisfactory for a given system demand, then the addition of Auxiliary Electric Storage Components (AESCs) can be added to improve the system behaviour. Supercapacitors, batteries and flywheels are such components with high power-to-energy ratio, which allows for fast discharging in milliseconds, seconds or minutes. In a system consisting of both AESCs and fuel cells, the AESCs can deliver electric power during fast load increments and at peak load, which results in lower performance requirements of the fuel cells, but lowers the total system power density. [3]

The hybridisation of fuel cells with auxiliary electric storage components can also be desirable in situations where the fuel cell is able to respond sufficiently fast to load changes. The degradation of the fuel cell is related to load transients and also increases at higher power outputs, so a system hybridisation can improve the lifetime and long-term performance of fuel cell. [3]

4.4.1 Performance characteristics of electric storage components

Which storage component(s) to add to a fuel cell system depends on the types of system response improvements that are desired.

Supercapacitors have relatively low energy capacity, but very high power density and low cycle degradation, which make them suitable for fast dynamic response and peak shaving in the time scale of milliseconds and seconds [3].

Batteries have a lower power-to-energy ratio than supercapacitors and have a limited number of charge-discharge cycles. Batteries are therefore best applied to handle fuel cell start-ups, large load transients and peak shaving that lasts on the scale of minutes or hours. [3]

Flywheels may be considered a hybrid of supercapacitors and batteries in terms of power and energy density, but at the cost of having a lower round-trip efficiency and high self-discharge. This may, however, possibly be compensated for with comparable cost savings. [3]

5 Energy Carriers for Fuel Cells

Depending on the type of fuel cell, different types of fuel can be used. Low-temperature fuel cells use platinum catalysts in order to achieve a sufficient reaction rate. However, platinum has two major drawbacks as a fuel cell catalyst. One is cost and the other is that carbon monoxide reacts strongly with platinum and can therefore be considered a strong contaminator of the platinum catalyst. Low-temperature fuel cells like the PEM fuel cell can therefore not run on fuels containing carbon, but should rather use high-grade hydrogen with minimal contamination. [3]

For higher temperature fuel cells, platinum catalysts are not required to achieve good performance and less expensive catalysts can be used instead. This avoids the problem of CO-poisoning of the catalyst and makes it possible for carbon-containing compounds to be used as fuel for the fuel cells. [3]

5.1 Hydrogen (H_2)

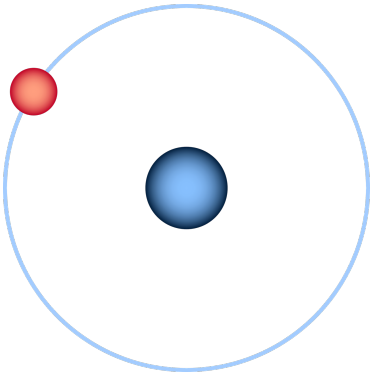

Figure 27: The hydrogen atom (H) with one electron.

5.1.1 Chemical properties

Hydrogen has a very high gravimetric energy density with a Lower (LHV) and Higher Heating Value (HHV) of 120.0 MJ/kg (33.$\overline{33}$ kWh/kg) and 141.8 MJ/kg (39.39 kWh/kg), respectively. The volumetric energy density, however, is much lower due to a volumetric mass density of just 89.87 kg/m^3 when stored in gas state. The atomic mass of a hydrogen atom (H) is just 1.00794 g/mol. Hydrogen exists as a gas at room temperature and atmospheric pressure with a melting and boiling point of mere -259.35 °C and -252.99 °C, respectively — neither of which are far from absolute zero (0 Kelvin) at -273.15 °C. [70, 71, 72, 73]

5.1.2 Production and efficiency

It is possible to produce hydrogen from numerous energy sources, both renewable and non-renewable, and through several different processes. Hydrogen can be manufactured by means of steam reforming of fossil fuels (in particular methane), oil reforming, coal gasification, water electrolysis and by biomass processes. A more comprehensive overview of different methods and sources can be explored in fig. 28. [74]

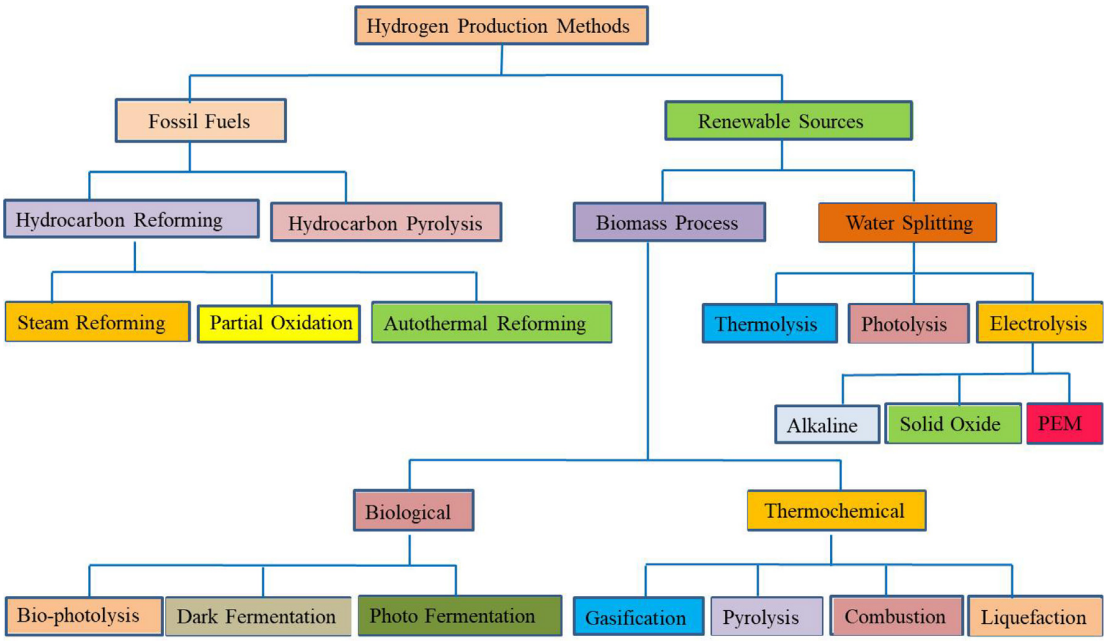

Figure 28: An overview of methods and sources for hydrogen production. Source: [74]

Water electrolysis is an especially simple and environmentally friendly way to produce hydrogen and works by basically running a hydrogen fuel cell in reverse. Electricity of at least 1.23 volts is added to water, resulting in hydrogen and oxygen forming at the cathode and anode, respectively. Renewable energy sources can be used as power source for the hydrogen production, reducing climate gas emissions to a minimum. The basic reaction for hydrogen production through water electrolysis is shown in eq. (15) and requires 285.8 kJ per mole of produced hydrogen. By taking into account the atomic mass of H_2, a theoretical energy consumption of 39.382 kWh/kg can be calculated, which is very close to the Higher Heating Value quantified in section 5.1.1. The efficiency of industrial water electrolysis equipment is in the range of 55% to 60%, so the industrial energy consumption is expected to be around 65 kWh/kg. [70, 74, 75]

$$H_2O + \text{Electricity}\left(237.2\frac{\text{kJ}}{\text{mol}}\right) + \text{Heat}\left(48.6\frac{\text{kJ}}{\text{mol}}\right) \longrightarrow H_2 + \frac{1}{2}O_2 \qquad (15)$$

5.1.3 Storage

Hydrogen as a fuel is very suitable for fuel cells due to fast electrochemical oxidation kinetics, which allow for high system power density and efficiency. When considering energy density it is clear that hydrogen has a very high gravimetric energy density, but at the same time a very low volumetric energy density due to its simple molecular structure. In other words, one unit of energy stored in hydrogen weights very little, but takes up a considerable volume. Hydrogen's extremely low volumetric density "[...] makes its storage a technical challenge for a hydrogen-oriented economy" [73, p. 15073]. An overview of hydrogen storage densities for different temperature and pressure conditions are illustrated in fig. 29. [3, 70, 73]

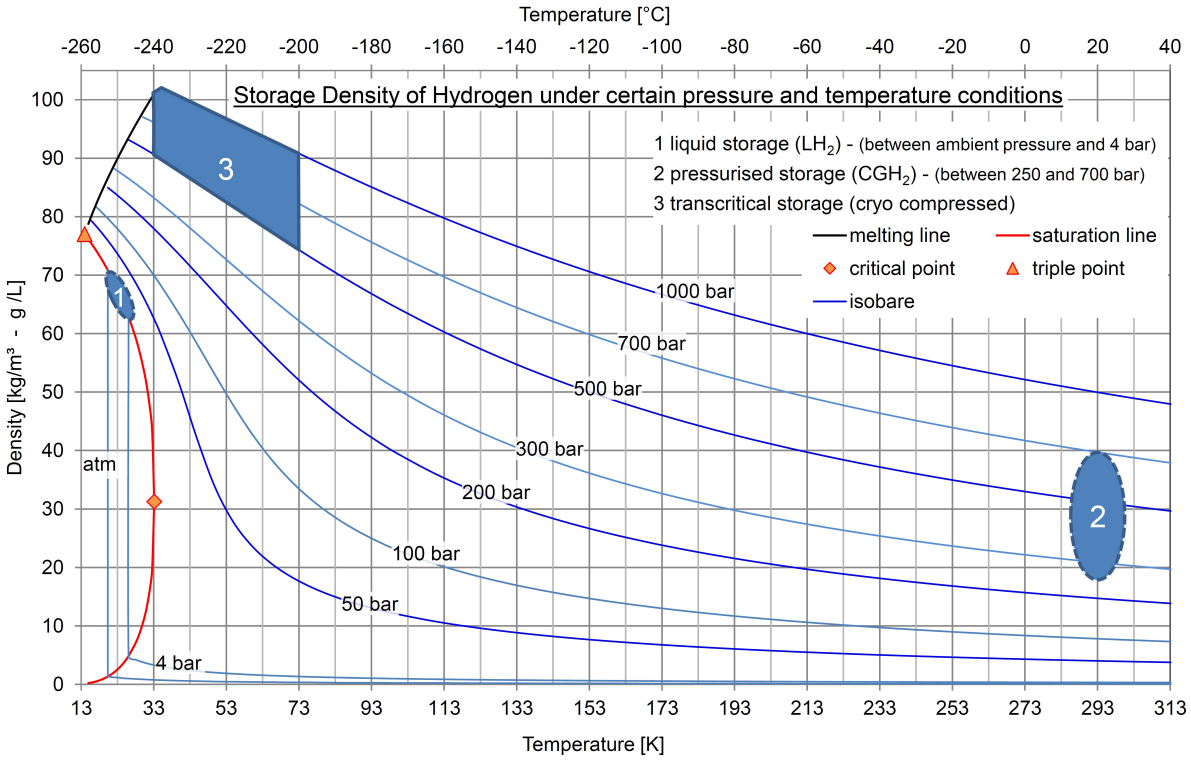

Figure 29: Storage density in kg/m^3 for hydrogen under different temperature and pressure conditions. Creator: Moritz Kuhn, ILK Dresden

Hydrogen's low volumetric density is a problem for volume critical applications like mobile energy production. Two ways to handle this problem are to

compress hydrogen to a very high pressure (usually at 350, 690 or 700 bar) or to liquify it at 20 K (-253°C) and atmospheric pressure - alternatively at 33 K (-240°C) and 13 atm. Regardless of the chosen method, the cost of these procedures comes in the form of energy loss during compression or liquefaction. Compressing hydrogen to a pressure of 700 bar requires circa 3 kWh pr kg of hydrogen, while the theoretical energy consumption for hydrogen liquefaction of one kilo of hydrogen is around 3 to 4 kWh. However, the actual energy consumption needed to liquify hydrogen is typically in the order of 10 to 13 kWh/kg. Given that hydrogen has a lower heating value (LHV) of 33.33 kWh/kg, hydrogen compression and liquefaction constitutes an energy loss of 9% and 30-39%, respectively. Additionally, fast-filling a storage tank with hydrogen at 700 bar requires an input gas pressure of 880 bar with the gas precooled to -40 °C to cope with the heating that takes place during the refilling process, according to the US Department of Energy (DoE) [76]. [3, 70, 73, 77, 78, 79, 80]

Hydrogen is often stored in storage vessels made of steel, aluminium and sometimes the stronger, but more expensive, material of carbon fibre reinforced plastic composite. Liquid hydrogen requires special double-walled storage tanks with appropriate insulation to avoid heat leakage. [73]

Hydrogen has several disadvantages when it comes to storage aspects. As mentioned, hydrogen has a low volumetric density and therefore needs to be compressed or liquified at a low temperature to increase the energy density, but at a cost of lower overall system efficiency. Hydrogen is also volatile and highly flammable, which poses challenges from a security standpoint. [42]

5.1.4 Safety

Hydrogen is flammable in air, but hydrogen and oxygen (oxyhydrogen) only react with each other at normal temperatures in the presence of a catalyst, such as platinum or palladium. A temperature of at least 550 °C is required for a reaction to develop without a catalyst, and hydrogen has an autoignition temperature of 585 °C (858 K). For comparison, typical gasoline has an autoignition temperature in the range of 192 °C to 470 °C (465 to 743 K). Hydrogen gas is both flammable and explosive, and especially so if two volume units of hydrogen are mixed with one volume unit of oxygen. A hydrogen–air mixture is flammable for hydrogen concentrations in the range of 4.0% to 75%, and explosive for concentrations between 18.3% and 59%. For hydrogen mixed with air at atmospheric pressure, 0.02 mJ is the minimum spark ignition energy. [70, 81]

Hydrogen is susceptible to leakage in both a liquid and gaseous state, due to a low molecular weight and low viscosity. "Hydrogen diffuses extensively, and when a liquid spill or large gas release occurs, a combustible mixture can form over a considerable distance from the spill location" [81, Sec. 6.4.2, p. 8]. However, hydrogen's high diffusibility also means that hydrogen quickly

diffuses to a nonexplosive mixture, partly because hydrogen is lighter than air. A ground-spill experiment of almost 1900 litres (500 gallons) demonstrated that hydrogen became nonexplosive after approximately 1 minute. [81]

Hydrogen gas has no colour or odour, and is therefore undetectable by human senses. It is recommended that hydrogen detectors are placed in the proximity of possible leak points and adequate ventilation is required for chambers containing hydrogen components. [70, 81]

5.2 Liquid Organic Hydrogen Carriers (LOHCs)

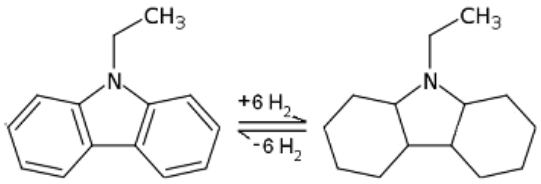

Figure 30: A structural model of Iminodibenzyl ($C_{14}H_{13}N$) illustrating the reversible processes of using Liquid Organic Hydrogen Carriers for hydrogen storage. Source: [80]

5.2.1 Conceptual overview

Much like ammonia (section 5.4, page 67) and methanol (section 5.5, page 73), Liquid Organic Hydrogen Carriers (LOHCs) function as chemical energy carriers and can be used as storage medium for hydrogen. LOHCs have, however, the added property of completely reversible dehydrogenation without the need to extract CO_2 or nitrogen from the atmosphere for each cycle. The reversibility of the organic compounds means that the compounds themselves need only to be generated once, and can then be repeatedly hydrogenated and dehydrogenated without altering the core structure. The downside of this is that LOHCs occupies storage space also after hydrogen extraction. [80]

Hydrogenation is the process of adding hydrogen to organic and inorganic chemical compounds, while dehydrogenation refers to the process of extracting hydrogen from a compound, as illustrated in figs. 30 and 35 [82].

Even though LOHCs are considered an emerging technology for hydrogen and energy storage, the history of organic hydrogen carriers date back to the 1970's and the technology is assessed as mature in industrial processes used for instance in oil refineries. [80]

5.2.2 Overview of chemical compounds

Table 1 lists some cyclic hydrocarbons with name, molecular formula and hydrogen capacity for both the hydrogenated and dehydrogenated states. The listed chemical composites have a hydrogen mass fraction in the range of 6.2 to 7.3 wt%, meaning that, for instance, 1000 kg of cyclohexane with a hydrogen mass fraction of 7.2 wt% contains 72 kg extractable H_2 when dehydrogenated back to benzene. The heat released during dehydrogenation is between 62 to 71 kJ mol^{-1} H_2. [80]

The following sections list pairwise the chemical components that together

Table 1: Overview of some cyclic hydrocarbons [80]. Each row list a LOHC with and without the number of carried hydrogen molecules indicated in the third column from the left. The rightmost column gives the mass fraction of *extractable* hydrogen during dehydrogenation for the respective hydrogenated compounds.

Dehydrogenated	**Molecular formula**	**Hydrogen storage capacity**	**Hydrogenated**	**Molecular formula**	**Hydrogen storage capacity [wt%]**
Benzene	C_6H_6	$+3\ H_2 \longleftrightarrow$	Cyclohexane	C_6H_{12}	7.2
Toluene	$C_6H_5CH_3$	$+3\ H_2 \longleftrightarrow$	Methylcyclohexane	C_7H_{14} or $C_6H_{11}CH_3$	6.2
Naphthalene	$C_{10}H_8$	$+5\ H_2 \longleftrightarrow$	Decalin	$C_{10}H_{18}$	7.3
Biphenyl	$C_{12}H_{10}$ or $C_6H_5C_6H_5$	$+6\ H_2 \longleftrightarrow$	Bicyclohexyl	$C_{12}H_{22}$	7.1

constitute one liquid organic hydrogen carrier. In the pairs, the hydrogen deficient form will be listed first, followed by the hydrogenated form.

5.2.3 Benzene / Cyclohexane

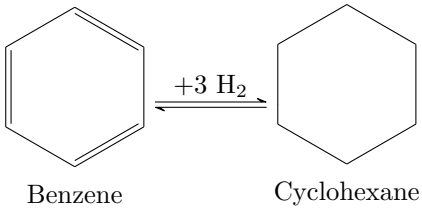

Figure 31: Reversible hydrogenation of benzene to cyclohexane.

Benzene (C_6H_6) is the simplest aromatic hydrocarbon and is a colourless, highly flammable, water insoluble liquid with a melting point of 5.5 °C and a boiling point of 80 °C. At 20 °C, benzene has a density of 876 kg/m^3. Benzene can be technically extracted from coal tar, a historical source, but is now mainly produced by cracking or reforming of petroleum fractions. Benzene is an acutely narcotizing chemical that is irritating to skin and mucous and can cause anaemia by damaging blood-producing structures in the body. [80, 83, 84]

Cyclohexane (C_6H_{12}) is a colourless, highly flammable liquid with a petroleum-like odour, a melting point of 7 °C and a boiling point of 81 °C. 778 kg/m^3 is the density for cyclohexane. The chemical is slightly soluble in water where microorganisms may slowly break it down. Cyclohexane is considered very toxic to aquatic life, both acute and long term, and can depress the central nervous system in humans with symptoms such as headache, dizziness, narcosis and even death if the exposure concentrations are high enough. A concentration of

250 ppm for 4 hours results in eye irritation and dry throat. [80, 85]

5.2.4 Toluene / Methylcyclohexane

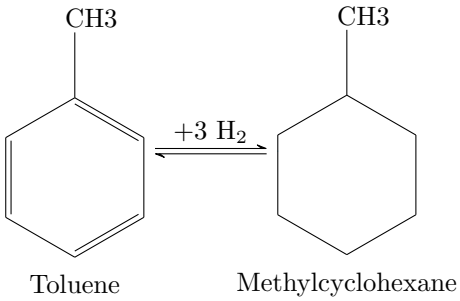

Figure 32: Reversible hydrogenation of toluene to methylcyclohexane. Toluene and methylcyclohexane have an extra methyl group (CH_3) compared with benzene and cyclohexane, respectively, and therefore have a reduced mass fraction hydrogen storage capacity [wt%] compared with benzene and cyclohexane.

Toluene ($C_6H_5CH_3$) is a clear, colourless and highly flammable liquid with a distinct aromatic smell similar to benzene. Toulene is produced during production of gasoline and other fuels from crude oil and has a melting point of -95 °C, a boiling point of 111 °C and a density of 862 kg/m^3. The compound can damage the central nervous system through aerial exposure, after which it can lead to symptoms like confusion, weakness, memory-loss and nausea. Extremely high concentrations can cause permanent brain damage and death. [80, 86]

Methylcyclohexane (C_7H_{14} or $C_6H_{11}CH_3$) is, like many of the chemicals listed so far, a clear, colourless, highly flammable liquid with a melting point of -127 °C and a boiling point of 101 °C. Measurements at 20 °C gives a density for methylcyclohexane at 769 kg/m^3. The liquid is not soluble in water and may be fatal if it is swallowed or enters the airways. Methylcyclohexane is, among other things, used as a fuel additive and as a cleaning solvent. Methylcyclohexane can be produced from toluene or a high temperature reaction between benzene and methane. An experiment showed that methylcyclohexane biodegraded 75% during 192 hours (8 days) at a temperature of 13 °C and from an initial concentration of 0.05 µg/litre. [80, 87]

5.2.5 Naphthalene / Decalin

Naphthalene ($C_{10}H_8$), also known as white tar, has a melting point temperature of 80 °C and a boiling point temperature of 218 °C, which means that naphthalene is in a solid state at room temperature and up to 80 °C. At 20 °C, naphthalene has a density of 1162 kg/m^3. Naphthalene has a white colour, has a strong coal tar odour and is made from petroleum distillation or coal tar. As

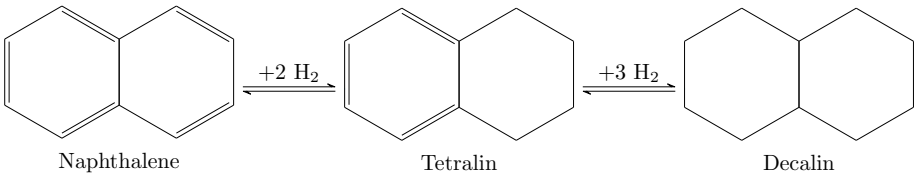

Figure 33: Reversible hydrogenation of naphthalene to decalin with tetralin as an intermediate product.

with most hydrocarbons, naphthalene is also damaging to health and aquatic life, but evaporates easily from both water and soil surfaces, and will be broken down within approximately one day by moisture and sunlight in air. The effects of naphthalene poisoning are much less severe than for other hydrocarbons and include symptoms like nausea, vomiting and diarrhoea. [80, 88]

Decalin ($C_{10}H_{18}$), also known as decahydronaphthalene, is a clear colourless, water-insoluble liquid with an aromatic odour, and is used in many cleaning products. The chemical has a melting point of -41 °C and a boiling point of 156 °C. The density is 878 to 888 kg/m^3 at 20 °C. Decalin can be made from hydrogenation of naphthalene and acetic acid at 25 °C and 130 bars in the presence of a platinum catalyst. This produces a mixture of 77% cis-decalin and 23% trans-decalin. Decalin can alternatively be made from naphthalene and hydrogen at a temperature of at least 100 °C local to a copper or nickel catalyst. Regarding hazards identification, decalin is flammable, very toxic to aquatic life and potentially fatal if swallowed or inhaled. Decalin does not degrade in marine water, but can degrade in stagnant water where biodegradation may take place. If released into water, decalin is likely to adsorb to suspended solids and sediment. [80, 89, 90]

5.2.6 Biphenyl / Bicyclohexyl

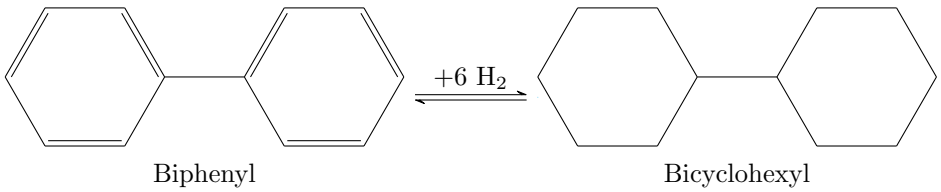

Figure 34: Reversible hydrogenation of biphenyl to bicyclohexyl.

Biphenyl ($C_{12}H_{10}$ or $C_6H_5C_6H_5$) consists of two benzene rings and can be manufactured from benzene (page 55). Biphenyl has a melting point of 70 °C and a boiling point of 255 °C, and is therefore a solid at room temperature like naphthalene. At 20 °C biphenyl has a density of 1155 kg/m^3. In a liquid state, biphenyl is clear and colourless with a pleasant odour. Nonetheless, biphenyl

can cause symptoms such as moderate irritation of eyes, nose, throat and skin, coughing, nausea and vomiting. The chemical is also considered very toxic to aquatic life. If released to air, biphenyl will degrade due to a reaction with hydroxyl (OH) radicals. This reaction has an estimated half-life of two days. If, however, biphenyl is released into water, then it will most likely adsorb to suspended solids and consequently sediment. [80, 91, 92]

Bicyclohexyl ($C_{12}H_{22}$) is, unlike its LOHC associate biphenyl, a liquid at room temperature with a melting point of 4 °C and a boiling point of 228 °C. The density is approximately 887 kg/m^3 at 20 °C. From a safety perspective, bicyclohexyl causes skin and eye irritation and is very toxic to aquatic life. [80, 93, 94]

5.2.7 Cyclic process properties

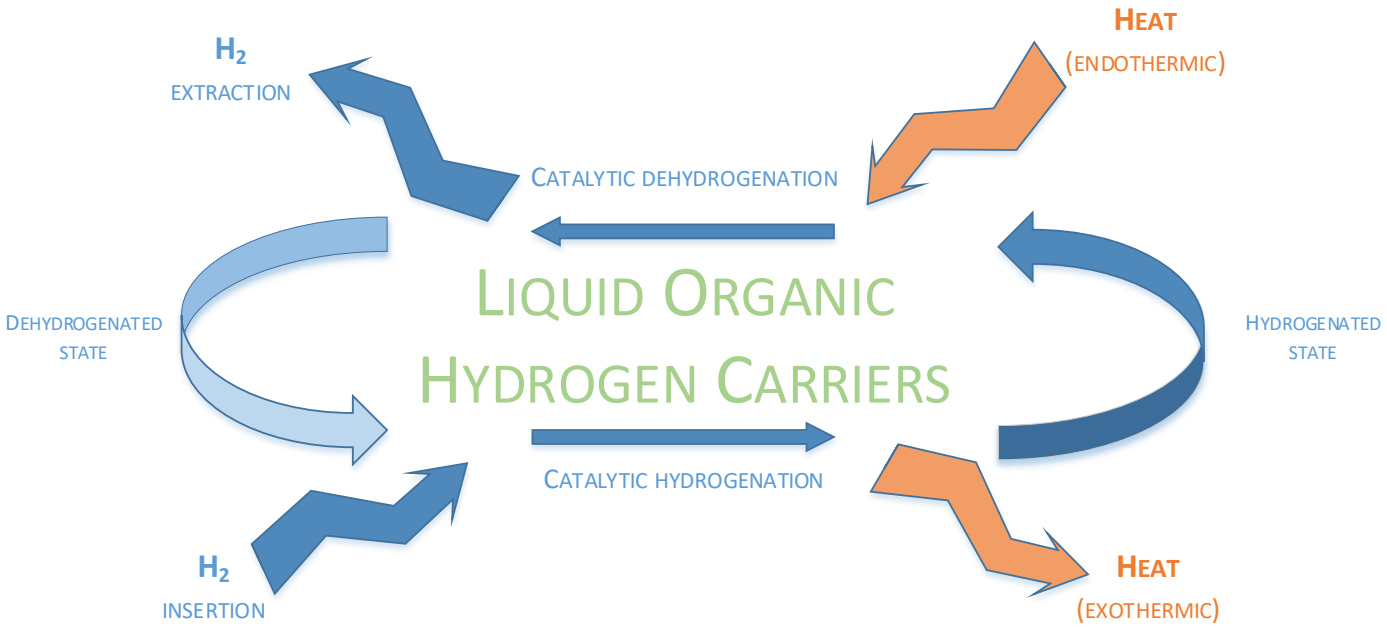

Figure 35: Schematic overview of the production–consumption cycle for Liquid Organic Hydrogen Carriers (LOHCs). Hydrogen is exothermically and catalytically added to a LOHC for storage and later released endothermically and catalytically for use in fuel cells, storage or other purposes. The dehydrogenated organic compound is kept for re-hydrogenation, and a complete regenerative cycle is formed.

LOHCs consist of many different hydrogen-carrying compounds with different properties for (de)hydrogenation and with different numbers of aromatic rings. For instance, benzene (C_6H_6) has one aromatic ring and requires a temperature in the range of 300 °C to 350 °C to dehydrogenate (ie. removal of

the hydrogen); naphthalene ($C_{10}H_8$) has two fused aromatic rings and requires 250 °C to 300 °C for dehydrogenation; nitrogen-containing heteroaromatics have one to three aromatic rings and release hydrogen between 50 °C to 200 °C. [80]

Dehydrogenation, in which the hydrogen is extracted from an organic compound, is an endothermic process that consumes heat. The heat is later released during hydrogenation, although at a lower temperature [80]. Overall system efficiency can be improved by utilising waste heat from the fuel cell stack in the dehydrogenation process.

The hydrogenation and dehydrogenation processes can be improved with heterogeneous metal catalysts [80]. Catalysts are materials that improve chemical reactions — with respect to factors like reaction temperature, energy requirements and reaction rates — by providing an alternative chemical reaction pathway for the reactants without the catalyst being expended in the process. A heterogeneous catalyst is a solid catalyst where the reaction occurs at the catalyst surface and the catalyst and the reactants are in different phases. [95, 96]

5.2.8 Temperature ranges for liquid storage

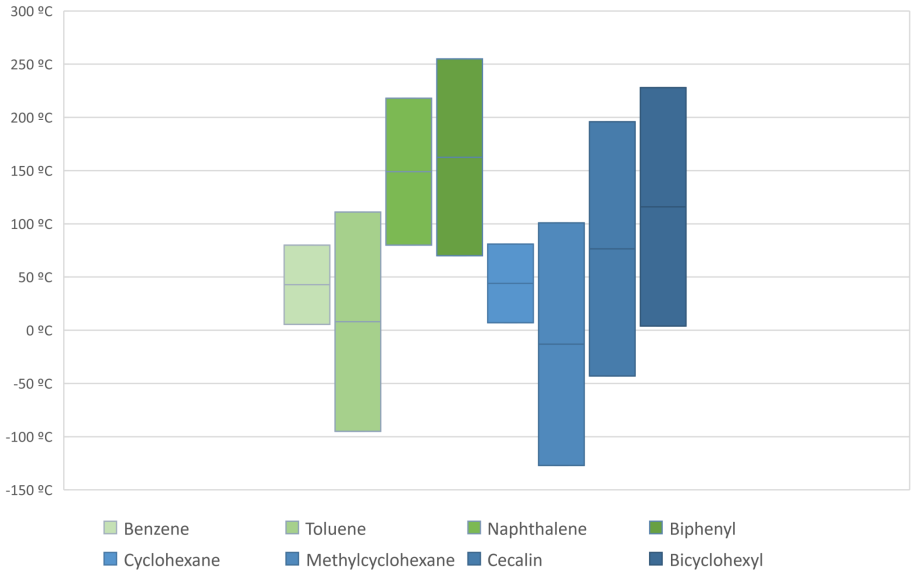

Figure 36: Overview of the temperature ranges in which the respective dehydrogenated (green shades) and hydrogenated (blue shades) LOHCs are in a liquid state at atmospheric pressure. In other words, the lower bounds indicate melting point temperatures and the higher bounds indicate the boiling point temperatures. The temperatures are plotted in Celsius degrees.

Figure 36 summarises the temperature ranges in which the previously mentioned Liquid Organic Hydrogen Carriers are in a liquid state at atmospheric

pressure. From the plot all the compounds, with the exception of naphtalene and biphenyl, can be identified to be in a liquid state at room temperature. The two LOHC exceptions are in a solid state after the release of stored hydrogen from cecalin or bicyclohexyl.

Of the four LOHC compound combinations, benzene/cyclohexane or toluene/methylcyclohexane should be selected as LOHC if it is deemed a priority to keep the compounds in a liquid state both before and after the extraction of hydrogen for fuel cell consumption. In addition, it is also worth considering that benzene/cyclohexane have a larger hydrogen storage mass fraction than toluene/methylcyclohexane, but also have a more restricted temperature range for remaining in a liquid state. It then becomes a question for the system designer if energy storage density is more important than the temperature range for liquid state or not. Benzene and cyclohexane need a temperature between 7 °C and 80 °C to remain in a liquid state, while toluene and methylcyclohexane are liquid at atmospheric pressure for a temperature range from -95 °C to 101 °C.

5.2.9 Hydrogen energy capacity

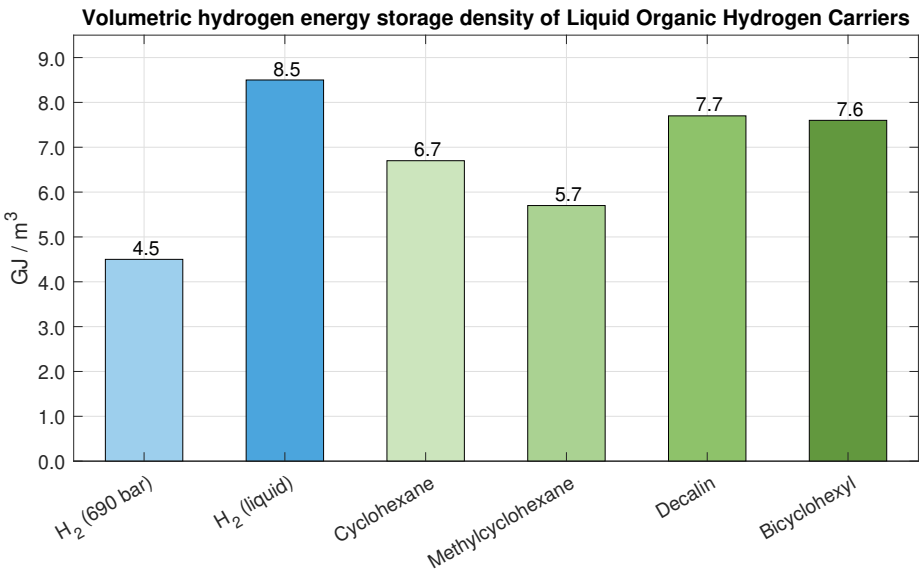

Figure 37: Hydrogen storage capacity of different Liquid Organic Hydrogen Carriers (LOHCs). The hydrogen energy capacity is calculated based on the density of each compound, the mass fraction of reversibly extractable hydrogen for each compound and the Lower Heating Value (LHV) of hydrogen. Hydrogen (H_2: 690 bar and liquid) is added for comparison.

Figure 37 summarises the the energy density of the hydrogen that can be

reversibly extracted from each Liquid Organic Hydrogen Carrier (LOHC). The numbers are calculated as shown in equation eq. (16), where ρ_{LOHC} is the density of each LOHC in kg/m^3, α_{H_2} is the mass fraction of reversibly extractable hydrogen of each carrier and 0.120 is the energy content (lower heating value) in GJ for each kilo of hydrogen, as determined in section 5.1.1. The resulting unit then becomes GJ/m^3.

$$\rho_{LOHC} \cdot \alpha_{H_2} \cdot 0.120 \frac{\text{GJ}}{\text{kg}_{H_2}} \tag{16}$$

The extractable hydrogen content should not be confused with the total hydrogen content of each organic carrier. Some hydrogen will always remain in the LOHC compounds even after dehydrogenation. See table 1 on page 55 for more information.

From the above-mentioned figure, it may be observed that all of the four LOHCs have a higher hydrogen storage density than hydrogen compressed at 690 bar, but also a lower hydrogen storage density than liquid hydrogen. Liquid hydrogen requires, however, a storage temperature of -253 °C or lower, while the LOHCs can be stored at room temperature, as discussed in section 5.2.8.

5.2.10 Suitable Fuel Cells

Liquid Organic Hydrogen Carriers can be supplied to any fuel cell that can run on hydrogen if the LOHCs are first dehydrogenated. For low temperature fuel cells, like the Proton Exchange Membrane Fuel Cell (PEMFC), an extra step of hydrogen purification is needed to avoid severe catalyst degradation.

5.2.11 Efficiency

Hydrogenation and dehydrogenation of Liquid Organic Hydrogen Carriers have an estimated efficiency of 98% for each processing step [97]. An additional energy consumption of 2 to 4 kWh/kg$_{H_2}$ is needed for hydrogen purification [80] for low-temperature fuel cells.

Table 2 presents a system efficiency perspective for different combinations of electrolyser and fuel cell technologies, based on data from Schneider & Johannes [97]. The efficiency of the dehydrogenation process for the PEM fuel cell is lower because of necessary hydrogen purification, as mentioned above, to avoid catalyst degradation. CHP stands for Combined Heat and Power and is co-generation of heat and power from a heat engine. SOEC is a Solid Oxide Electrolyser Cell, which basically is a Solid Oxide Fuel Cell (SOFC) that runs in regenerative mode to produce, rather than consume, hydrogen gas and/or carbon monoxide (CO).

The efficiency given by Schneider & Johannes [97] for re-electrification with SOFC is a bit conservative given that the electrical efficiency of SOFCs can

be above 65% — and even up to 90% in a CHP setting. Naturally, fuel cell efficiencies depend on output power, because of kinetic, ohmic, mass transfer and system losses, so the efficiency numbers provided by Schneider & Johannes may be for a SOFC running at sub-optimal conditions like low power output.

For clarification, the choice of fuel cell technology does not depend on the technology used for electrolysis, unless it is desired that hydrogen or carbon monoxide gas production and consumption is performed regeneratively using the same unit and at the same location.

Table 2: Overview of power-to-power system efficiencies for electrolysis, hydrogenation and dehydrogenation of LOHCs and fuel cell power generation. Source: [97]

Process step	**PEM electrolysis + PEMFC**	**PEM electrolysis + CHP**	**PEM electrolysis + SOFC**	**SOEC + SOFC**
Electrolysis	70%	70%	70%	90%
Hydrogenation	98%	98%	98%	98%
Dehydrogenation	70%	98%	98%	98%
Re-electrification	55%	42%	50%	50%
El. round-trip efficiency	**26%**	**28%**	**34%**	**43%**
Waste heat temperature	< 150 °C	< 300 °C	< 400 °C	< 400 °C

5.2.12 Costs

Benzene (C_6H_6) and toluene ($C_6H_5CH_3$ or C_7H_8) are priced below €1 per kg and have an annual global production volume of approximately 50 Mt (2018). [80]

5.3 Metal hydrides

"Metal hydrides are known as a potential[ly] efficient, low-risk option for high-density hydrogen storage since the late 1970s" [98, p. 7780] and "[...] have been recognised as one of the most feasible solutions to store hydrogen in hydrogen-powered systems" [73, p. 15082]. Nonetheless, there are some challenges with storage capacity and slow kinetics for hydrides [73], which the following sections will consider in more detail.

5.3.1 Conceptual overview

While Liquid Organic Hydrogen Carriers (LOHCs) store hydrogen in a liquid state, metal hydrides are the conclusion of combining hydrogen with different metals. The result is a solid-state storage solution contained under moderate pressure and temperature. [73]

A generic example of the reversible unification of metal/alloy and hydrogen is presented in eq. (17).

$$\mathrm{M} + \frac{x}{2}\mathrm{H_2} \leftrightarrow \mathrm{MH_x} + \mathrm{Q} \tag{17}$$

The M can either be a metal, a solid solution or an intermetallic alloy. The x is a positive whole number. The resulting formed hydride is denoted MH_x, and Q is the reaction heat.

The reaction rate of eq. (17), and therefore a metal-hydrogen system, is a function of temperature and pressure. Metal hydrides can also be divided into low- and high-temperature hydrides, where the latter has the highest storage capacities. [73]

The main challenges with metal hydrides are weight and relatively low storage capacity for hydrogen in the low-temperature metal hydrides. For the high-temperature hydrides, slow kinetics and a temperature range between 300 °C and 400 °C for uptake and release of hydrogen can be problematic. [73]

5.3.2 Hydrogen capacity

The main driving force behind "[...] a wide usage of metal hydrides in the field of hydrogen storage is their huge capacity to accommodate a significant amount of hydrogen in their structures" [73, p. 15077]. Fascinatingly, it is actually

> "[...] possible to pack more atoms of hydrogen into a metal that forms a hydride lattice than into the same volume of liquid hydrogen because when such metal is brought in contact with gaseous hydrogen, the hydrogen molecules are first adsorbed onto the surface of the material" [73, p. 15077].

In other words, "more is less".

Hydrogen gas and liquid hydrogen have a storage density of 0.99 hydrogen-atoms/cm^3 and 4.2 hydrogen-atoms/cm^3 [73], respectively. Metal hydrides have a hydrogen storage capacity that is significantly higher. For instance, magnesium hydride (MgH_2) [99] can store 6.5 hydrogen-atoms/cm^3 [73] — 55% more than liquid hydrogen can on its own.

Figure 38 and 39 show the hydrogen storage capacity of the various metal hydrides in terms of weight percentage (wt.%) or GJ of hydrogen per cubic metre (GJ/m^3) of hydride.

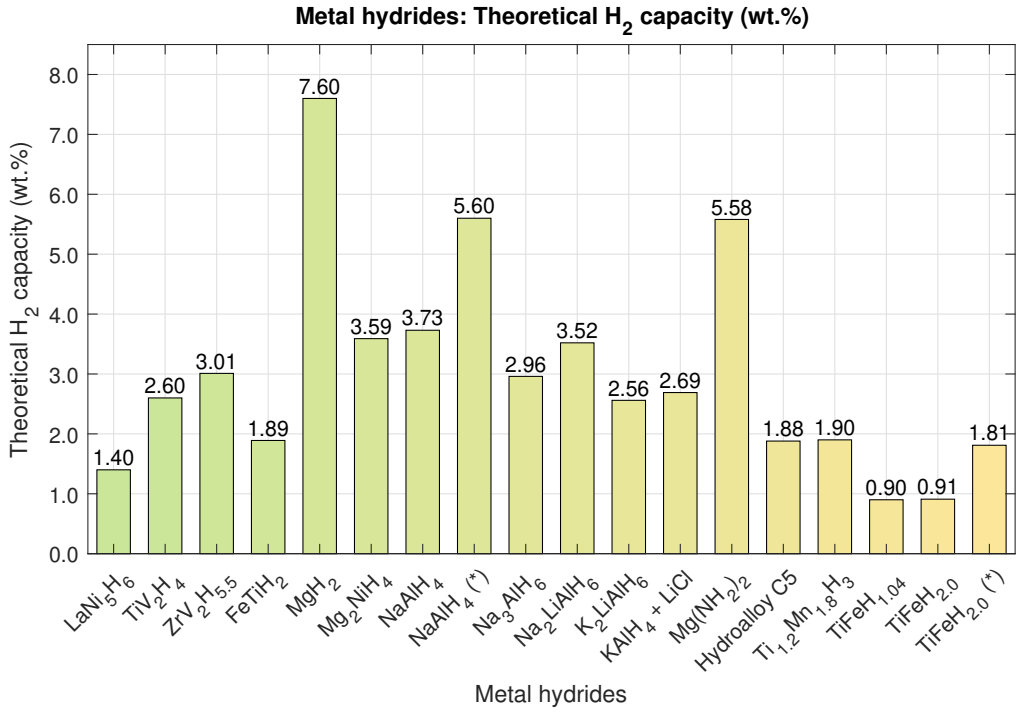

Figure 38: Theoretical hydrogen storage capacity of different metal hydrides. The values indicate the weight of hydrogen relative to the weight of the respective metal hydrides. The duplicates marked with a star (*) can be decomposed into different molecule combinations with different amounts of released hydrogen. Based on data from [73, 98].

5.3.3 Kinetics, catalysts and reversibility

If contamination is avoided, a metal hydride can in theory be indefinitely charged and discharged with hydrogen. [73]

To effectively absorb or desorb hydrogen, high hydrogen pressure or high temperatures are required; since the metals have an activation barrier that needs to be overcomed. [73]

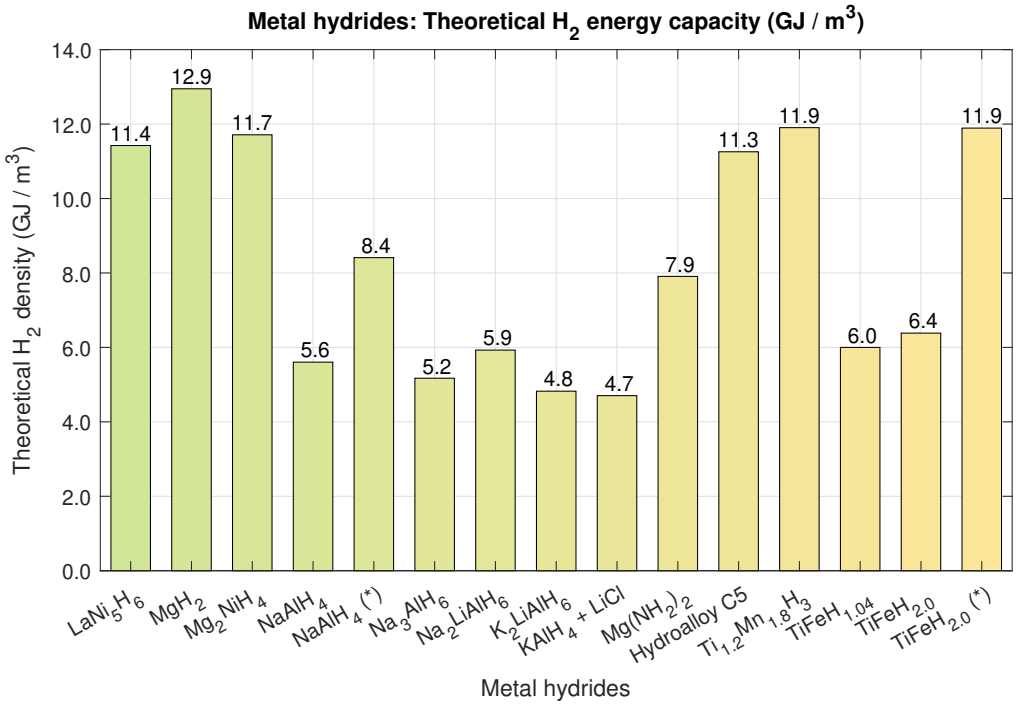

Figure 39: Theoretical hydrogen energy storage capacity of different metal hydrides. The duplicates marked with a star (*) can be decomposed into different molecule combinations with different amounts of released hydrogen. Based on data from [73, 98]. Data is missing for TiV_2H_4, $ZrV_2H_{5.5}$ and $FeTiH_2$.

Catalysts can also be used for improved hydrogen sorption kinetics. A catalyst made of palladium has the ability to "[...] take up large volumetric amounts of hydrogen at normal room temperature and atmospheric pressure [...] to reach a high hydrogen gas quality of 99.9999% purity" [73, p. 15079]. Platinum is also a good hydrogen catalyst and is often used in low-temperature fuel cells as discussed in the chapter on Fuel Cell Technologies. Alloys, such as $LaNi_{4.7}Al_{0.3}$, can be doped with small amounts of platinum and palladium so that they can be activated at room temperature with very low hydrogen pressure and with up to 100 times faster uptake and release of hydrogen compared to alloys without catalyst treatment. The biggest problem with palladium and platinum is that they are very expensive. Other and cheaper catalysts also exist for different metal hydrides. For instance, niobium pentoxide (Nb_2O_5) has shown good performance when coupled with magnesium hydride (MgH_2). [73]

Catalyst alloying has a direct effect on the energy of hydrogen sorption. Pure MgH_2 has an activation energy of 120 kJ/mol, while MgH_2 fused with an element called vanadium (V) almost halves the activation energy down to 62.3 kJ/mol. MgH_2 with Nb_2O_5 performs even better with the activation energy

reduced to 38 kJ/mol. [73]

5.3.4 Storage and safety

As initially mentioned, metal hydrides can be stored at moderate pressure and temperature. To be more specific, the pressure is generally between 3 and 30 bar; much lower than the 690 bar pressure that compressed hydrogen is usually stored under. The consequence is a much safer storage system than for compressed hydrogen. Additionally, there is no risk of hydrogen gas leakage or tank explosion with metal hydrides as there unfortunately is for hydrogen gas. [73]

On the negative side, metal hydrides are very heavy, since they are made of metals after all, while hydrogen is the lightest molecule in the universe. In research, there is hope to discover novel light materials that reduce the gravimetric density. [73]

5.3.5 Suitable Fuel Cells

Since metal hydrides release pure hydrogen, any hydrogen-compatible fuel cell can be used for power production given that the hydrogen is first desorbed from the hydrides.

5.3.6 Efficiency

The conversion efficiency of metal hydrides varies with the different metals, solid solutions and intermetallic alloys.

The maximum energy efficiency of a full hydrolysis cycle for MgH_2 is 45.3% [100]. A full hydrolysis cycle means that hydrogen is first added to the metal hydride and then later releases from the hydride, much like the hydration and dehydration processes for Liquid Organic Hydrogen Carriers (LOHCs). Since the overall efficiency is 45.3%, the process steps of adding and removing hydrogen from the hydride each have an average energy efficiency of 67.3%.

The two compounds $H-Mg_3La$ and $HeLa_2Mg_{17}$ have maximum energy efficiencies of 40.1% and 41.1%, respectively [100].

5.4 Ammonia (NH_3)

Ammonia is a promising energy carrier for fuel cells and may pose a practical solution to the challenges that arise with storage of molecular Hydrogen (H_2).

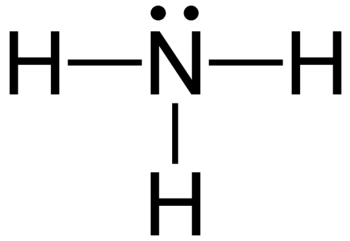

Figure 40: The molecular structure of ammonia.

5.4.1 Chemical properties

Ammonia has a melting and boiling point of -78 °C and -33.4 °C and a Lower (LHV) and Higher Heating Value (HHV) of 18.646 MJ/kg and 22.5 MJ/kg, respectively. Ammonia is therefore in a gas state at room temperature. [13, 101, 102]

Both "[...] hydrogen and ammonia are considered among the most significant clean fuel sources with no carbon emissions, and an increasing trend for their use in the near future" [103, p. 96]. This is in part because ammonia only consists of nitrogen and hydrogen atoms, as shown in figure 40, hence no CO_2-emissions can be directly attributed to the combustion of ammonia. Furthermore, ammonia's lack of carbon bonds means that it can be used without risk of carbon poisoning of catalysts in fuel cells. Furthermore, ammonia is fully recyclable and its substances are available almost everywhere in the environment. [103, 104, 105]

Ammonia can be considered an energy carrier for hydrogen, and ammonia has in fact the highest volumetric hydrogen density amongst many liquid fuels, including methanol, ethanol, gasoline, etc. [106]. To be more precise, ammonia has a hydrogen mass fraction of $(3 \cdot 1)/(14 + 3 \cdot 1) = 0.1765$, where 1 and 14 are the atomic weights of hydrogen and nitrogen, respectively. This means that 17.65 wt.% of any gravimetric amount of ammonia is hydrogen. And since hydrogen has a lower heating value of 33.33 kWh/kg (120.0 MJ/kg), it can easily be calculated that a kilo of ammonia contains approximately 5.88 kWh of hydrogen energy.

The liquid density of ammonia is 696 kg/m^3 [107]. Given ammonia's hydrogen mass fraction of 0.1765 and the lower heating value of hydrogen of 120 MJ/kg, the hydrogen energy density of ammonia can be computed to be 14.7 GJ/m^3 or 4.09 MWh/m^3.

5.4.2 Production

> "Ammonia is the most produced chemical worldwide and its production is based on a well-known and efficient technology. Moreover, ammonia is widely distributed, due to its utilization as fertilizer in agriculture and a logistic network is already present. Those aspects, along with a high energy density and a carbon free status, make ammonia a potential green and sustainable energy vector, especially if renewable energy is used to produce the basic chemicals (hydrogen and nitrogen) necessary for its synthesis" [58, p. 13583].

Ammonia can be produced through gasification from various sources including natural gas, oil and coal, or from waste heat and various renewable energy sources. As of 2019, natural gas and coal production stand for 72% and 22%, respectively, of worldwide ammonia production. Combining Carbon Capture and Storage (CCS) with ammonia production means that ammonia can be produced from fossil sources in an environmentally friendly way without CO_2-emissions. [103, 104]

There exists numerous different production processes in which ammonia is the end-product. The two most common ammonia production methods are the Haber-Bosch and Solid-State Ammonia Synthesis processes (SSAS) and their production routes are illustrated in fig. 41. These processes often use an air separation unit to deliver nitrogen from the air, but cryogenic (ie. very low temperature) air separation can also be utilised and is considered very effective and economical. [102, 103]

The Haber-Bosch synthesis process, in which ammonia is industrially formed from hydrogen and nitrogen, is considered highly efficient and retains 88% of the energy from the hydrogen molecules [105]. At temperature and pressure in the range of 350-600 °C and 100-350 bar, respectively, nitrogen and hydrogen are combined at a ratio of 1:3 in an exothermic process that results in ammonia. The net thermo-catalytic reaction then becomes as shown in eq. (18). [101, 102, 103, 108]

$$\frac{3}{2}\,H_2 + \frac{1}{2}\,N_2 \longrightarrow NH_3 + 45.2\,\mathrm{kJ/mol} \tag{18}$$

As mentioned, ammonia can also be produced using the Solid-State Ammonia Synthesis process, which is a solid-state electrochemical process driven by electricity and is considered more efficient than the Haber-Bosch method. A comparison of the two methods with respect to power consumption reveal that "[t]he Haber-Bosch combined with an electrolyser costs approximately 12,000 kWh/tonne-NH_3, where the required electricity for the SSAS process is 7000–8000 kWh/tonne-NH_3" [103, p. 98] [106]. In section 5.4.1 it was shown that ammonia has a theoretical hydrogen energy content of 5.87 kWh/kg-NH_3,

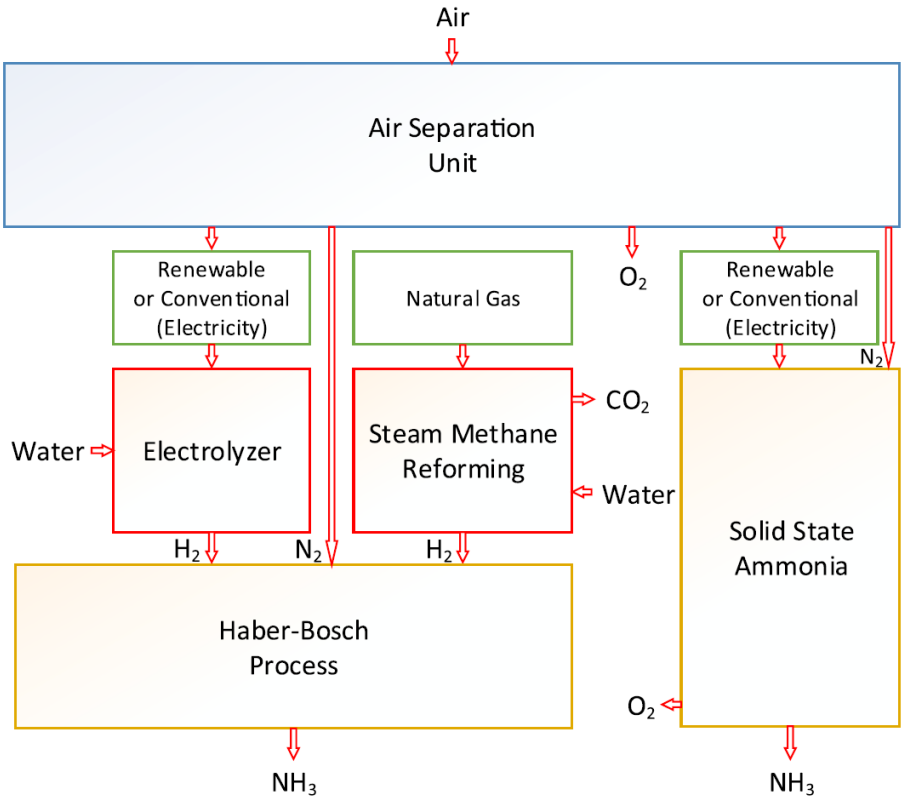

Figure 41: Production process flow for the Haber-Bosch and Solid-state ammonia synthesis processes with both conventional and renewable energy sources. Source: [103]

which translates to 5870 kWh/tonne-NH_3. The SSAS process then has an efficiency of 73.4% to 83.9%, while the Haber-Bosch method has an efficiency of just around 48.9%.

5.4.3 Storage

Ammonia is a viable alternative to hydrogen as a clean fuel source; in part because ammonia has several distinct advantages compared to hydrogen when it comes to storage considerations. From an economical standpoint, ammonia has only about one third of the costs associated with storage compared to hydrogen. This is due to ammonia's much higher melting and boiling point, which allows for significantly reduced storage requirements. While hydrogen often is compressed to a high pressure of 350 or around 700 bar, or cooled down to -253 °C to be stored in liquid form, ammonia can be stored in liquid form at room temperature at a modest pressure of 8 bar; or at -33 °C and a pressure of just 1 bar (atmospheric pressure). [70, 101, 103, 104]

"Moreover, the energy content of ammonia per unit of volume is comparable to that of gasoline which makes it a fuel attractive for transportation applications" [104, p. 459], and liquid ammonia contains approximately 70% more energy than liquid hydrogen for a given volume.

The physical properties of ammonia are equivalent to those of propane (C_3H_8), which allows for storage of ammonia as a liquid in inexpensive, low-pressure tanks [105].

5.4.4 Safety

Ammonia is considered to be a safe and efficient way to store hydrogen [103]. To be more specific,

> "[...] ammonia fuel has a narrow flammability range and therefore it is generally considered non-flammable when transported. If released into the atmosphere, ammonia's density is lighter than that of air and thus it dissipates rapidly. In addition, because of its characteristic smell the nose easily detects it in concentrations as low as ~5 ppm" [104, p. 459] (parts per million),

or even below 1 ppm [105]. Concentrations of ammonia in the air in the range from 25 to 100 ppm will induce noticeable irritation of the nose and throat [105]. For comparison, hydrogen is a gas without smell and taste [70]. Exposure to an ammonia concentration level of 300 ppm or above is considered "Dangerous to Life or Health" (IDLH) [106] and concentrations higher than 1000 ppm is extremely irritating an may lead to death if the exposure lasts more than a few minutes [105]. Nonetheless, ammonia has an excellent safety record in commercial applications, partly due to "[t]he wide range in concentrations between detectability and lethal effects [...]" [105, p. 1764].

Ammonia is toxic and harmful to living species, but becomes non-toxic after being processed by a reformer or a fuel cell. The aspect of toxicity is relevant in the case of tank leakage or spillage. It is possible to completely eliminate the the danger of toxicity if ammonia is embedded in metal amines, as it takes a temperature of at least 350 °C to release the ammonia from the porous media. The downside of this solution is that energy is required to release the ammonia from the amines, which increases costs. [104, 108]

5.4.5 Suitable Fuel Cells

Ammonia can be used as a fuel in PEM fuel cells if the ammonia is first reformed catalytically and separated into nitrogen and high purity hydrogen. The process of ammonia decomposition to nitrogen and hydrogen is endothermally driven at a temperature of 300-400 °C in a heat source with a catalyst prior to the PEM

fuel cell. The heat can be generated by combustion of a minor fraction of the generated hydrogen, and efficiencies of at least 97.0% have been reported [109]. For low-temperature fuel cells based on acidic membranes, like the PEMFC, directly fed ammonia is considered incompatible and degrade the membrane and catalyst even for ammonia concentrations as low as 1 ppm [110, 111] and 13 ppm [112], depending on sources. It is recommended that ammonia concentrations in hydrogen for PEM fuel cells have an upper bound of 0.1 ppm. Normal decomposition of ammonia at temperatures between 500 °C and 550 °C produce hydrogen with ammonia concentrations of about 1000 ppm. It is therefore very important to properly purify the hydrogen extracted from ammonia to be within acceptable concentration levels. [104, 106, 110, 111, 113]

Alternatively, "[a]mmonia can be used directly as a fuel in alkaline and solid oxide fuel-cells (SOFCs) [...]" [104, p. 460], in addition to direct ammonia solid electrolyte fuel cells and other high-temperature fuel cells without prior reforming and hydrogen purification. [13, 53, 58, 104, 106, 110, 113]

For SOFCs, ammonia can be made use of as a direct fuel in both proton conducting (SOFC-H) and oxygen anion conducting (SOFC-O) electrolyte based fuel cells. It is worth mentioning that the SOFC-O technology has 3 times the power density than SOFC-H. [13]

5.4.6 Reforming and hydrogen purification

Research from Japan shows that residual ammonia concentrations can be reduced from 1000 ppm to between 0.01 and 0.02 ppm by using an absorbent made of Li-exchange X-type zeolite (Li-X), as a processing step after conventional ammonia decomposition, to remove surplus ammonia from hydrogen. The extracted ammonia is then stored in the Li-X material, which can be recycled by heating the material to 400 °C. Li-X has a gravimetric adsorption capacity of 5.7 wt% of ammonia. Ammonia extracted with Li-X results in a hydrogen purity of at least 99.97%. [111]

Another pathway for ammonia decomposition to ultra-clean hydrogen is the use of Multi-Stage Fixed Bed Membrane Reactors (MSFBMR) with inter-stage heating. "A rigorous heterogeneous mathematical model [...]" [112, p. 2] show that this process achieves complete (100%) ammonia conversion, and therefore has a promising potential for high-purity hydrogen extraction from ammonia. [112]

Figure 42 illustrates the numerical results of ammonia decomposition to hydrogen with the MSFBMR process. As can be seen in the figure, each stage (bed 1–4) repeats the process with increasing levels and decreasing rates of ammonia to hydrogen conversion [112]. For reference, 40 kmol of hydrogen is equivalent to 80.6 kg of H_2, given an atomic weight of 1.00794 g/mol for a single hydrogen atom.

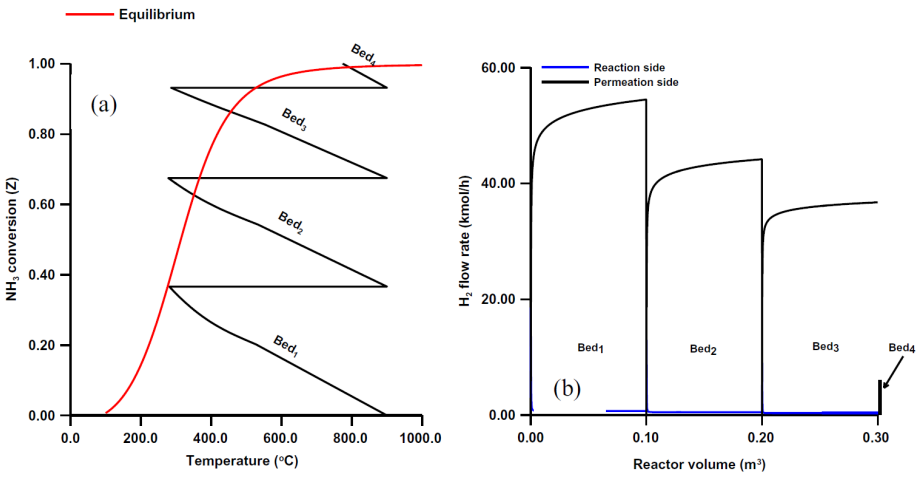

Figure 42: (a) The temperature levels of the successive stages of ammonia decomposition using a Multi-Stage Fixed Bed Membrane Reactor (MSFBMR) with inter-stage heating. The red line shows the amount of converted ammonia (NH_3). (b) The hydrogen (H_2) flow rates for each stage and the respective reactor volumes. Source: [112]

5.5 Methanol (CH_3OH)

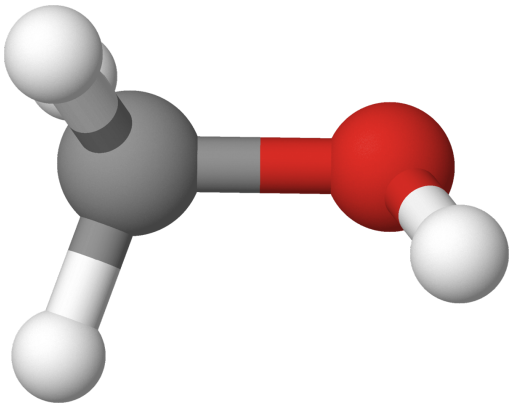

Figure 43: Molecular model of methanol. The grey and red sphere are carbon and oxygen atoms, respectively. The white spheres are hydrogen atoms. [114] (By: Johannes Botne; License: CC BY SA 3.0)

5.5.1 Chemical properties

Methanol is a simple oxygenated hydrocarbon, which means that it consists of oxygen, hydrogen and carbon atoms. Structurally, one methyl group (CH_3) is connected to a hydroxyl group (OH), as illustrated with the molecular model in fig. 43. Sometimes this molecule is abbreviated as MeOH, where Me is a reference to methanol's methyl group.

Methanol has a melting and boiling point of -97.8 °C and 64.8 °C, respectively, meaning that methanol is in a liquid state at room temperature. The density of methanol is 796 kg/m^3 and the Lower (LHV) and Higher Heating Value (HHV) is 20.094 MJ/kg and 22.884 MJ/kg, respectively. [71, 79, 114, 115]

5.5.2 Production

Methanol is one of the five most widely traded chemicals in the world and is used in a number of different consumer products from paints, LCD screens and pharmaceuticals. In the last few years, methanol has been increasingly used for energy applications, with an estimated yearly methanol fuel production of around 20 million tons. [79]

As a result of containing carbon, methanol "[...] does produce hydrocarbon emissions at a similar level to gasoline (albeit of different species) [...]" [79, p. 45]. There are, however, several alleviating factors to consider from an environmental perspective. Methanol consists of a single carbon molecule and has a combustion characteristic which results in lower emissions of Particulate Matter (PM) and nitrogen oxides compared to more complex hydrocarbon

fuels. Furthermore, methanol may be considered carbon neutral if produced with renewable energy and if the input carbon is sourced from aerial capture of CO_2, thus confining the carbon to a closed emission and production cycle as illustrated in fig. 44. [79]

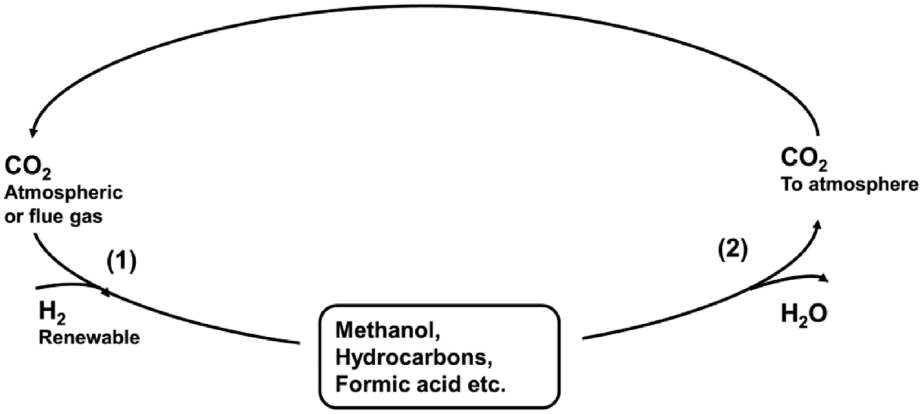

Figure 44: Overview of circular hydrocarbon carrier cycles. If CO_2 is extracted from the atmosphere for hydrocarbon production, then the cycle is closed without net Greenhouse Gas Emissions. Source: [80]

Traditionally, methanol has been made from fossil sources, including natural gas, coal and steam reformation, but the fuel can also be made from biogenic feedstocks and waste. Unlike (bio)ethanol (C_2H_5OH), methanol can be thermochemically made from any chemical compound containing carbon, and is therefore not restricted to slow biological processes and production pathways that also compete with food-producing agriculture land, as is the case for ethanol. Methanol can also be produced using electric energy from renewable energy sources and the necessary chemical compounds for synthesis can be harvested from the atmosphere. An electric production pathway in effect makes methanol an 'electrofuel' in the sense that electricity is converted and transported using a chemical medium, much like, for instance, hydrogen and ammonia. By this classification, methanol is the "[...] the simplest *liquid* electrofuel and an excellent hydrogen carrier" [79, p. 50], and is also the "[...] the cheapest liquid electrofuel that can be produced" [79, p. 51]. [79, 116]

The topic of fuel costs is up for debate and will be further discussed in section 5.7.

The multi-step production process of methanol is as follows. The first step is the production of synthesis gas, also called syngas, which is a mixture of H_2, CO, and CO_2. The syngas can be produced through reforming of natural gas or from other fossil or renewable materials. The second step is then conversion of the synthesis gas to methanol. It is estimated that the efficiency of these steps is in the order of 75%. Methanol is a polar molecule, like water, and can

even absorb water from the atmosphere. Consequently a third step of methanol distillation is required to remove the water content and produce high grade methanol. When atmospheric CO_2 and renewable hydrogen are used as input materials, the chemical reaction is as shown in eq. (19), and it is clear from this equation that one mole of water is produced for each mole of methanol. The reaction is exothermic, which means that the process releases thermal energy. [79, 116, 117]

$$CO_2 + 3\,H_2 \longleftrightarrow CH_3OH + H_2O - \text{Heat}\left(50\frac{\text{kJ}}{\text{mol}}\right) \tag{19}$$

The maximum theoretical efficiency for electricity-to-methanol is 74%. This efficiency can be improved to 79% by reusing the "waste" heat in a high-temperature electrolysis process. Further improvements to an efficiency of 84% can be attained by reducing CO_2 to CO by co-electrolysis — although some of this improved efficiency must be sacrificed for CO_2-separation. [117]

"Methanol is favorable due to its ready availability, high-specific energy and storage transportation convenience [...]" [5, p. 944], and is a very promising alternative to hydrogen [5].

5.5.3 Storage

Methanol is in a liquid state at Standard Temperature and Pressure (STP), unlike hydrogen and ammonia, since the fuel is in a liquid state for temperatures in the range of -97.8 °C to 64.8 °C. This allows for easy storage, transportation and efficient production without a need for energy demanding liquefaction or gas compression. [79]

Methanol has several advantages compared to hydrogen. More specifically, methanol has a higher energy density compared with hydrogen and is safer and easier to handle with respect to storage and transportation. This makes methanol a "[...] very suitable, abundant and economical fuel nowadays for different applications" [42, p. 1].

Figure 45 shows a comparison of methanol and different energy carriers with respect to volumetric energy density (kWh per litre) including and not including the volume of the storage tank itself. Methanol in a liquid state has an energy density of approximately 4.4 kWh per litre, while hydrogen at 700 bar pressure has approximately 1.3 kWh of energy per litre, when including the volume of the storage tank into the calculation [42]. Methanol also has the capacity, as a result of its hydrogen-dense molecular structure, to store 40% more hydrogen per unit of volume than liquid hydrogen (LH_2) [79], without requiring energy input for compression or liquefaction. It is worth noting that the above-mentioned figure depicts the energy content of the fuels themselves without taking into account the redox efficiency of the fuel cells and therefore also the usable electric energy

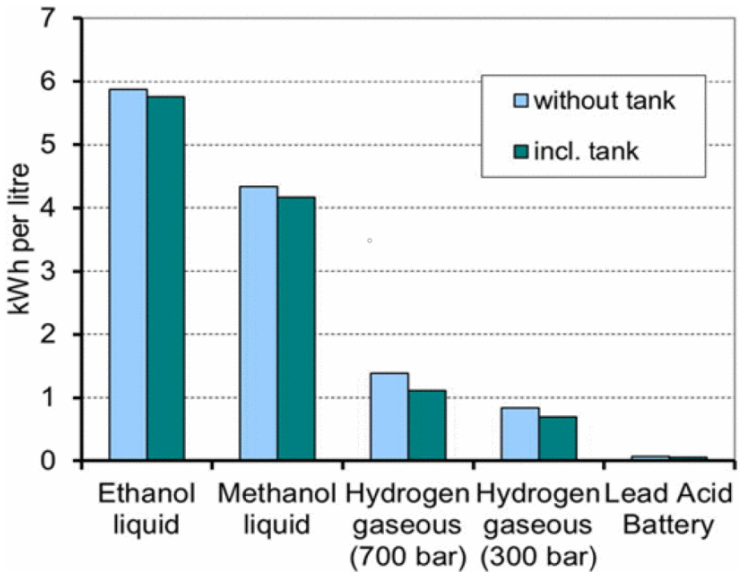

Figure 45: Comparison of different fuels and lead acid battery with respect to volumetric energy density. Source: [42]

output of the fuels. A more comprehensive energy density assessment will take place in section 5.6 and 6.2.

5.5.4 Safety

Methanol is considered a dangerous and toxic agent, but that is also true for all fuels that can be used as a substitute for gasoline and diesel. Both alcohols in general and methanol specifically are toxic for skin and eye contact, inhalation and ingestion. The human body can metabolise small amounts of methanol (CH_3OH), but an overloaded digestive system results in high concentrations of formaldehyde (HCHO) and formic acid (HCOOH), both toxic intermediate products in the chemical reaction pathway as shown in eq. (20). A fatal dose is in the range of 1 to 2 ml of methanol per kg of body weight. [79, 116]

$$CH_3OH \longrightarrow HCHO \longrightarrow HCOOH \longrightarrow CO_2 + H_2O \tag{20}$$

> "Symptoms of acute methanol poisoning from direct ingestion include dizziness, nausea, respiratory problems, coma and finally death. However, the process takes between 10 and 48 hours after ingestion and the cure is well understood, consisting of intravenous administration of ethanol, which the body preferentially metabolizes while the methanol is ejected. Accidental ingestion of methanol or ethanol can be avoided by appropriate design of fuel dispensing systems and by making the fuel completely unpalatable to human taste through

> additives such as denatonium benzoate [...]. Skin or eye contact with methanol, as well as inhalation of methanol vapours are generally of much lower concern, as long as it does not persist for hours" [79, p. 51].

Methanol has a flammability index close to diesel, but produce flames that are almost invisible in sunlight. The flames can be made more visible with additives. The polar nature of methanol molecules gives the compound high miscibility with water, allowing water to effectively extinguish methanol fires. [79]

In case of spilling, methanol is biodegradable on a timescale of a few days and any spills will therefore mostly self-clean, leading to the inference that light alcohols, such as methanol, are "[...] attractive as marine fuels, since any spill quickly disperses due to their infinite solubility in water, and then biodegrades simply" [79, p. 52] and so fast that "[...] dangerous concentrations are never reached" [79, p. 76]. This is in sharp contrast to more complex hydrocarbons, which give rise to significant consequences in the event of a marine fuel spillage. [79, 116]

5.5.5 Suitable Fuel Cells

Methanol can be used directly in a Direct Methanol Fuel Cell (DMFC) or a Solid Oxide Fuel Cell (SOFC), or reformed to hydrogen locally/on-board and then used in any low or high-temperature fuel cell that can run on hydrogen. [79]

In a reformer, heat causes the decomposition of methanol to hydrogen (H_2), carbon monoxide (CO) and carbon dioxide (CO_2). The hydrogen, and potentially carbon monoxide, can then be used either directly in a fuel cell or stored in a buffer tank for later utilisation or handling. Catalytic reforming of methanol can be executed at temperatures above 200 °C. [79, 108]

As a reminder, carbon monoxide can only be used as fuel in high-temperature fuel cells that are not susceptible to carbon poisoning. Low-temperature fuel cells like the PEMFC are, however, very susceptible to catalyst poisoning by carbon and therefore require an additional step after reformation to purify the hydrogen. Carbon monoxide concentrations even as low as 5 to 10 ppm are sufficient to "[...] severely poison the active sites of the platinum catalyst at the anode, resulting in transient cell potential oscillations and a profound drop in the overall efficiency of the PEM fuel cell (Oetjen et al., 1996; Farrell et al., 2007)" [112, p. 2].

The hydrogen purification process consumes energy in the order of 2 to 4 kWh per delivered kilo of hydrogen [80], which is equivalent to a conversion loss of 6.0% to 12.0% of the input hydrogen energy, since hydrogen has a lower heating value of $33.\overline{33}$ kWh/kg.

As mentioned in section 2.2.1, the PACF/HT-PEMFC is less susceptible to CO-degradation than the LT-PEMFC and can tolerate around up to 3% carbon monoxide gas without degrading. Since the CO content of methanol reformate gas is less than 3%, hydrogen purification is not necessary for the PAFC/HT-PEMFC. On the other hand, the PAFC/HT-PEMFC has a lower efficiency than the LT-PEMFC.

With reference to the section on Compatible energy carriers; Internal and external fuel reforming on page 30, methanol can be directly fed to a Solid Oxide Fuel Cell for temperatures as high as 1000 °C. However, carbon formation and deposition can occur at lower temperatures, effectively encapsulating the catalyst surface and reducing its activity. Consequently, for fuel temperatures of 700 to 975 °C, "[...] methanol must be firstly converted to methane and other small molecular weight products in the [external] catalytic reformer (IIR)" [5, p. 949]. The carbon formation side effect can be circumvented by means of sufficient space volume at the entrance of the anode chamber where methanol is homogeneously converted to CH_4, CO, CO_2, and H_2 before reaching SOFC anode" [5, p. 951], and thus allowing for direct feeding of methanol to SOFCs. [5, 118]

5.6 Comparison of storage requirements for energy carriers

5.6.1 Hydrogen storage density

Figure 46 shows the absolute hydrogen density of various fuels and compares them with liquid hydrogen. As can be seen in the figure, all the listed fuels have around 35% to 70% more hydrogen per volume than liquid hydrogen, and ammonia is the most hydrogen dense fuel.

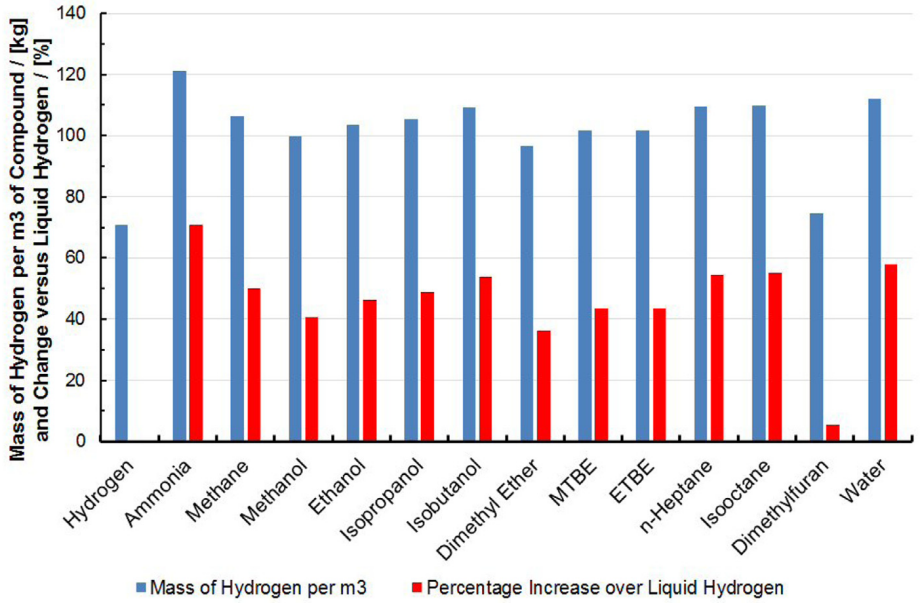

Figure 46: A comparison of the hydrogen density in various fuel compounds, in terms of kg/m^3 and relative concentration [%] for each compound compared with liquid hydrogen (LH_2). All the fuels are considered in their liquid state. MTBE and ETBE stand for Methyl Tert-Butyl Ether ($(CH_3)_3COCH_3$) and Ethyl Tert-Butyl Ether ($C_6H_{14}O$), respectively. Source: [79]

5.6.2 Energy storage density

Figure 47 shows the minimum amount of theoretical hydrogen energy that is stored in different energy carriers. The numbers are based on the gravimetric density of each fuel [kg/m^3], their respective hydrogen storage mass fractions [wt.%] and the lower heating value of hydrogen. The values do not take into account energy losses occurring during reforming, purification or conversion to electric power in fuel cells. An analysis that takes into consideration these conversion losses will take place in section 6.2 Total electrical energy density.

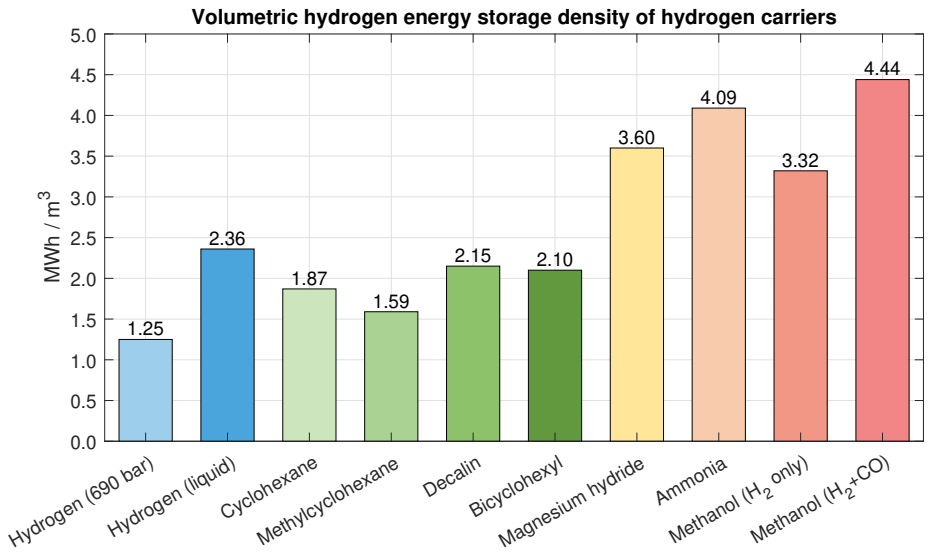

Figure 47: Hydrogen energy storage capacity of different energy carriers. Based on the calculations shown in appendix A.

As a baseline, hydrogen compressed at 690 bar pressure can store 1.25 MWh/m^3 of hydrogen energy and liquid hydrogen can store 2.36 MWh/m^3.

Methanol has two application pathways that are very different in terms of energy content, and has therefore been split into two separate columns. Methanol can be fed directly to a Solid Oxide Fuel Cell, and is in this case more of a complete fuel than a hydrogen carrier. Therefore, the rightmost methanol column gives the energy content of methanol when considering the molecule's complete lower heating value for such use. In other words, the energy content of both the carbon monoxide and the hydrogen is accounted for. The leftmost methanol column, on the other hand, only accounts for the energy content of the hydrogen embodied in the methanol molecules, as this is a more relevant perspective for low-temperature fuel cell applications like the PEMFC and PAFC.

LOHCs

As can be further observed in fig. 47, the LOHCs (green shades) have higher hydrogen energy concentrations than pure hydrogen compressed at 690 bar pressure, but also less hydrogen energy per volume than liquid hydrogen. The LOHCs cyclohexane, methylcyclohexane, decalin and bicyclohexyl can reversibly store and release 1.87 MWh/m^3, 1.59 MWh/m^3, 2.15 MWh/m^3 and 2.10 MWh/m^3 worth of hydrogen, respectively. These energy densities are in the range of 27% to 68% higher than compressed hydrogen at 690 bar and 9% to 33% less than liquid hydrogen. Regardless of the energy density disadvantage compared to liquid hydrogen, liquid hydrogen loses a lot of energy for liquefaction and need cryogenic temperatures for storage, which LOHCs do not. Liquid Organic Hy-

drogen Carriers do, however, need energy for hydrogen purification if supplied to PEMFCs, giving an additional 6% to 12% energy loss to the system efficiency. LOHC purification losses are not calculated for in fig. 47, but will be analysed more closely in section 6.2.

Metal hydrides

The metal hydride with the highest volumetric hydrogen energy density is magnesium hydride (MgH_2) with 3.60 MWh/m^3. This gives magnesium hydride an energy density that is 188% higher than hydrogen compressed at 690 bar, and 52% higher than liquid hydrogen.

Ammonia

Figure 47 also shows that both ammonia and methanol markedly outperform hydrogen with respect to volumetric energy storage density. Ammonia, with more hydrogen atoms per molecule than hydrogen itself, can store 4.09 MWh/m^3 of hydrogen energy, which is 228% more energy dense than compressed hydrogen (690 bar) and 73% more than liquid hydrogen. Ammonia is therefore an excellent hydrogen carrier and also has the advantage of much more moderate requirements for compression, liquefaction and storage than pure hydrogen molecules, as described in section 5.4.3 on page 69.

Methanol

When considering only the hydrogen energy content of methanol, then methanol has an energy storage density of 3.32 MWh/m^3, 165% more than compressed hydrogen at 690 bar and 41% more than liquid hydrogen. Nonetheless, methanol has a lower hydrogen energy density than ammonia, and is therefore from a storage consideration less beneficial than ammonia for low-temperature fuel cells like the PEMFC. On the other hand, if a high-temperature fuel cell like the SOFC is deployed, methanol surpasses ammonia with respect to energy density since more of the molecular energy of methanol can be employed for electric power generation. Fully combustible methanol has a total energy density (lower heating value) of 4.44 MWh/m^3, 255% more than compressed hydrogen (690 bar) and 88% more than liquid hydrogen. Methanol also has the advantage as an electrofuel of having a liquid state in room temperature and at atmospheric pressure, which ammonia and hydrogen do not. Methanol is for these reasons a better choice than ammonia for high-temperature fuel cells from a purely storage-technical perspective.

5.7 Cost analysis: Power-to-tank

Presented in fig. 48 is a complete power-to-tank cost analysis and comparison of the energy carriers Hydrogen (H_2), Ammonia (NH_3) and Methanol (CH_3OH) based on carbon-neutral pathways and renewable electricity. In other words,

the figure takes into account the complete respective costs of environmentally friendly production of each fuel and transferring the products to storage tanks in what can also be termed power-to-tank costs.

An American cost analysis [31] include the costs of: hydrogen production and storage; capital costs for synthesis plants for ammonia and methanol; nitrogen and carbon dioxide air separation and extraction; long-distance fuel transportation; local distribution; and refueling of storage tanks from fuel storage stations.

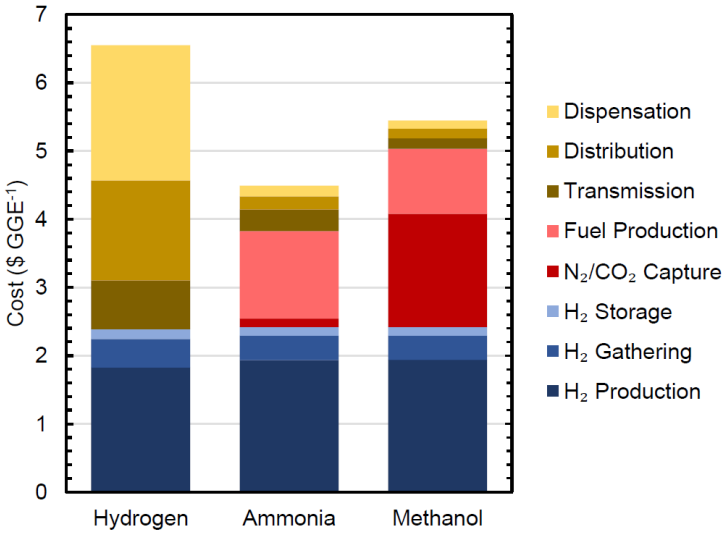

Figure 48: Power-to-tank cost comparison for the energy carriers hydrogen, ammonia and methanol. Gasoline Gallon Equivalent (GGE) is the energy in a gallon of gasoline, which amounts to 33.41 kWh/gallon or 8.83 kWh/litre [119, 120, 121, 122]. Source: [31]

The quantified power-to-tank costs for each fuel is 6.55 USD/GGE for hydrogen, 4.50 USD/GGE for ammonia and 5.46 USD/GGE for methanol [31], where a Gasoline Gallon Equivalent (GGE) is the energy in a gallon of gasoline, which amounts to 33.41 kWh/gallon or 8.83 kWh/litre [119, 120, 121, 122]. These specific fuel costs are therefore equivalent to 196.05 USD/MWh for hydrogen, 134.69 USD/MWh for ammonia and 163.42 USD/MWh for methanol. Based on these costs, ammonia and methanol cost approximately 31% and 17% less, respectively, to produce, transport and refuel than compressed hydrogen.

The relatively high cost of hydrogen production is attributed "[...] to high transmission, distribution, and dispensation costs (totalling \$4.16 GGE^{-1} as a compressed gas" [31, p. 2478]. Further, ammonia has a lower specific cost than methanol due to the high cost associated with extracting carbon dioxide from air [31].

A German fuel cost study estimated the well-to-tank, or power-to-tank, re-

newable production costs of hydrogen (H_2, 700 bar) and methanol (CH_3OH or MeOH) to be 0.047 EUR/MJ and 0.056 EUR/MJ [123], respectively, but did not calculate the cost of ammonia. This is equivalent to 169.2 EUR/MWh for hydrogen and 201.6 EUR/MWh for methanol. In this study, the cost of methanol production is therefore 19% higher than for hydrogen.

A Swedish study that reviewed several articles on energy carrier production costs found that the cost of hydrogen is in the range of 48 EUR/MWh to 157 EUR/MWh, and the cost range for methanol is between 79 EUR/MWh and 179 EUR/MWh [124]. However, the study further concludes that "[...] the range in the estimates is broad, partly due to the variations in the assumptions used in the studies" [124, p. 1877].

A master's thesis completed at NTNU in 2019 by M. Runnerstrøm on wind powered hydrogen production at Fosen in Norway estimates the hydrogen production cost to be from 28.22 NOK/kg to 31.51 NOK/kg, equivalent to about 850 to 950 NOK/MWh, depending on the type of electrolyser used for production [75]. These values are the break-even *costs* of production without margin for profit. The hydrogen market *price* will therefore be higher when accounting for profit margin, taxes, marketing, etc.

From the above-mentioned studies, it is clear that the production cost of hydrogen containing fuels depend significantly on regional and local production cost levels.

Since the production of both hydrogen, ammonia and methanol are based on hydrogen production, the *total cost* of the individual fuels correlate significantly with the cost of hydrogen electrolysis [31], and therefore also the cost of electricity. This also implies that the *cost difference* between the fuels "[...] is mostly insensitive to the cost of hydrogen production and storage" [31, p. 2476]. In fig. 48 it can be observed that the electrolysis costs ("H_2 Production") is approximately 2 USD/GGE, which is in the order of 30% to 45% of the total fuel costs for each fuel listed in the figure.

A cost comparison summary for the energy carriers is presented in fig. 49. The summary shows that hydrogen and ammonia, on average, is cheaper than methanol. This is contrast to the American study, where both ammonia and methanol are lower cost options to hydrogen. Either way, the range between minimum and maximum energy carrier costs is wide, so the values should be considered indicative rather than conclusive.

	Energy carrier	Studies/reports: American	German	Swedish: Lower bound	Swedish: Upper bound	Norwegian: Lower bound	Norwegian: Upper bound
Local currency	Hydrogen	196,05 USD/MWh	169,2 EUR/MWh	48,0 EUR/MWh	157,0 EUR/MWh	850 NOK/MWh	950 NOK/MWh
	Ammonia	134,69 USD/MWh					
	Methanol	163,42 USD/MWh	201,6 EUR/MWh	79,0 EUR/MWh	179,0 EUR/MWh		
NOK	Hydrogen	1841 NOK/MWh	1797 NOK/MWh	510 NOK/MWh	1667 NOK/MWh	850 NOK/MWh	950 NOK/MWh
	Ammonia	1265 NOK/MWh					
	Methanol	1535 NOK/MWh	2141 NOK/MWh	839 NOK/MWh	1901 NOK/MWh		
EUR	Hydrogen	172,5 EUR/MWh	169,2 EUR/MWh	48,0 EUR/MWh	157,0 EUR/MWh	80,0 EUR/MWh	89,5 EUR/MWh
	Ammonia	118,5 EUR/MWh					
	Methanol	143,8 EUR/MWh	201,6 EUR/MWh	79,0 EUR/MWh	179,0 EUR/MWh		

	Min.	Max.	Average
Hydrogen	510 NOK/MWh	1841 NOK/MWh	1269 NOK/MWh
Ammonia	1265 NOK/MWh	1265 NOK/MWh	1265 NOK/MWh
Methanol	839 NOK/MWh	2141 NOK/MWh	1604 NOK/MWh
Hydrogen	48,0 EUR/MWh	172,5 EUR/MWh	119,4 EUR/MWh
Ammonia	118,5 EUR/MWh	118,5 EUR/MWh	118,5 EUR/MWh
Methanol	79,0 EUR/MWh	201,6 EUR/MWh	150,9 EUR/MWh

Exchange rates	USD in NOK	9,39
	EUR in NOK	10,62
	USD in EUR	0,88

as of 2020-07-07

Figure 49: Cost comparison summary of hydrogen, ammonia and methanol. Sources: [31, 75, 123, 124]

6 System analysis: Fuel cells and energy carriers

This section aggregates and summarises data for the fuel cells and energy carriers presented in Fuel Cell Technologies and Energy Carriers for Fuel Cells.

6.1 Total electrical power-to-power efficiency

6.1.1 Production steps

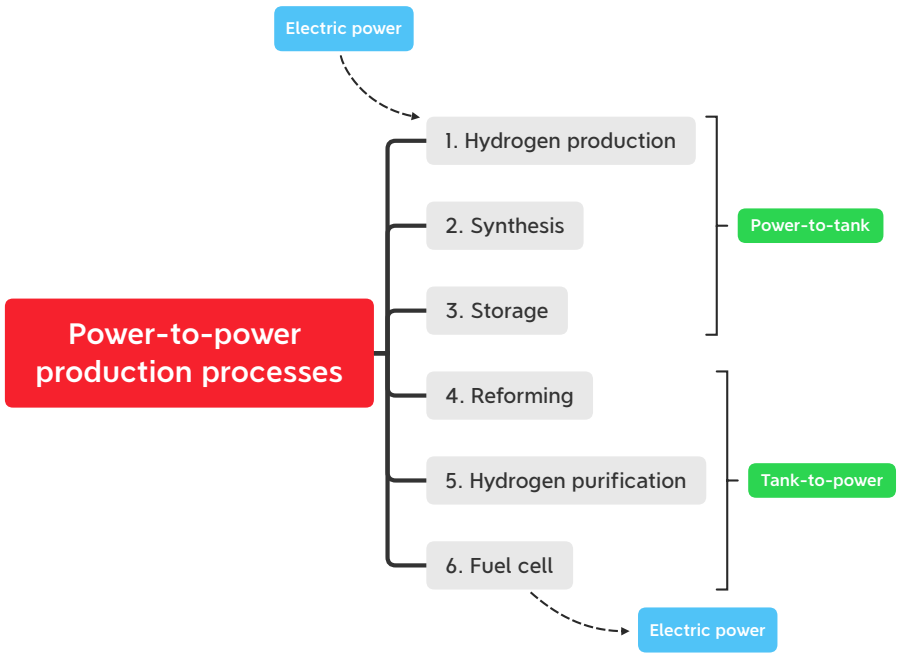

Figure 50: The power-to-power productions steps involved in energy carrier production and later conversion to electric power in a fuel cell.

The total electrical power-to-power efficiency of various combinations of fuels and fuel cells is calculated based on the efficiencies of several processing steps, as shown in fig. 50. The necessary processing steps depend on a case-to-case basis on the different energy carrier and fuel cell combinations.

Power-to-tank

The first step is the production of hydrogen by electrolysis, with an efficiency of approximately 60%.

For the other fuels, a second step is required to synthesise hydrogen with other chemical elements to form the more complex molecules that function as hydrogen carriers. The synthesis process has an efficiency of approximately 67%

for Metal hydrides, 79% for Methanol (CH_3OH), 84% for Ammonia (NH_3) and 98% for Liquid Organic Hydrogen Carriers (LOHCs).

Liquid Organic Hydrogen Carriers and methanol are in a liquid state at room temperature and therefore do not require any significant energy input for storage. In contrast, hydrogen and ammonia need to be either compressed or cooled down for storage. The storage efficiency is 91%, 70% and 98% for compressed hydrogen, liquid hydrogen and ammonia, respectively.

Tank-to-power

Depending on the combination of energy carrier and fuel cell, a hydrogen extraction reforming step is necessary before the fuels are delivered from the storage tank to the fuel cells. Usually this step has an efficiency in the order of 95% to 98%. For metal hydrides, the efficiency of this step is as low as 67.3%, as discussed in section 5.3.6. LOHC, ammonia and methanol distributed to LT-PEMFCs also need hydrogen purification after the reforming process to avoid catalyst contamination. Purification efficiencies are 91% for ammonia and methanol, and 94% for LOHC. The respective reforming and purification efficiency values are included in fig. 51 for the fuel cell – energy carrier combinations that require these processing steps.

The final electrical power production step is the chemical to electrical energy conversion that takes place in the fuel cells. With the exception of the Direct Methanol Fuel Cell (DMFC), which has an efficiency of only 35%, the selected fuel cells in fig. 51 have peak efficiencies in the range of 50% to 67%.

6.1.2 Total efficiency

Metal hydrides and the combination of methanol and a direct methanol fuel cell have the lowest total power-to-power efficiency of around 16.3% to 17.7%, and are therefore not recommended solutions based on an energy efficiency assessment. For all the other combinations listed in fig. 51, the total efficiency is between 22.5% for the combination of methanol and PAFC/HT-PEMFC to 37.5% for paring LOHCs with a SOFC stack.

The total efficiency for liquid hydrogen is relatively low because of the high energy requirements for cryogenic (extremely low temperature) liquefaction.

Ammonia and methanol have mid-range total efficiencies that mostly fall between compressed and liquid hydrogen in terms of power-to-power efficiency, but this depends a lot on the choice of fuel cell.

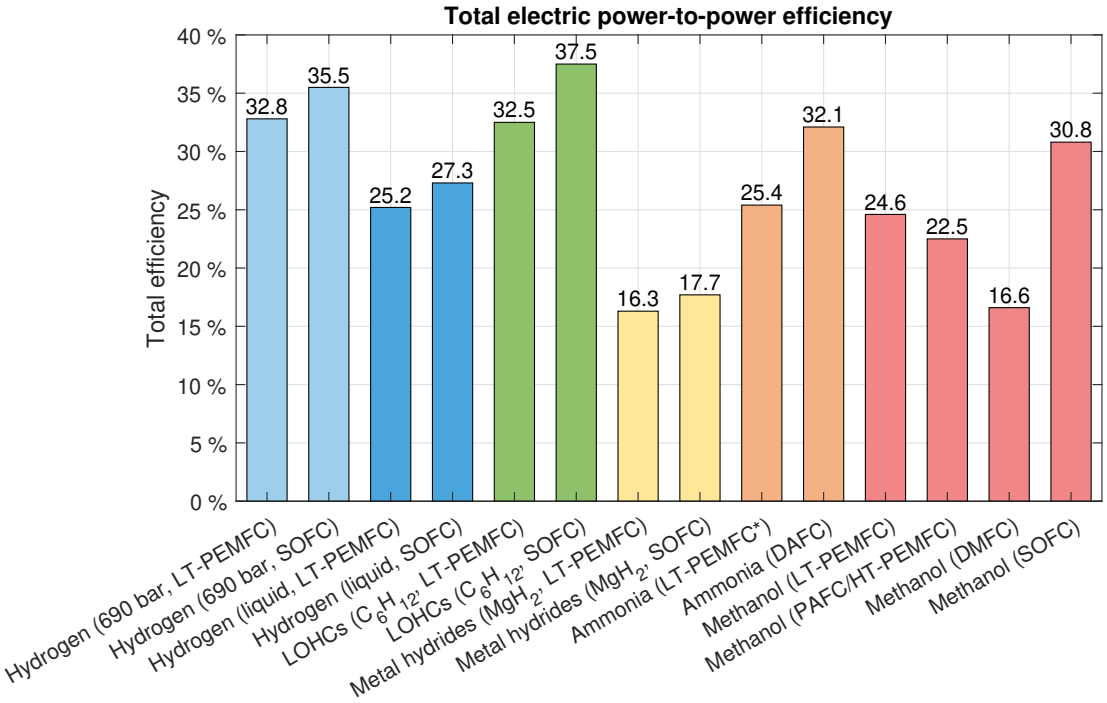

Figure 51: Life cycle power-to-power fuel efficiency analysis for combinations of fuels and fuel cells. The total efficiency takes into account the efficiency of hydrogen production, fuel synthesis[1], storage[2], reforming[1] and hydrogen purification[3] as well as the efficiency of the different fuel cells. *The storage efficiency of ammonia has been estimated to 95%; The efficiency of ammonia purification for PEMFC has been set to 91% based on the purification efficiency of methanol. The calculations for the graph can be found in appendix B.

[1]Only applicable for Liquid Organic Hydrogen Carriers (LOHCs), Metal hydrides, Ammonia (NH_3) and Methanol (CH_3OH).

[2]Only applicable for Hydrogen (H_2) and Ammonia (NH_3).

[3]Only applicable for Liquid Organic Hydrogen Carriers (LOHCs), Ammonia (NH_3) and Methanol (CH_3OH) in combination with Proton Exchange Membrane Fuel Cell (PEMFC), or for ammonia combined with Phosphoric Acid Fuel Cell (PAFC/HT-PEMFC).

6.2 Total electrical energy density

An important question when scaling a fuel cell-based electrical power production system is "How much electrical energy can be produced from a cubic metre of a given fuel when processed by a specific type of fuel cell?". Figure 52 essentially answers this question.

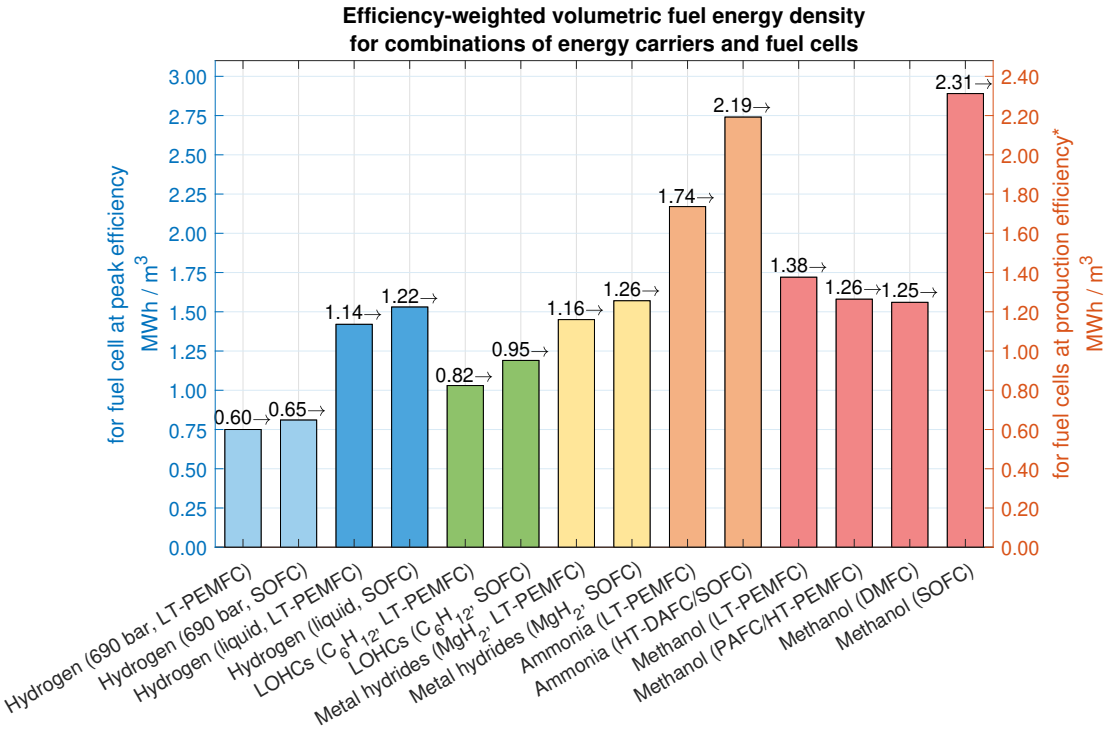

Figure 52: The expected electrical power production from a cubic metre (m^3) of various fuels adjusted for the tank-to-power efficiencies (see fig. 50), consisting of reformation, purification and fuel cell efficiencies. The left ordinate (y-axis) quantifies the energy density when the fuel cells operate at their peak efficiency (which for cells such as the PEMFC happens at low power output). The right ordinate quantifies the energy density when taking into account the fuel cell efficiencies that occur when the fuel cells operate at a wider range of power production output. The calculations for the graph can be found in appendix A and B. *The production efficiency has been set to 80% of peak efficiency.

The data in fig. 52 results from taking the volumetric hydrogen energy density of the various fuels, and subtracting for the efficiency losses that occur between the fuel storage tank and the power output from the fuel cells. These losses include the reforming, hydrogen purification and the electrical power production losses in the fuel cells. Note that only some of the fuel cell/fuel-combinations need reforming or purification.

The production efficiency of the fuel cells has been set to 80% of peak fuel cell efficiency, based on the data presented in section 7.4.3.

The data used for the calculations can be found in Appendix A and B.

The combination of methanol and SOFC is much higher than methanol with HT-PEMFC and DMFC, because the SOFC operates at temperatures high enough to utilise the energy content of the carbon in methanol. This allows for the Lower Heating Value of the whole methanol molecule to be used for power production instead of only the LHV of the hydrogen contained in the methanol compound.

Even though there are Liquid Organic Hydrogen Carriers with somewhat higher densities (+15%), Benzene / Cyclohexane has been chosen to represent the LOHCs in fig. 52, because this LOHC-pair has the highest energy density when only considering LOHCs that are liquid both in the hydrated and dehydrated state. This selection has limited impact on the results.

The reforming efficiency of methanol has been estimated to 95% and the post-reforming hydrogen purification of ammonia has been estimated to 91% based on the purification efficiency of methanol.

Axis scaling

The efficiency of fuel cells depends on the load factor (actual power output divided by rated power output) of the cells. To handle this complexity, fig. 52 has been equipped with two y-axes. The left y-axis is the appropriate scale for determining the post-fuel cell energy density of the listed energy carriers when the given fuel cells are operating at peak efficiency. Comparably, the right y-axis is the reference scale for the fuel energy density when considering the fuel cells operating at more realistic production load factors and efficiencies. For simplicity, the right y-axis has been scaled to 80% of the left y-axis. This is an estimate, based on the discussion in section 7.4.3, and should give a good indication of the electrical energy that can be produced by energy carriers employed in a more realistic production scenario. The value labels above the data columns refer to the right y-axis scale, but the height of each bar can be interpreted with both the left and right y-axis.

6.2.1 Performance discussion

In fig. 52 it can be seen that the volumetric energy density is the lowest for compressed Hydrogen (H_2) and Liquid Organic Hydrogen Carriers (LOHCs), with values ranging from 0.60 to 0.95 MWh/m^3 for the fuel cells, when operating at realistic production efficiency.

Due to the condensed nature of liquid hydrogen, this type of fuel has a fuel cell efficiency-weighted energy density of almost twice that of compressed hydrogen with densities between 1.14 MWh/m^3 and 1.22 MWh/m^3 for Proton

Exchange Membrane Fuel Cell (PEMFC) and Solid Oxide Fuel Cell (SOFC), respectively.

Figure 52 further shows that Ammonia (NH_3) and Methanol (CH_3OH) compare very well to hydrogen, LOHCs and metal hydrides when it comes to fuel energy density — especially if Proton Exchange Membrane Fuel Cell (PEMFC) or Solid Oxide Fuel Cell (SOFC) are considered. For LT-PEMFCs, ammonia and methanol have a fuel energy density of 1.74 MWh/m^3 and 1.38 MWh/m^3, respectively, which is 190% and 130% better than for compressed hydrogen. For Solid Oxide Fuel Cells, the fuel density of ammonia and methanol is even better with the energy densities being 2.19 MWh/m^3 and 2.31 MWh/m^3, vastly outperforming all the other alternatives in terms of electrical energy density.

By using a SOFC instead of a LT-PEMFC, the efficiency-weighted energy density of ammonia and methanol increases with 25.9% and 67.4%, respectively.

For ammonia, the rather large difference in energy density between the LT-PEMFC and DAFC is the result of a conglomerate of factors: Ammonia needs to go through reforming and hydrogen purification processes in order to be used in a PEMFC, but not for a DAFC or SOFC. Additionally, the DAFC has a higher efficiency.

As mentioned earlier, the reason for the high density of methanol in combination with SOFC, compared to HT-PEMFC, is that the carbon monoxide (CO), in addition to the hydrogen, in methanol also becomes a fuel at the high temperatures that exist in a SOFC. In other words, a larger part of the energy content of the molecule is utilised for power production and the effective energy density of the fuel is therefore higher.

For methanol it is interesting to compare the effect of combining the fuel with either LT-PEMFC or PAFC/HT-PEMFC, as the latter option doesn't require hydrogen purification of methanol, but has lower fuel cell efficiency. From fig. 52 it can be calculated that the LT-PEMFC gives about 9.5% more electrical energy output per cubic metre (m^3) of methanol, despite the energy cost required for hydrogen purification.

6.3 Energy carrier storage tank sizing

Figure 53 is effectively the inverse of fig. 52 and essentially answers the question of "How much fuel storage volume (m^3) is needed per unit of electrical energy (MWh) produced by a specific type of fuel cell?", and can be used to dimension fuel tanks if the energy requirements are known.

As in section 6.2, it is clear that ammonia significantly outperform hydrogen, LOHCs and metal hydrides. The storage volume requirements for Ammonia (NH_3) is only 35% compared to that of compressed hydrogen, 66% of liquid hydrogen, 47% of LOHCs and 67% compared to metal hydrides. Methanol (CH_3OH) also outperform the above-mentioned fuels, albeit to a lesser extent

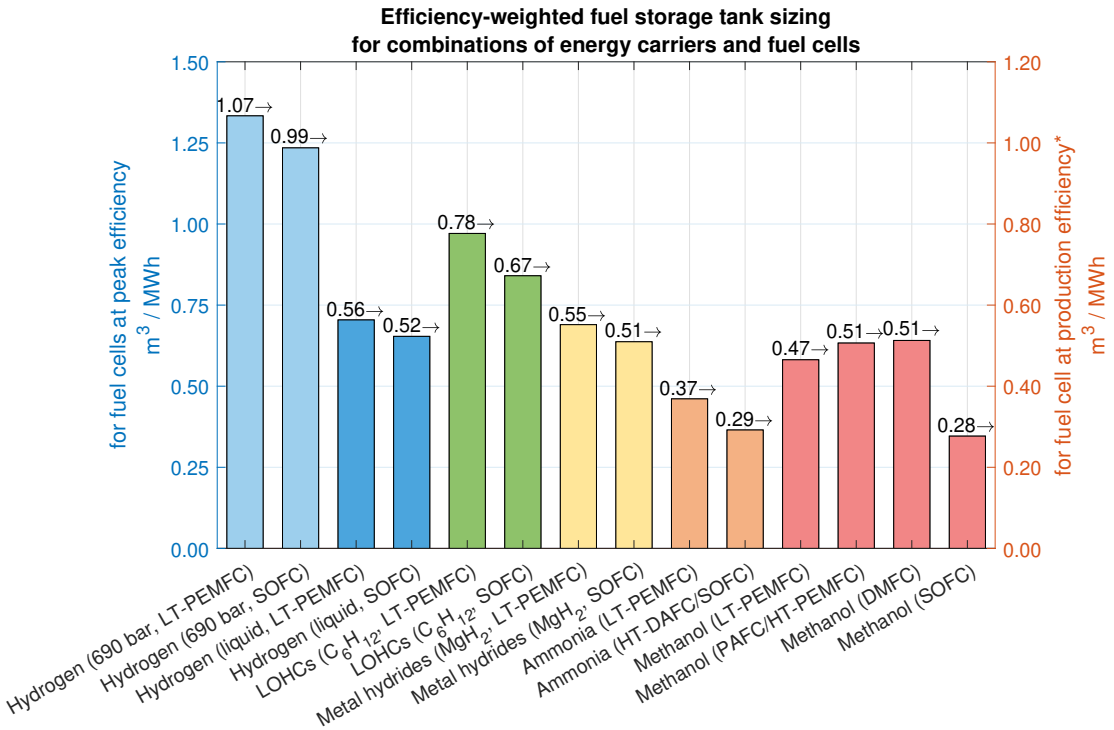

Figure 53: Inverse plot of fig. 52 to show the tank volume requirements per MWh of electrical power generated by the fuel cell. The data columns can be interpreted both with the left and right y-axis, depending on whether it is desired to analyse fuel storage requirements as a function of either peak or a more production realistic fuel cell efficiencies (80% of peak efficiency).

than ammonia for the PEM fuel cell.

Both ammonia and methanol perform very well in terms of tank-to-power efficiency-weighted energy density. Interestingly enough, ammonia is the best choice in terms of electrical energy density for the Proton Exchange Membrane Fuel Cell (PEMFC) and the Phosphoric Acid Fuel Cell (PAFC/HT-PEMFC), but methanol is the best choice for the Solid Oxide Fuel Cell (SOFC) — although with a margin of just around 5% (0.015 m^3/MWh) to ammonia.

6.4 Technology recommendations

Be advised that this thesis, and this section in particular, presents recommendations based on a technological analysis without considering economical factors like investment (CAPEX) and operation costs (OPEX) to any great extent. Decision makers are therefore advised to supplement this master's thesis with an economical analysis of the fuel cell and energy carrier recommendations presented herein.

In the technology selection matrix in fig. 54 on page 94 is a concise overview of important aspects worth considering when deciding on a combination of fuel cell and energy carrier. Since the matrix is quite information-dense, each technology combination has been colourised to provide better overview and make the information more accessible. The colour coding ranks the combinations based on performance and limiting properties, but does not consider costs.

Due to the feature complexity of the different technologies and possible technology combinations, it is not a straightforward task to select one single fuel cell–energy carrier combination as the "best" one, as all the possible combinations have one or more limitations and what can be considered the most optimal technology solutions will depend on the specific system application requirements. For instance, some system designs may be very volume critical, while others may prioritise efficiency, low system complexity, high power density, load transient following capabilities or might not be very limited by the requirements for hydrogen storage.

The low-temperature Direct Ammonia Fuel Cell (DAFC) may be a good choice for the future, in combination with ammonia as fuel, but is still considered to be in a development state and needs further research. Similarly, the Anion Exchange Membrane Fuel Cell (AEMFC) is a fuel cell that is gaining momentum in research, but has so far only showed low power densities and short lifetimes. In contrast, the Direct Methanol Fuel Cell (DMFC) does have an impressive durability, but falls short on power density and to some degree fuel efficiency, unless as part of a CHP system.

The Proton Exchange Membrane Fuel Cell (PEMFC), the high-temperature Direct Ammonia Fuel Cell (DAFC) and the Solid Oxide Fuel Cell (SOFC) are all mature technologies that perform very well in terms of power density and efficiency and are therefore all good choices for electrical power or combined heat and power (CHP) generation. CHP generation has the potential to drastically increase system efficiency, but comes at the cost of system complexity and capital costs.

Ammonia (NH_3) and Methanol (CH_3OH) perform very well in energy density, have acceptable values for total electrical power-to-power efficiency and are both much easier and safer to store in tanks than compressed or liquid hydrogen. Ammonia also has the added benefit of costing less than both hydrogen and methanol, at least according to the data presented in section 5.7, and is storable in liquid form at modest temperature and pressure requirements, while methanol has the advantage of being liquid at atmospheric pressure and room temperature. The high density of these fuels may be a very important technology selection factor for applications with considerable sailing time and distances between refueling or where the fuel tank volume is an important limiting factor. Larger vessels may also be better suited for the system complexity that ma-

terialises with fuel reforming and purification, high-temperature fuel cells and combined heat and power generation.

Good combinations of fuel cells and energy carriers are therefore the PEMFC or the HT-DAFC/SOFC with either ammonia or methanol. This is under the assumption that hydrogen of sufficiently high purity can be reformed and extracted from ammonia or methanol so that the catalyst surface of the PEMFCs is not contaminated with ammonia or carbon (monoxide). Another assumption is that methanol is produced in a carbon-neutral production-consumption cycle so that the energy carrier can be considered environmentally friendly.

The PAFC/HT-PEMFC can also be considered as a suitable fuel cell for methanol. This fuel cell type has a lower efficiency and power density than the LT-PEMFC, but higher carbon tolerance that circumvent the need for carbon-removing hydrogen purification of methanol, which can potentially reduce system complexity and costs.

Some applications may favour an electrical power production solution consisting of compressed or liquid hydrogen processed with the LT-PEMFC, as the LT-PEMFC is a very high-performance and simple to manage fuel cell technology, and pure hydrogen doesn't require post-storage processing. This especially applies to applications with short sailing distance between refueling, and where the tank volume and placement do not strain the system design to any considerable degree.

Technology Selection Matrix

	Hydrogen	LOHC	Metal hydrides	Ammonia	Methanol
LT-PEMFC	Low (gas) volumetric energy density High (liquid) volumetric energy density Demanding fuel storage High efficiency Very high power density Fast dynamic response Long lifetime	Medium volumetric energy density High efficiency Very high power density Fast dynamic response Requires dehydrogenation and hydrogen purification Long lifetime	High volumetric energy density High efficiency Fast transient response Very high power density Fast dynamic response Low power-to-power efficiency Requires dehydrogenation Long lifetime	Very high volumetric energy density High efficiency Fast transient response Very high power density Fast dynamic response Requires reforming and hydrogen purification Long lifetime	High volumetric energy density High efficiency Fast transient response Very high power density Fast dynamic response Requires reforming and hydrogen purification Long lifetime
PAFC/HT-PEMFC	Low (gas) volumetric energy density High (liquid) volumetric energy density Demanding fuel storage Medium efficiency and power density Long lifetime	Medium volumetric energy density Medium efficiency and power density Requires dehydrogenation Long lifetime	High volumetric energy density Medium efficiency and power density Low power-to-power efficiency Requires dehydrogenation Long lifetime	Very high volumetric energy density Medium efficiency and power density Requires reforming and hydrogen purification Long lifetime	High volumetric energy density Medium efficiency and power density Requires reforming Long lifetime
AEMFC	Low (gas) volumetric energy density High (liquid) volumetric energy density Demanding fuel storage Very short lifetime	Medium volumetric energy density Requires dehydrogenation Very short lifetime	High volumetric energy density Low power-to-power efficiency Requires dehydrogenation Very short lifetime	Very high volumetric energy density Very short lifetime	High volumetric energy density Very short lifetime
LT-DAFC	Low (gas) volumetric energy density High (liquid) volumetric energy density Demanding fuel storage High efficiency Medium power density Needs more research	Medium volumetric energy density High efficiency Medium power density Requires dehydrogenation Needs more research	High volumetric energy density High efficiency Medium power density Low power-to-power efficiency Requires dehydrogenation Needs more research	Very high volumetric energy density High efficiency Medium power density No reforming necessary Needs more research	High volumetric energy density High efficiency Medium power density Unknown compatibility Probably requires reforming Needs more research
DMFC	Low (gas) volumetric energy density High (liquid) volumetric energy density Demanding fuel storage Very low efficiency and power density Long lifetime	Medium volumetric energy density Very low efficiency and power density Requires dehydrogenation Long lifetime	High volumetric energy density Very low efficiency and power density Low power-to-power efficiency Requires dehydrogenation Long lifetime	Very high volumetric energy density Very low efficiency and power density Unknown compatibility Probably requires reforming Long lifetime	High volumetric energy density Very low efficiency and power density Low power-to-power efficiency Long lifetime
MCFC	Low (gas) volumetric energy density High (liquid) volumetric energy density Demanding fuel storage Very low power density Medium efficiency Very long lifetime	Medium volumetric energy density Very low power density Medium efficiency Requires dehydrogenation Very long lifetime	High volumetric energy density Very low power density Medium efficiency Low power-to-power efficiency Requires dehydrogenation Very long lifetime	Very high volumetric energy density Very low power density Medium efficiency Very long lifetime	High volumetric energy density Very low power density Medium efficiency Very long lifetime
SOFC	Low (gas) volumetric energy density High (liquid) volumetric energy density Demanding fuel storage High power density and efficiency Very high operating temperature Slow dynamic response Very long lifetime	Medium volumetric energy density High power density and efficiency Very high operating temperature Slow dynamic response Requires dehydrogenation Very long lifetime	High volumetric energy density High power density and efficiency Very high operating temperature Slow dynamic response Low power-to-power efficiency Requires dehydrogenation Very long lifetime	Very high volumetric energy density Very high efficiency High power density No reforming necessary Very high operating temperature Slow dynamic response Very long lifetime	Very high volumetric energy density Very high efficiency High power density No reforming necessary Very high operating temperature Slow dynamic response Very long lifetime

Figure 54: Overview of fuel cell–energy carrier combinations based on the most prominent technological aspects. Color codes: **green**: potentially good combination for certain applications; **yellow**: viable combination with some limitations; **orange**: possible combination, but several drawbacks; **red**: not recommended.

7 Case study: Service Operation Vessel

In this chapter, case study simulations are presented of a fuel cell powered Service Operation Vessel (SOV). The purpose of the case study is to investigate and exemplify the performance, effects and feasibility of implementing fuel cell technology in microgrids and maritime applications.

The Solid Oxide Fuel Cell (SOFC) has been chosen for the simulations as this type of fuel cell was one of the better fuel cell options, as discussed in chapter 6, and is readily compatible with high-density energy carriers such as Ammonia (NH_3) and Methanol (CH_3OH). Additionally, the SOFC is a high-temperature technology with a relatively slow dynamic response. This makes it possible to demonstrate the effectiveness of using fuel cells — even as slow as the SOFC — in an electric battery-supported, hybrid power production environment. The results will also indicate the recommended battery capacity required for a "worst-case" fuel cell, in terms of dynamic response capability.

7.1 Operational load demand profile

Kongsberg Maritime has kindly provided for this master's thesis a load profile based on real measurements for a Service Operation Vessel used to construct offshore wind turbines in the North Sea. The load profile consists of several distinct phases, which have been averaged and combined by Kongsberg Maritime to a daily load profile to keep proprietary information confidential, while still providing realistic values.

Figure 55 presents the load profile, which consists of the following successive stages: Harbour (300 kW); Standby (500 kW); Long Transit (3000 kW); and a Technical Operation-phase (≈1000 kW) that is repeated every 30 minutes during this period.

The repeating pattern of the Technical Operation-phase can be studied closer in fig. 56. The different Technical Operation phases are as follows: Acceleration (1000 kW); Transit (800 kW); Deceleration (1500 kW); Manoeuvring (1100 kW); Dynamic Positioning at turbine (900 kW); and some more Manoeuvring (1000 kW). Dynamic Positioning (DP) is a control concept that seeks to automatically maintain a vessel's position and heading at sea using propellers, thrusters and the rudder [125]. DP is used during turbine assembly.

Integrating the various phases of the load profile given above results in an electric power consumption of 23.0 MWh per day.

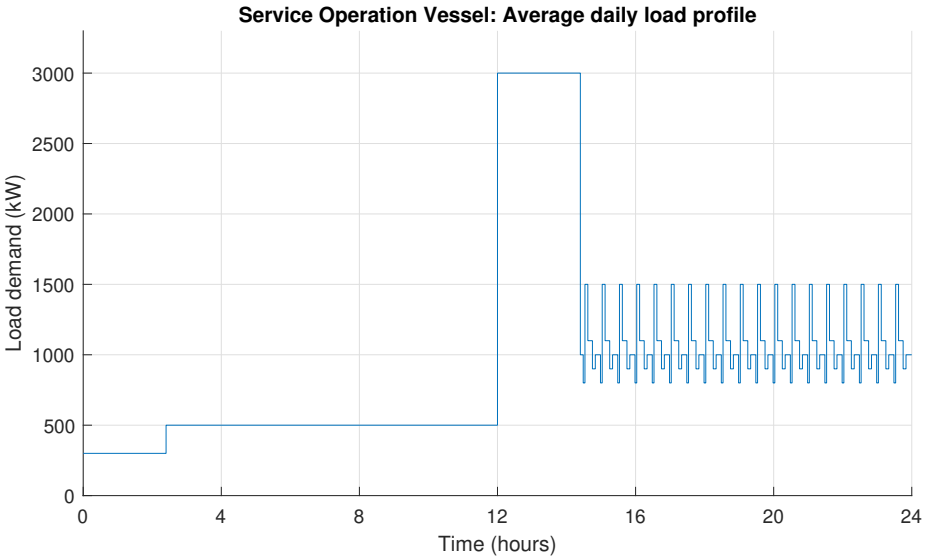

Figure 55: Average load profile of a Service Operation Vessel (SOV) deployed to assemble offshore wind turbines.

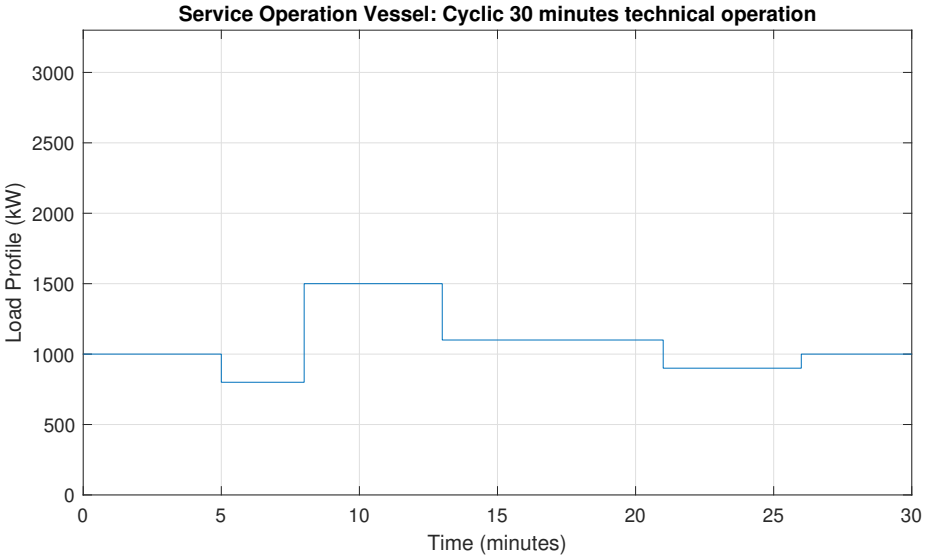

Figure 56: Zoomed in view of the 30 minutes repeating technical operation period of the load profile given in fig. 55.

7.2 Simulation model

7.2.1 Model evolution

Mark I

Initially, a very detailed simulation model was developed in Simulink for this master's thesis and the preceding project thesis [1] to model the dynamic nature of fuel cell stacks in a detailed electrical system for maritime vessels.

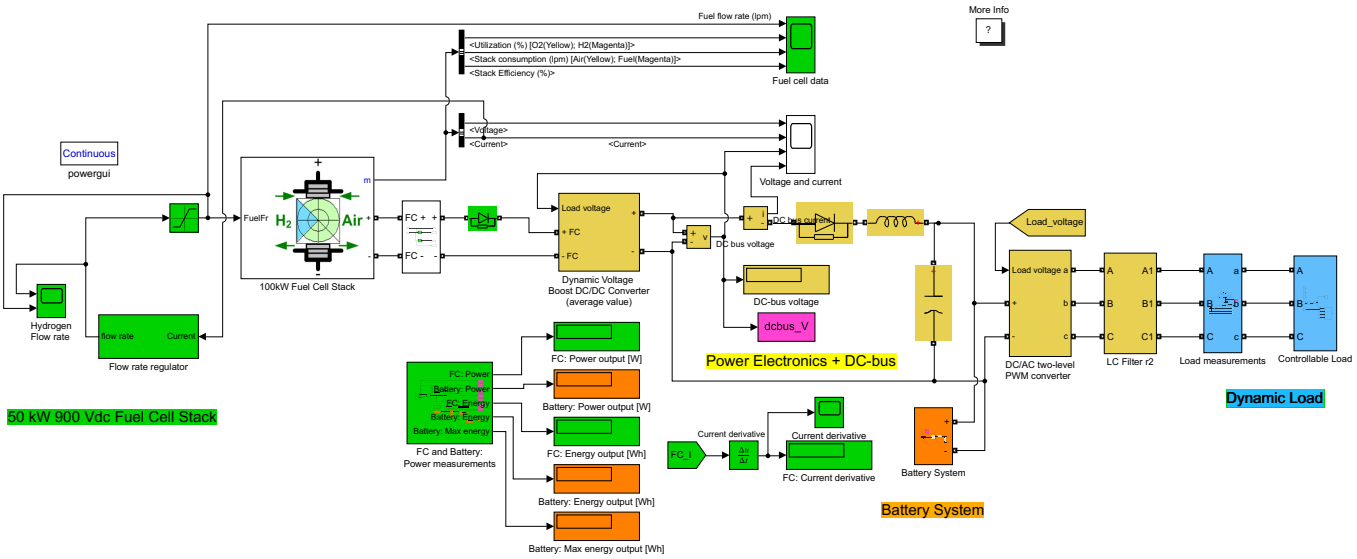

Figure 57: Mark I simulation model of a fuel cell integrated electrical system on board a maritime offshore vessel.

The model included the fuel cell stack, battery system, and ship propulsion. These components were further coupled by detailed models of power electronic converters (DC-DC boost and two-level DC-AC) that connected the fuel cells with the DC bus and the battery, and further to the 690 V AC-network that through voltage smoothing LC-filters sent power to the propulsion machinery of the ship, as presented in fig. 57. This level of detail meant that the Simulink-model was very demanding of computational power and needed around 3 minutes of computational time on a decent computer to simulate 5 seconds of simulation time — acceptable for simulations in the order of minutes, but too time-demanding to model a 24-hour load profile like the one given in section 7.1 (it would take more than a month to run one simulation). A new simulation model was therefore developed for this purpose.

Mark II

The Mark II simulation model has been specifically constructed for this master's

thesis using only the most essential components for a power flow analysis. These components consist of the fuel cell system, a battery system, a simplified DC-DC converter with average modelling and a controllable DC load that simulates load demand profiles. In addition, measuring devices and data collectors are included for component and system analysis. The simulation system can be observed in fig. 58.

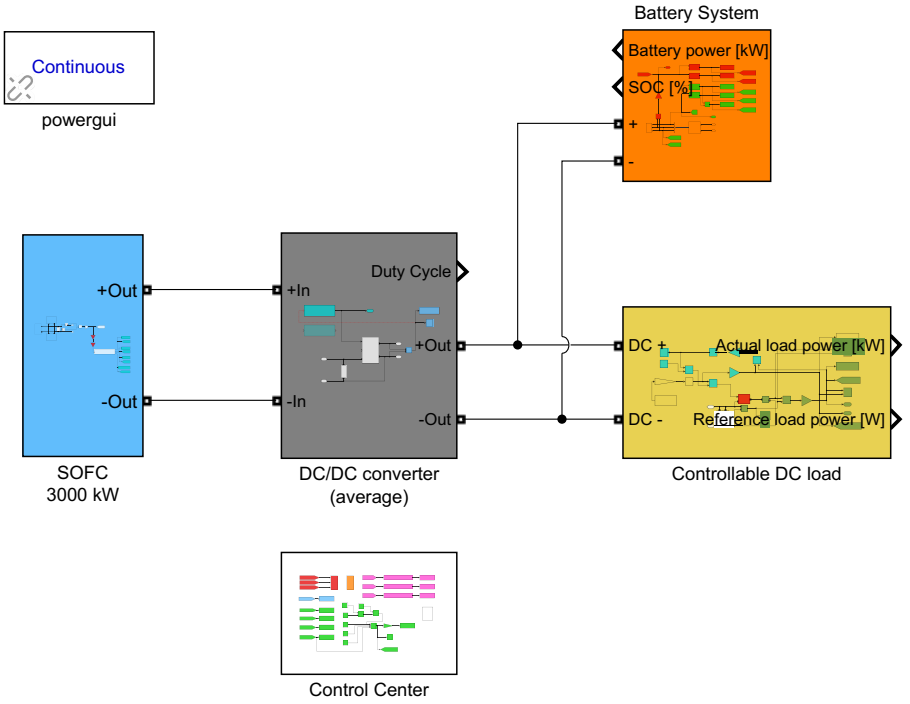

Figure 58: Mark II simulation model for power flow analysis of a fuel cell system on board a maritime offshore vessel.

This model is significantly faster than the Mark I-version and can simulate a 24-hour load profile in a matter of minutes. The loss of system complexity does not significantly reduce the data accuracy for long-duration power flow analysis, as such analyses do not need to simulate transients with milli- and microsecond accuracy. The removal of the two-level DC-AC converter excludes some losses of the system, but this is still mostly negligible as power electronics generally have very little losses.

7.2.2 Fuel cell system

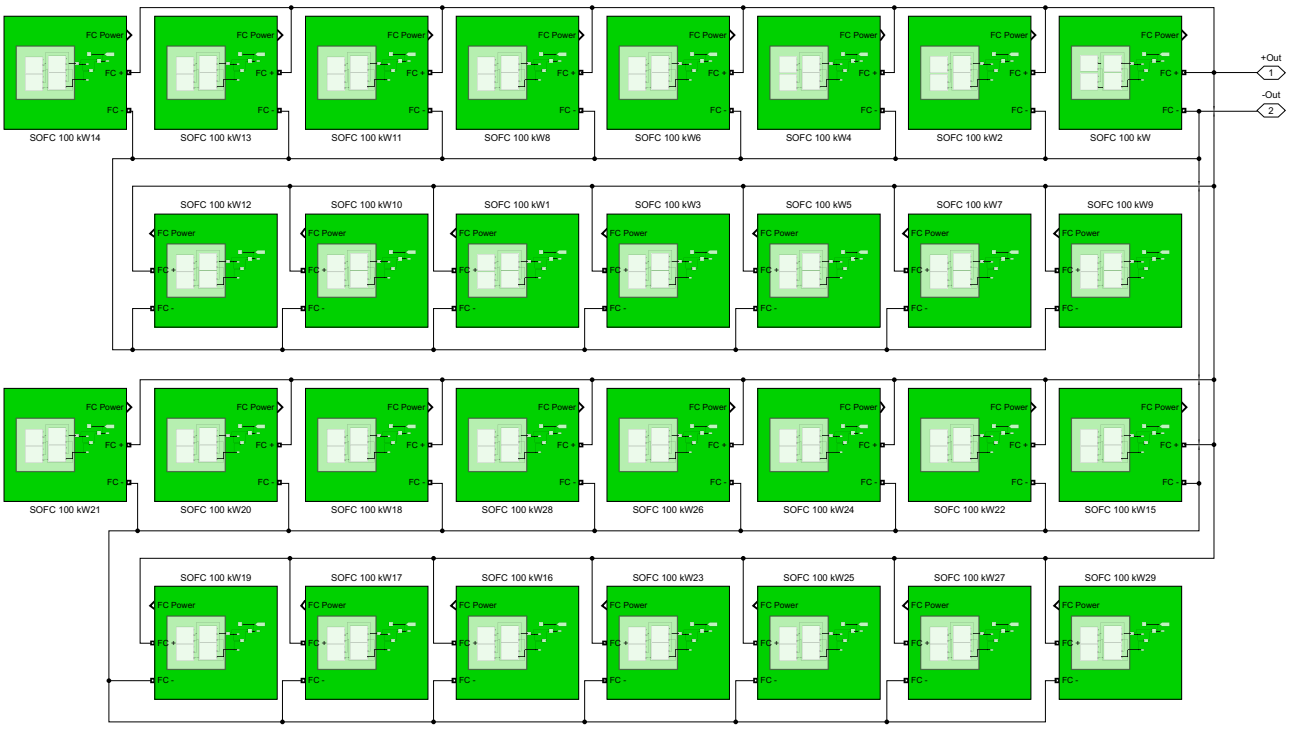

Figure 59: The simulated solid oxide-based fuel cell system with a power capacity of 3000 kW.

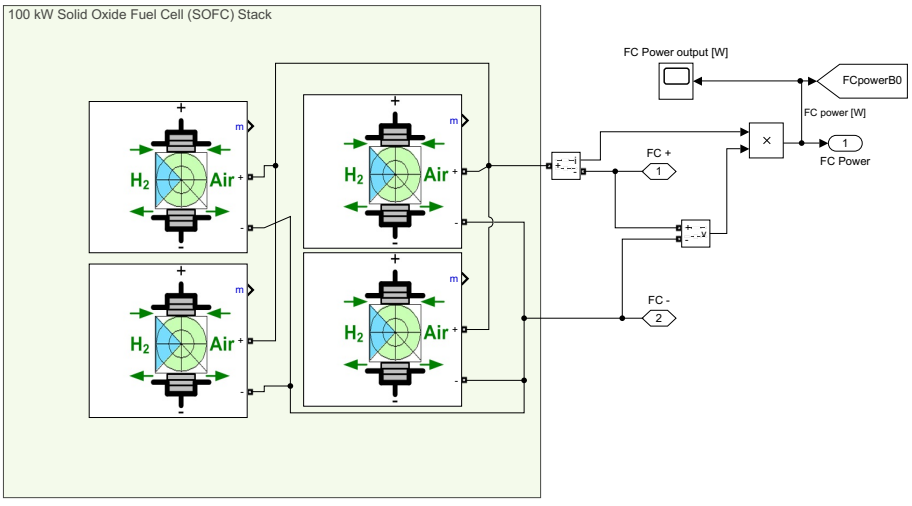

Figure 60: One of the 100 kW Solid Oxide Fuel Cell modules.

The fuel cell system consists of 30 fuel cell modules of 100 kW power capacity each, connected in parallel as shown in fig. 59, summing up to a total power delivery capacity of 3000 kW (3 MW). Each module further consists of 4 Solid Oxide Fuel Cell (SOFC) stacks of 25 kW peak power with a nominal voltage of 630 V_{AC}. One such 100 kW fuel cell module is displayed in fig. 60. Configuring a fuel cell system with a specific power rating then simply comes down to the process of duplicating the 100kW modules until the desired power rating is achieved, and connecting the modules to a common connection point. This explains the multi-module setup in fig. 59. It is possible to obtain a desired power rating with other approaches, but the effect of doing so would not affect the simulation results.

Efficiency calculations

Based on SOFC efficiency graphs kindly provided by Ceres Power (fig. 13) and Forschungszentrum Jülich (fig. 14), regression analysis has been performed in MATLAB to determine a polynomial that fit the data from the graphs. The data points used as input and the resulting polynomial graph can be seen in fig. 61. The data from Ceres Power lack information for power levels below 25%, but data from Forschungszentrum Jülich show that the efficiency approaches zero for low power levels.

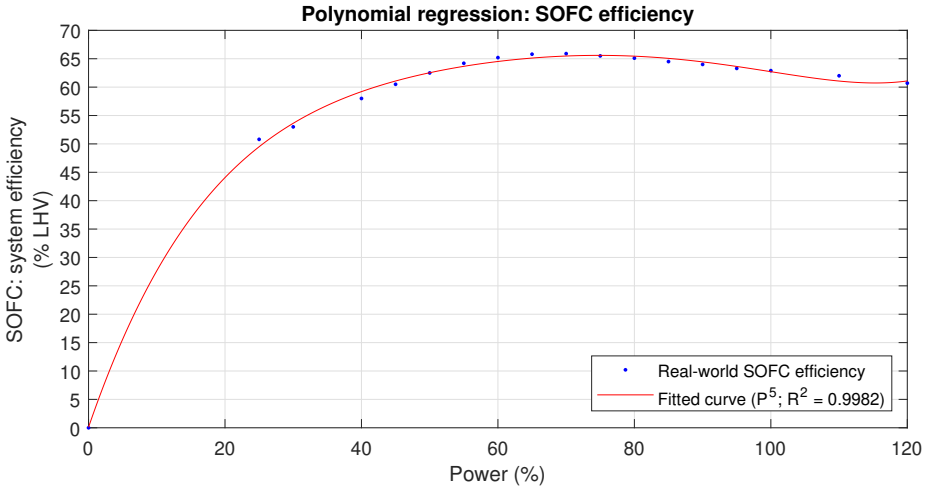

Figure 61: Regression analysis of Solid Oxide Fuel Cell (SOFC) system efficiency as a function of power output.

A fifth degree polynomial seems to give the best compromise between accuracy ($R^2 = 0.9982$) and number of coefficients. The resulting polynomial for the system efficiency is quantified in eq. (21), where the variable p represents the fuel cell stack output power as a percentage of rated power.

$$\eta(p) = 2.292 \cdot 10^{-8} p^5 - 8.113 \cdot 10^{-6} p^4 + 0.00114 p^3 - 0.08448 p^2 + 3.493 p + 0.1 \quad (21)$$

Fuel consumption calculations

The fuel consumption has been calculated by dividing the instantaneous fuel cell stack power output with the instantaneous stack efficiency, which is calculated as described above. To arrive at units of energy (kWh) rather than power (kW), the continuous fuel consumption has been further divided with 3600 (seconds per hour) and integrated over time. Mathematically, this can be represented with eq. (22), where C_{fuel} is fuel consumption in kWh, P is fuel cell stack power in kW, $\eta(p)$ is the stack efficiency in percent as a function of relative output power, p.

$$C_{fuel} = \int_0^T \frac{P}{\eta(p)/100\%} \cdot \frac{1 \text{ hour}}{3600 \text{ seconds}} dt \quad (22)$$

7.2.3 DC bus

The DC bus is a direct current bus that connects the Fuel cell system (through the DC-DC converter), the Battery system and the Controllable load to a single electrical network.

Ships with a generation capacity that is smaller than 5 MW, usually have a three-phase AC network rated at 690 V [126]. If the ship has equipment for DC power generation or consumption, this equipment would then be connected to the AC network through a DC-AC power electronics converter from the DC bus.

If a two-level DC-AC Voltage Source Converter (VSC) is used to connect the DC and AC networks, then the minimum DC network voltage level can be determined using eq. (23),

$$V_{DC} \cdot m_\alpha = \frac{2 \cdot \sqrt{2}}{\sqrt{3}} V_{AC} \quad (23)$$

where m_α is a modulation index variable ($m_\alpha \in [0, 1]$) used in the VSC to modulate the output voltage level on the AC-side of the converter [1, 127].

For an AC voltage level of 690 V_{AC}, the minimum DC bus voltage would be 1126.8 V_{DC}. To ensure sufficiently high DC voltage at all times for DC-AC conversion, the voltage of the DC bus has been configured to 1200 V in the simulation model.

7.2.4 DC-DC converter

The DC-DC boost-converter connects Fuel cell system with the DC bus and, by extension, the Battery system and the Controllable load. For high perfor-

mance simulation, the converter is modelled as a duty cycle controlled average switching-function model converter so that computational-intensive PWM-simulations are not necessary.

The converter has three primary functions.

The first function is to increase the voltage of the fuel cell system to the voltage of the DC bus, which has been set to 1200 V. This is necessary because the fuel cell system voltage is much lower than 1200 V and also varies with the electric power output.

The second function of the converter is to regulate the power flow from the fuel cells to the battery system and the load. As mentioned earlier in section 3.5 and 4.2, fuel cell degradation increases significantly with dynamic load variations, as this alters the internal thermo-chemical balances of the cells and leads to degradation-inducing stresses. It is therefore important from a durability point of view to operate the fuel cells with high stability and slow load transients.

The converter is regulated by a Proportional Integral (PI) controller that is tuned to limit the load rate change of the fuel cells to a maximum of approximately 100% load change per hour. To exemplify, this allows the converter to change the load output of the fuel cell system with up to $8.\overline{3}\%$ every 5 minutes or up to $16.\overline{6}\%$ every ten minutes. The schematics of the PI controller is presented in fig. 62.

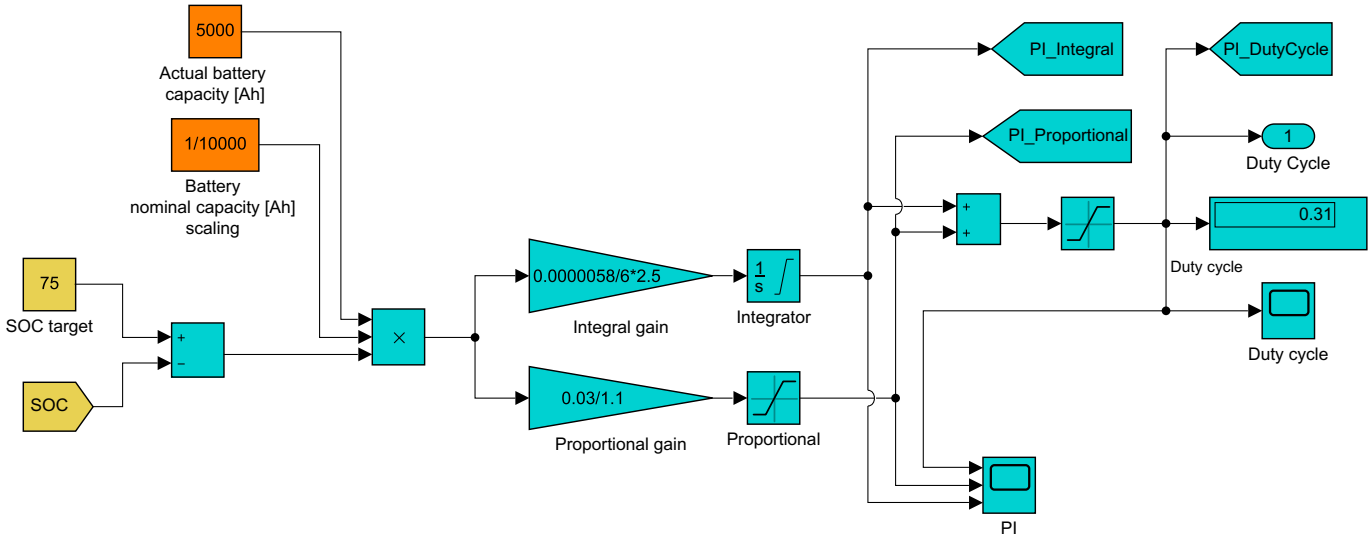

Figure 62: The Proportional Integral controller that regulates the power flow from the fuel cell system to the DC bus-connected battery system and load.

The third function of the DC-DC converter and the PI controller is to automatically ensure that the battery system is charged up to a certain State of

Charge (SOC) level after the battery has discharged to handle load changes. In the simulation model the SOC target has been set to 75%, but may be set to any other desired level. Many batteries wear down faster for both high and low SOC levels [128], so 75% is a good compromise.

The PI controller functions according to classic closed-loop control theory: A measured state is compared with a reference or target state, and the difference is calculated and defined as the error. For this controller, the measured state is the State of Charge of the battery pack and the reference state is 75% SOC. The error is then multiplied with the proportional gain and integrated with the integral gain, separately, before being summed together to establish an appropriate control signal with the objective of minimising the error. The dynamic nature of the control signal is dictated by the size and rate of change of the error, as well as the proportional and integral gain constants, and fluctuates over time unless steady state is in effect.

For power electronic converters, like the DC-DC boost converter, the control signal is labeled the duty cycle and is essentially the fraction of time (in the range from 0 to 1) that the high frequency switches of the converter are conducting power from the input side to the output side of the converter.

A more in-depth explanation of control theory, PI(D)-controllers and power electronics is beyond the scope of this thesis.

7.2.5 Battery system

Figure 63 shows the battery system used in the Simulink-simulation model. The battery pack has been configured with a rated capacity of 5000 Ah and a nominal voltage of 1108.5 V so that the battery voltage for a 75% SOC is almost exactly 1200 V. Just like the output voltage of fuel cells vary with the power output, the battery voltage changes with SOC. Nonetheless, for large batteries, like the one in question, the voltage does not change considerably during operation. It was therefore not found necessary to implement a two-way power electronics converter between the battery and the DC bus in this case. The maximum voltage deviation in the DC bus during load simulation of the load profile in section 7.1 was less than 0.85% from the nominal voltage of 1200 V — more about this in the Simulation results: Base case. If propulsion and other ship loads are AC-bound, then a DC-AC converter can compensate for this voltage deviation on the DC-side and provide an even more stable voltage on the AC-side. Even so, in a real world scenario it is probably a good idea to equip maritime vessels with one or more dedicated DC-DC converters for the battery system to facilitate improved control (regulation) over the battery, further improve voltage stability in the DC bus and handle plug-in charging, etc.

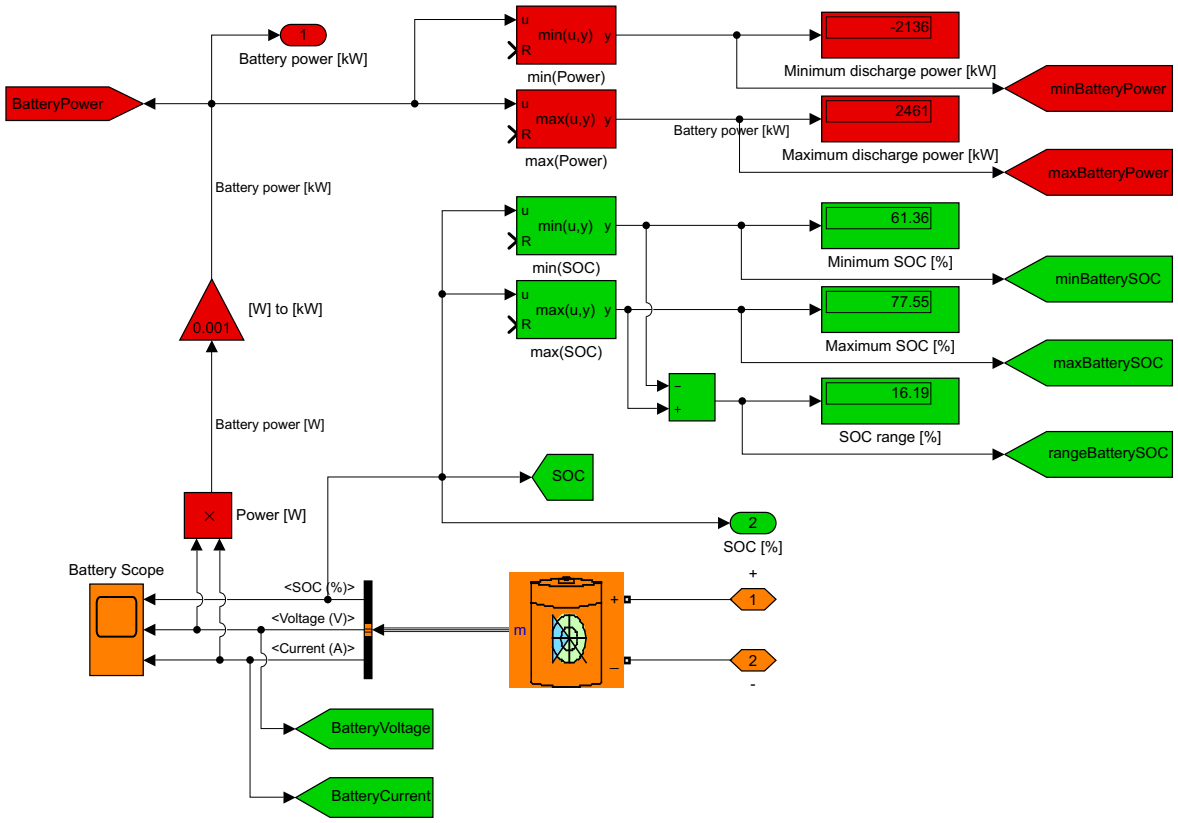

Figure 63: The simulated battery system. The red and green colours indicate measuring devices for power, voltage, current and State of Charge of the battery pack. These data are then send to the Control Center in the model for further data processing.

7.2.6 Controllable load

To simulate load profiles, a controlled DC-load has been implemented by means of a controlled current source, as shown in fig. 64. By dividing the power signal from the load profile with the DC bus voltage, a current signal is established for the current source, which functions as the load.

In fig. 64, the red component is the controlled current source, the yellow components are handling the load profile input and the green components are for measurements and data analysis. The cyan coloured component group is a simple integral controller that compensates for any offset in the actual DC bus voltage from the targeted 1200 V. This voltage correction ensures that the power consumption at the load does not deviate in any significant amount from the power reference given by the load profile.

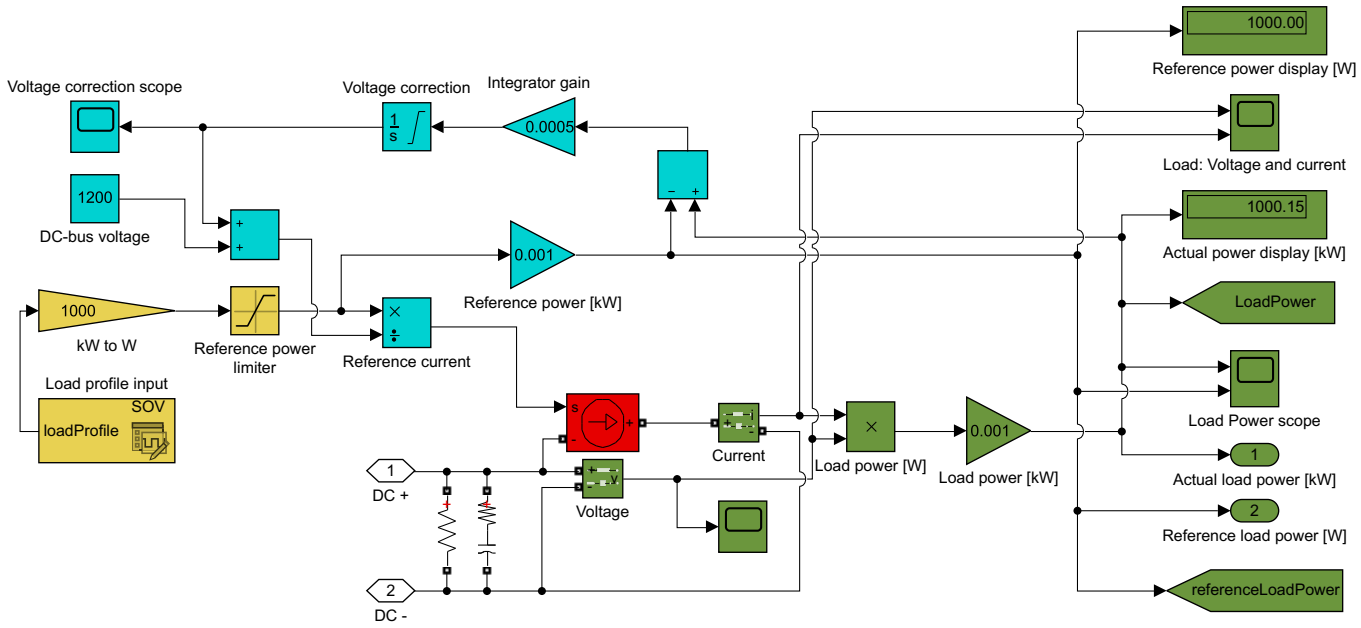

Figure 64: Overview of the controllable DC-load.

7.2.7 Control centre

Figure 65 visually lays out the control centre of the simulation model.

The recommended minimum battery size is calculated as follows: The difference between the minimum and maximum State of Charge of the installed battery system is determined as *rangeBatterySOC*, which is calculated in the Battery system. This SOC-range is then multiplied with the actual battery capacity in kWh and divided with a percent constant of 100, to deduce the minimum amount of energy that a battery must be able to deliver or absorb to function as a buffer between the load and the fuel cells for a specific load profile. As mentioned in section 7.2.4, the lifetime of batteries deteriorate fast at both high and low levels of SOC. The previously mentioned minimum buffer energy that the battery must handle is therefore divided by a factor of 0.6 so that the battery system can operate with a State of Charge ranging from 20% to 80%. Lastly, the so-far calculated battery size is multiplied by a durability scaling factor of 1.2, since "[f]or most [battery] products, 20% capacity fade (80% of initial battery capacity) is considered the battery's end of life (EOL)" [14, p. 3]. This last calculation step is mostly a techno-economic optimisation and serves to prolong the usable lifetime of the battery pack.

After these calculations a number for recommended minimum battery size is established for the current fuel cell stack size and load profile. A system designer is recommended to further scale up this number to handle specific

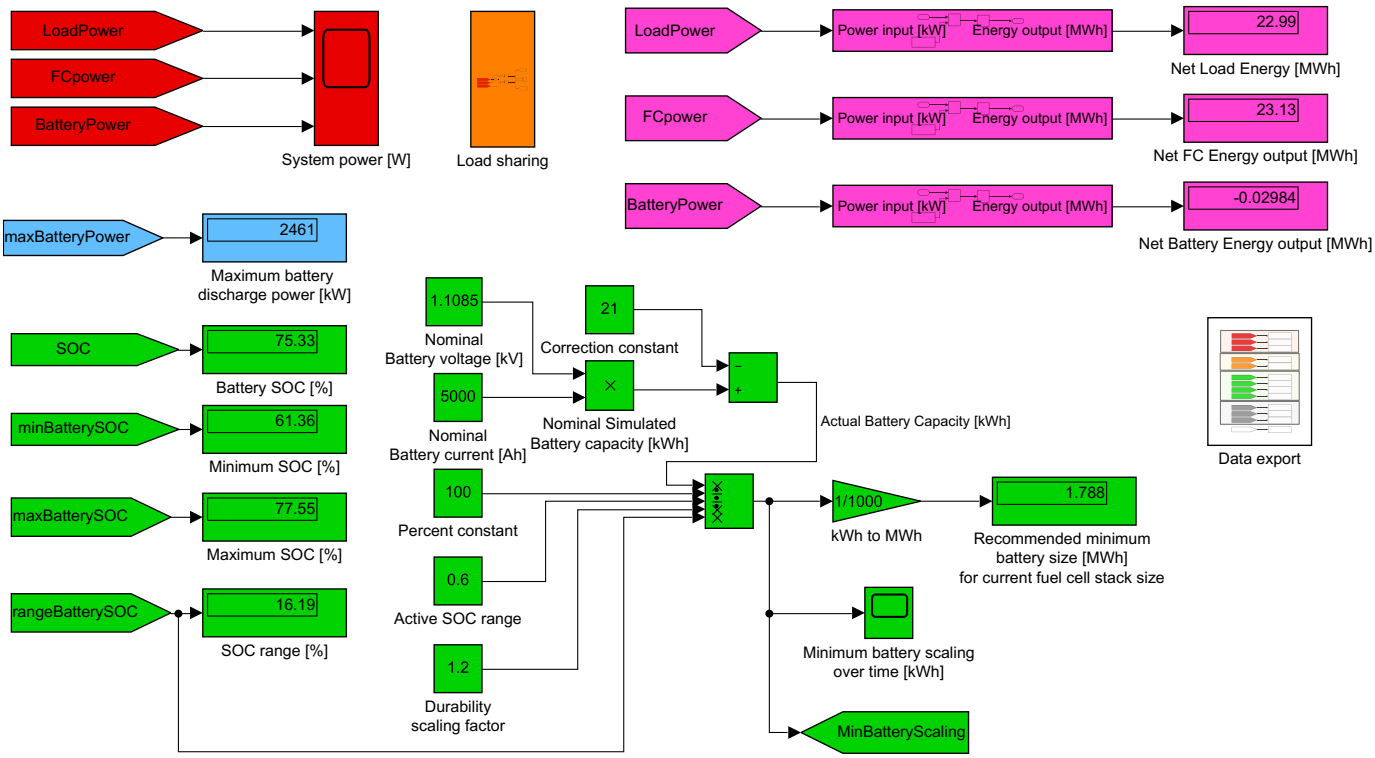

Figure 65: The control centre of the simulation model. Here the most important data measurements are processed. This is also where the battery sizing calculations are performed.

system requirements, such as safety margins and additional equipment like diesel generator sets.

7.2.8 Data export

Finally, the most important simulation data is exported from Simulink to MATLAB with the components shown in fig. 66. The data is processed in MATLAB to generate the data plots presented in the Simulation results: Base case and Sensitivity analysis: Fuel cell power capacity.

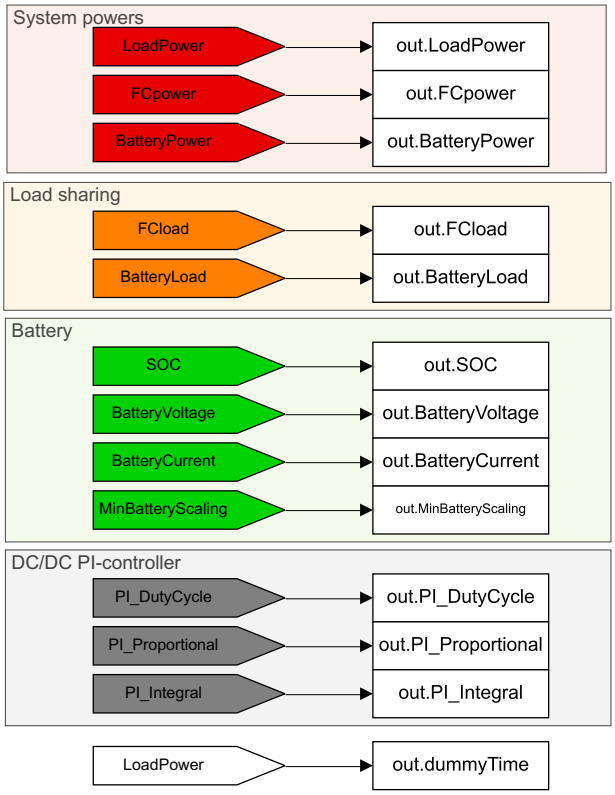

Figure 66: Data extraction from the Simulink-model to MATLAB for further analysis.

7.3 Simulation results: Base case

7.3.1 Power balance

Figure 67 shows the simulation of the 24-hour load consumption profile provided in section 7.1 Operational load demand profile, and how the fuel cell and battery systems operate in unison to deliver the required power to the load.

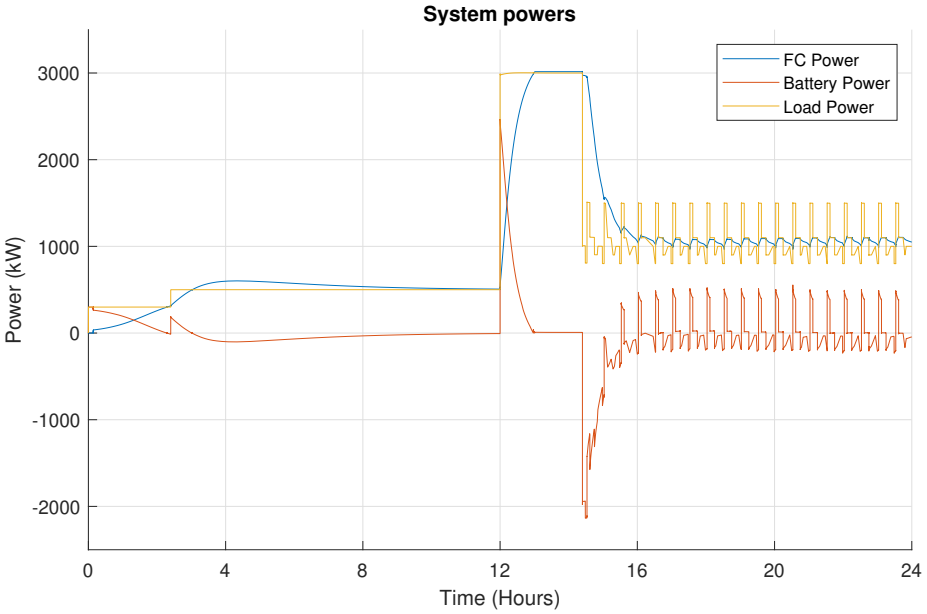

Figure 67: Overview of system powers. The load power is positive for power consumption, while the fuel cell and battery power is positive for power delivery.

Harbour and standby

Initially at zero hours simulation time, the battery system handles all of the load power dispatching. As a direct result, the State of Charge of the battery system starts dropping as the battery pack discharges. The SOC is plotted in fig. 70 on page 112. The decreasing SOC is registered by the DC-DC converter, which in response gradually increases the power output from the fuel cells to the DC bus. Between the approximately 3 and 12 hour mark of the simulation, the fuel cell power delivery is higher than the load consumption, in order to recharge the battery pack back to 75% SOC. The recharging of the battery eventually leads to a steady state power balance between the fuel cells and the load. Consequently, the battery system assumes an idle state in which neither charging nor discharging are taking place.

Transit

By the 12-hour mark, the load increases sharply from 500 kW to 3000 kW

as the simulated ship goes from harbour to transit mode. The fuel cells are still delivering about 500 kW at this time, so the battery takes on the role of "spinning" reserves and immediately provides the load with the necessary intermediate power. Once again the fuel cell system output is steadily increased to match the load consumption and phase out the power delivery from the battery pack. However, since the load requires the fuel cell system to operate at nominal power capacity, there is no surplus fuel cell power to recharge the battery until the load consumption drops after 14.4 hours. As a result, the battery SOC flattens out at approximately 61% during this period.

If the peak fuel cell power was set higher than the peak load power, the fuel cells would have had extra capacity to recharge the battery even at peak load. At the same time the battery SOC is, as previously mentioned, almost constant in this high-load phase, so the need for recharging is limited. Besides, at peak load, the load is expected to eventually drop followed by a period of surplus fuel cell power production. This surplus power will automatically lead to a recharging of the battery pack.

Technical operation

At the 14.4 hour mark, the load consumption drops considerably from 3000 kW to an average load of around 1000 kW as the SOV enters a technical operation phase at an offshore work site. In response, the fuel cell power output is gently downregulated by the DC-DC converter and its PI controller. As already alluded to, the reduction in the load and the slow regulation of the fuel cell power leads to a recharging of the battery back to the reference SOC level.

The technical operation phase involves many moderate up and down regulations of the power demand to the propulsion systems. The power fluctuations are mostly buffered by the battery system. Simultaneously, the power output from the fuel cells does also oscillate with the load, but to a much lesser extent than the battery, and also handles the average load.

7.3.2 Load sharing

Figure 68 is a derivation of fig. 67 and has been constructed by dividing the fuel cell and battery power production with the load consumption. The result is an overview over how much of the load the fuel cells and the battery system handles at any point in time, in terms of percentage. It is very clear from this figure that the fuel cell system generally has approximately 100% of the load share, while the battery pack functions as an energy buffer to handle any short-term imbalances in power between the load and the fuel cells.

Unless charged from a secondary energy source like a diesel generator set or from a grid connection, the battery does not provide any power delivery beyond the energy it buffers from the fuel cells. Any discharging of the battery

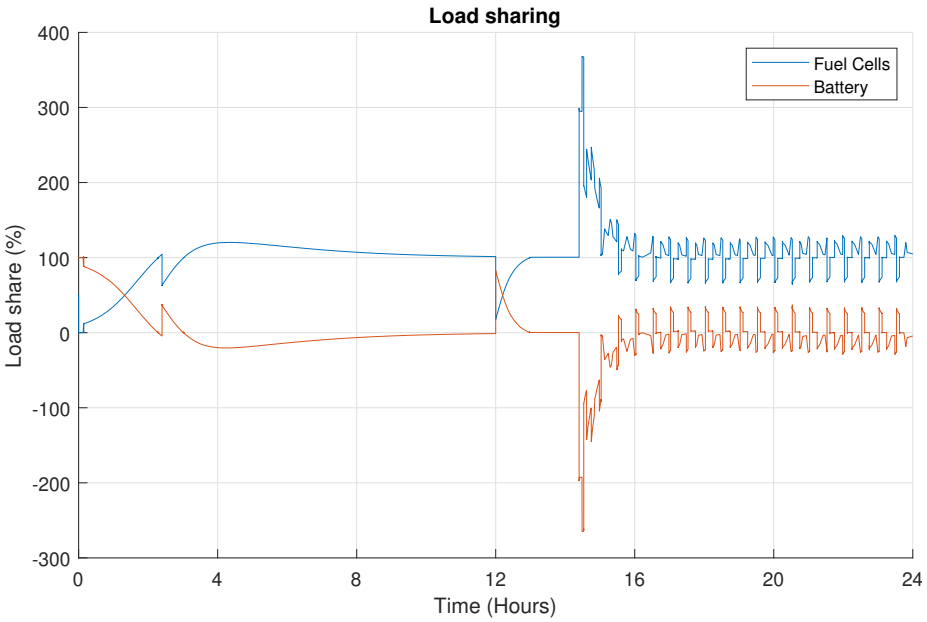

Figure 68: This plot is derived from fig. 67 and shows the fuel cell and battery power delivery as percentage of the instantaneous power consumption at the load.

is followed by a charging of the battery by the fuel cells system.

Figure 68 also shows that when the fuel cell load share is higher than 100%, the battery pack has a negative load share, signifying recharging of the battery.

7.3.3 Energy carrier consumption

While the electric energy consumption of the Operational load demand profile is 23.0 MWh, the energy carrier consumption for a 3000 kW SOFC system is 44.2 MWh, in terms of LHV, due to the conversion losses in the fuel cell system.

In section 5.6.2 the Energy storage density of various energy carriers was established in MWh/m^3. By inverting these energy densities and multiplying them with 44.2 MWh and 14 days, the fortnightly volume requirements for the different energy carriers can be calculated in cubic metres. This should give a good idea of the energy carrier tank volume needed on board a Service Operation Vessel to operate the vessel for 14 days, and allows for easy calculations for longer or shorter periods of sailing time.

The values in section 7.4.4 have been compensated for the losses occurring during dehydrogenation of LOHCs and magnesium hydride, but not for hydrogen purification of any fuel or reforming of fuel such as ammonia and methanol. This is because dehydrogenation of LOHCs and metal hydrides is required regardless of fuel cell, while hydrogen purification or reforming of am-

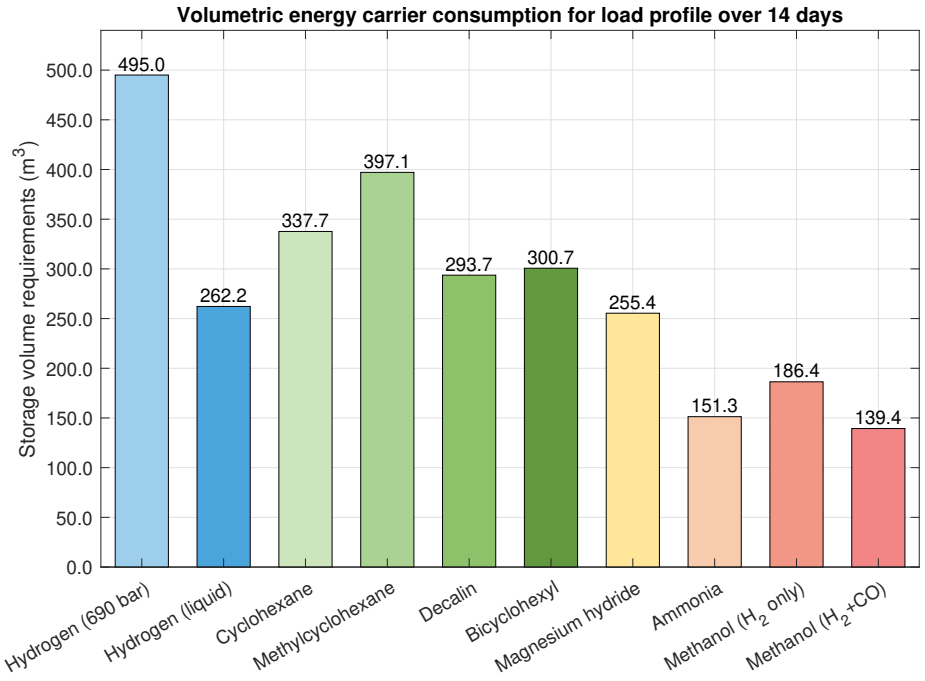

Figure 69: The amount of required storage volume for the various energy carriers for the Operational load demand profile repeated over 14 days. Based on a daily energy consumption, in terms of LHV, of 44.2 MWh per day, as simulated in section 7.4.4, and adjusted for the numbers presented in section 5.6.2. The volume requirements for the LOHCs and magnesium hydride have also been adjusted for the efficiency associated with dehydrogenation of these energy carriers.

monia, methanol and other energy carriers is not necessarily required. Without the low efficiency for dehydrogenation, magnesium hydride would perform on par with ammonia and methanol.

7.3.4 Battery system

In fig. 70 it can be seen that the State of Charge (SOC) of the battery pack begins at 75% and gradually falls down to below 70% during the first hours of simulation; since it takes time for the fuel cell stack to match its power production with the load demand. Simultaneously, the battery voltage falls from 1200 V to 1198 V and the output current from the battery system is positive.

Eventually, the power delivery from the fuel cells is ramped up enough to charge the battery back to the target of 75% SOC. The charging slightly increases the voltage back to almost 1200 V and slowly reduces the battery output

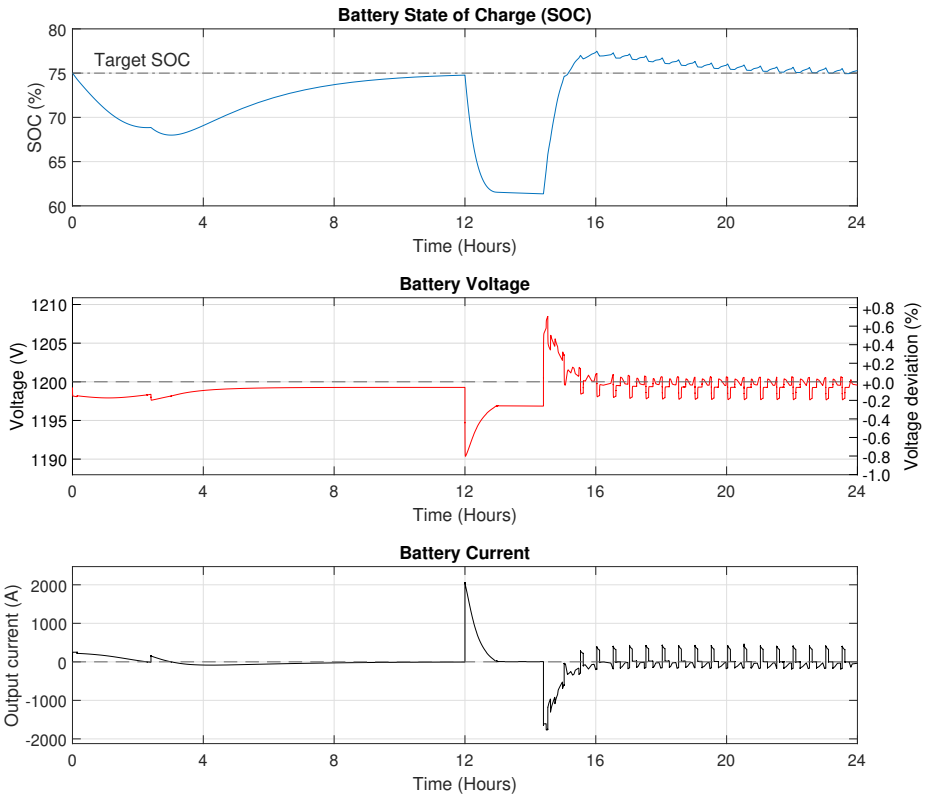

Figure 70: Subplots of the State of Charge (SOC), voltage and output current for the battery system. Positive current means that the battery delivers power to the DC bus and is discharging. Negative output current means that the battery pack is charging.

current from slightly negative to near zero.

At the 12-hour mark, the load demand is stepped up significantly, as described in the sections Operational load demand profile and Power balance. Hence, the battery voltage drops sharply from 1199.3 V to 1190.4 V, equivalent to a voltage deviation of (-)0.80% from the reference voltage. In absolute numbers, 0.80% is the maximum voltage deviation in the DC bus for this simulation. The voltage falls because of the rush of current (up to 2081.2 A) from the battery to the load. The voltage later stabilises at 1196.9 V as the fuel cells boosts power production to a load share of 100%. By this time, the power delivery from the battery pack has reduced the SOC to a simulation minimum of 61.4%.

After 14.4 hours of simulation time, the load demand is stepped down, allowing the fuel cells to start charging the battery back to 75% SOC, overshooting a bit and maxing out at 77.5%. The sudden step down in power consumption at the load consequently increases the battery voltage to 1205.8 V, due to the

surplus of power being fed to the DC bus from the fuel cells. In fig. 70 it can furthermore be observed that the battery output current during this phase is negative, as energy rushes in from the fuel cells to the battery at a rate of up to 1768.9 A.

During the technical operation phase of the SOV, the battery SOC remains relatively stable and close to 75%, after recharging, while the battery voltage and current oscillates in buffer-synchrony with the load demand pattern to offload transit loads from the fuel cells.

The maximum power output from the battery system during the simulation of the SOV load profile is 2461 kW.

Recommended minimum battery capacity

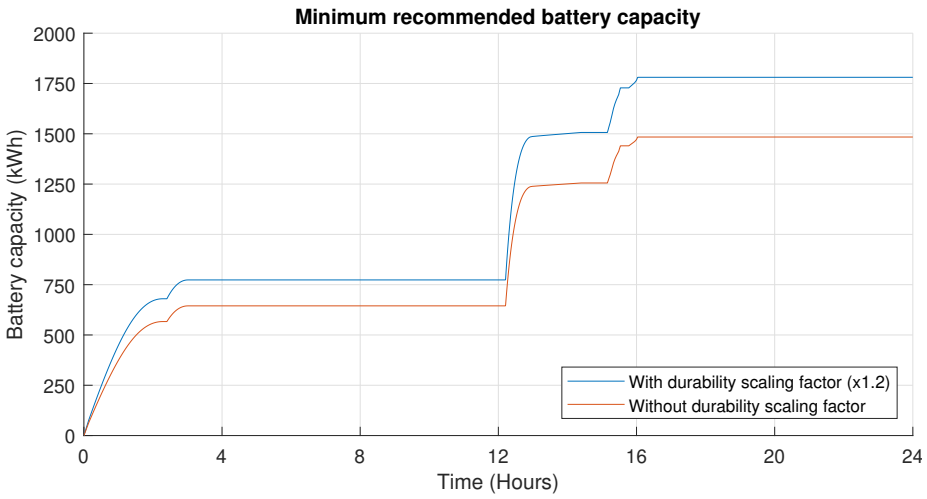

Figure 71: Recommended minimum battery capacity as a function of time.

Figure 71 outline the time-related development of the recommended minimum battery capacity — calculated as described in section 7.2.7 and shown in fig. 65. The only dynamic variable in the Simulink-calculations is the range of battery SOC, meaning that any new values of minimum or maximum SOC will increase the recommended battery capacity proportionately. Ultimately, the recommendation reaches an energy capacity of 1780.7 kWh, or almost 1.8 MWh. Note that this includes the durability scaling factor of 1.2. Without this factor, the recommendation is just under 1.5 MWh. Any further scaling considerations are left to the system designer.

7.3.5 Fuel cell power flow regulation

Figure 72 shows how the DC-DC converter is regulated by the PI controller, configured as shown in fig. 62. Since the DC-DC controller regulates the power

flow from the fuel cell stack, this also gives an insight into the tuning of the fuel cell performance.

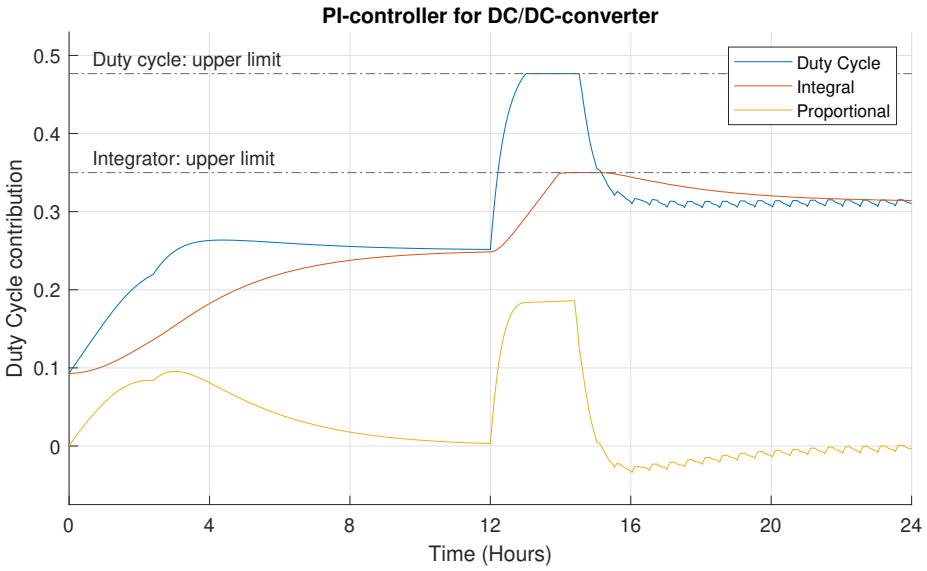

Figure 72: Plot of the integral and proportional contribution of the PI controller to the duty cycle used to control the power flow through the DC-DC converter.

The duty cycle has been limited to 0.4767 to limit the maximum power transfer from the fuel cells to 3000 kW, which is the nominal power capacity of the fuel cell system. The integrator has been limited to an upper limit of 0.35 to avoid integral wind-up, which could otherwise limit the PI controller's ability to regulate the DC-DC converter. In addition, the initial condition of the integrator has been set to 0.093, which corresponds to the minimum duty cycle level for power transfer in the DC-DC converter.

In fig. 72 it can be observed that the duty cycle is at the upper limit between 13.0 and 14.6 hour after the start of the simulation. During this period the fuel cell system is operating at rated power production. The integrator is in saturation for an hour between 14.2 and 15.3 hours in simulation time.

The integrator saturation limit is reached because the battery state of charge remains far from the reference value of 75% for a significant time. Moreover, the fuel cell system is already delivering maximum power output to the load and does not have surplus power capacity to recharge the battery until the load demand drops at 14.4 hours. A fuel cell system with a much higher nominal power capacity than the one used in the simulation could have reduced the chance of integrator wind-up/oversaturation. The same effect can also be achieved with an integrator limiter, which is the solution provided in the simulation model.

Fuel cell power as a function of duty cycle

The correlation, or rather causality, between the duty cycle of the DC-DC controller and the power output from the fuel cell stack is not strictly proportional or linear. In fig. 73 it is apparent that a linear relationship is only present in the region for duty cycle values greater than approximately 0.25. Knowledge about this nonlinearity can possibly be used to improve the regulation of the power production from the fuel cell stack. For instance, the duty cycle can be changed faster in the region below 0.25 to give a faster fuel cell response at low power levels, if desired.

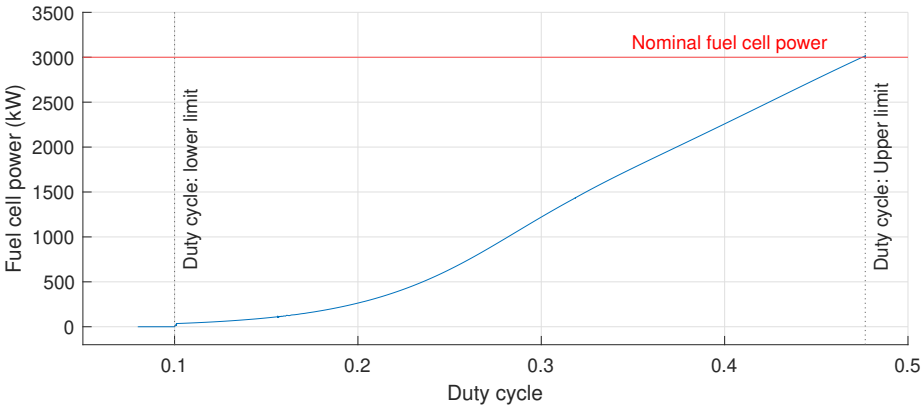

Figure 73: Relationship between the duty cycle of the DC-DC converter and the power output from the fuel cell stack.

7.4 Sensitivity analysis: Fuel cell power capacity

This section expands upon the setup in Simulation results: Base case by performing a sensitivity analysis on fuel cell power capacity. This is done by changing the rated power of the fuel cell system in steps of 500 kW between 2000 kW and 4000 kW in the simulation model, and analysing the effect this has on Fuel cell efficiency, Fuel cell power production and Battery system scaling.

As mentioned in section 7.2.2, the base case was configured with a 3000 kW fuel cell system.

All simulation components remain as in the base case setup except for:

1. changing the power capacity of the fuel cells, as described above;
2. minor re-tuning of the PI controller in the DC-DC converter, to adapt the converter to the different fuel cell stack sizes;
3. addition of a few new sensors for data logging.

This makes it possible to isolate and analyse the effect of scaling the fuel cell system.

7.4.1 Fuel cell power production

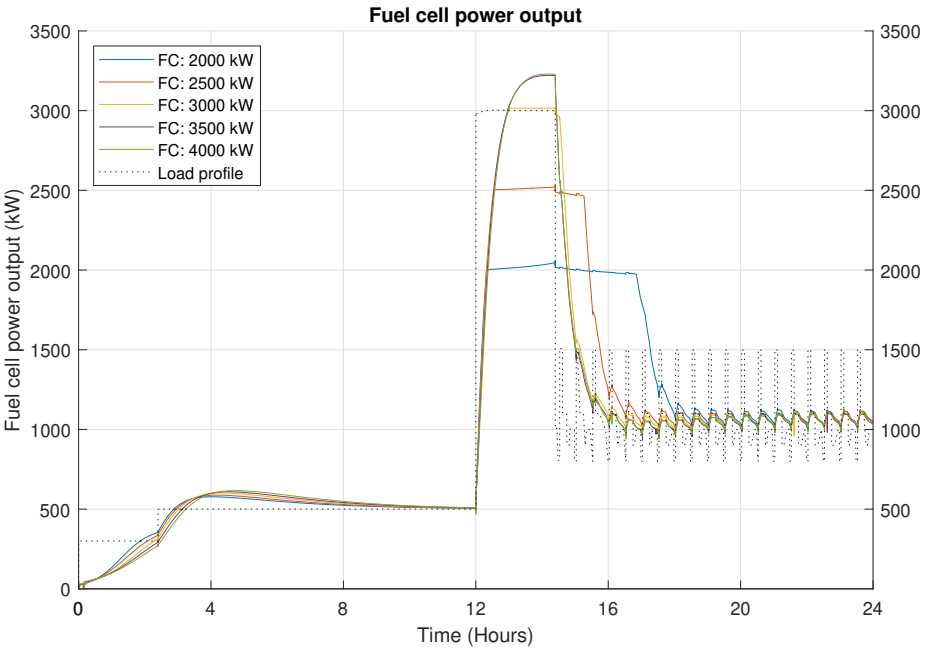

Figure 74: Power output from fuel cell stacks with different maximum power capacities.

Upregulation

Figure 74 shows the effect different fuel cell power capacities have on the power flow from the fuel cells. The grey dotted line in the plot is the unchanged load consumption profile presented in Operational load demand profile on page 95.

From the figure it is clear that all the different fuel cell sizes perform rather similarly for the low load consumption that take place up until the 12-hour mark. But once the load steps up significantly to 3000 kW, the difference in maximum power production of the fuel cell systems become quite pronounced. Naturally, the 2000, 2500 and 3000 kW fuel cell stacks are limited to their rated power, and require the battery system to cover any remaining load share until the load consumption later decreases. The 3500 and 4500 kW systems, however, have more than enough rated power to cover the load and can even charge the battery system during peak load, to recover the SOC to the target level. While this initially may appear desirable, two factors reduce the necessity of recharging the battery at peak or high loads:

1. Any fast load reductions will automatically lead to a recharging of the battery.

2. The battery system needs to absorb surplus fuel cell power production when the load consumption sooner or later is reduced, and until there is established a new power balance between the fuel cells and the load. The combination of high load and recharged battery could therefore increase the SOC above 80%, which reduces the battery life. In a worst case scenario, caused by either a badly configured power production system or unforeseen events, the battery could potentially reach 100% and force the fuel cells to change power output much faster than desirable.

Downregulation

To continue the analysis of the fuel cell power output plotted in fig. 74, it can be pointed out that the distinctly sized fuel cell stacks also behave differently after the large load reduction at the 14.4-hour mark. All the stacks with rated power including and above 3000 kW follow an almost indistinguishable pattern where a fast unloading of the fuel cells starts immediately with the load reduction. For the 3500 and 4000 kW fuel cell stacks, the fast downregulation (although within the rate limits described in section 7.2.4) takes place because the battery SOC is already close to the target SOC when the load consumption is stepped down. Consequently, the SOC therefore overshoots the target. For the 3000 kW fuel cell stack, the battery SOC is still low when the load consumption drops, but quickly returns to near target SOC as a result of the load reduction.

For the fuel cell stacks rated below peak load consumption, the situation is dissimilar to the situation for the $\geq$3000 kW stacks. Since the lower performing

stacks did not have sufficient power capacity to cover 100% of the load consumption at peak load, the battery pack has been discharging continuously and at a high rate since the load was increased to 3000 kW. As a result, the smaller fuel cell stacks need to continue max power output long after the large load reduction, to recharge the battery back to the target SOC. This is the cause of the delayed drop of the 2000 and 2500 kW fuel cell systems in fig. 74, and also the cause of the increased battery capacity requirements that will be discussed in section 7.4.6.

7.4.2 Relative power production

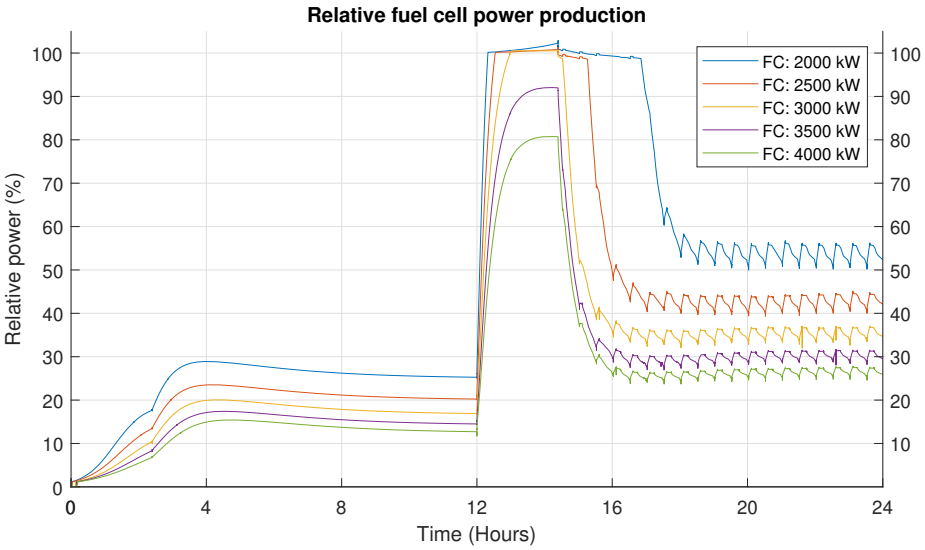

Figure 75: Power output from the fuel cell stacks relative to rated power.

While fig. 74 quantifies the absolute power production by the fuel cells, fig. 75 gives insight into how much power each fuel cell stack is producing as a percentage of their respective rated power. Not surprisingly, the smaller stacks work the longest at 100% power. For instance, the 2000 kW FC stack maintain maximum power production for about 1 hour and 40 minutes after the load demand is reduced from 3000 kW to approximately 1000 kW at the beginning of the technical operation phase. In contrast, the 3500 kW and 4000 kW fuel cell systems never quite reach their max power output potential for this specific load profile.

7.4.3 Fuel cell efficiency

Instantaneous efficiency

Since the efficiency of fuel cells varies with the power output level, it is interesting

to study the impact that scaling a fuel cell system up or down in rated power has on the fuel-to-power efficiency.

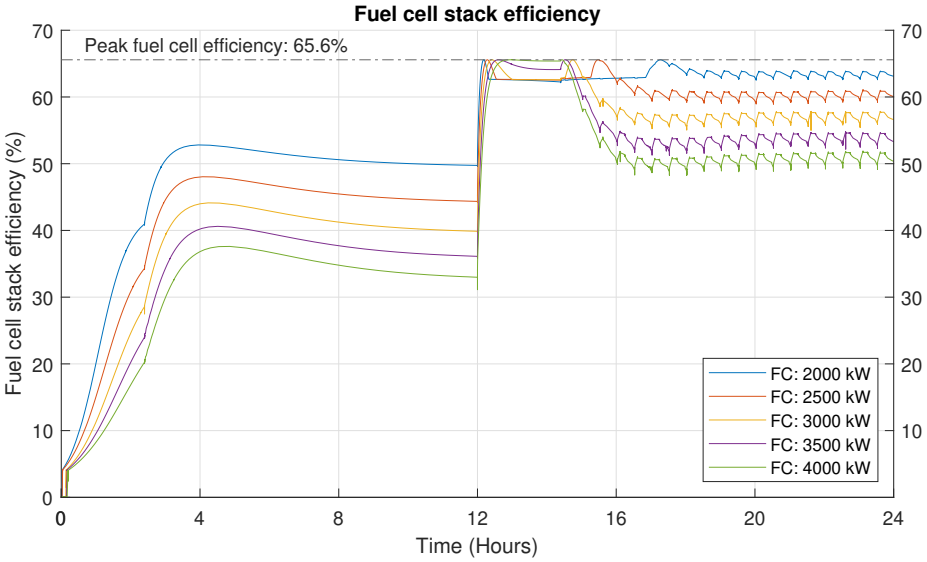

Figure 76: Instantaneous efficiency for fuel cell stacks with different maximum power capacities. The FC stack analysed in Simulation results: Base case had a capacity of 3000 kW.

As can be seen in fig. 76, the efficiency of the fuel cell systems does vary notably with the various system sizes. And, for most of the simulated load profile, there is also a clear trend: fuel cell systems with small power ratings perform better than the larger systems. The only exception seems to be during the time where the fuel cell stacks are operating at 100% power output, as very high power outputs are correlated with sub-peak efficiencies for the fuel cells.

The smaller fuel cell systems also operate at max power output for a longer period than the larger systems, to recharge the battery after the high load consumption period between 12 and 14.4 hours of simulation time. Nonetheless, the efficiency loss associated with max rated power production is limited and its effect can potentially be dealt with by altering the control logic of the DC-DC converter. For instance, the max power output of fuel cells could be somewhat reduced, to optimise fuel cell efficiency, during time periods in which the battery State of Charge (SOC) is considered high enough for efficiency optimisation to take place.

It is also worth noting that the various fuel cell efficiencies are especially low during the first three hours of simulation, as the power demand is quite low during this interval. In other words, there exist a potential for further fuel cell efficiency optimisation. For instance, some of the battery recharging can be moved to off-peak hours or a smaller fuel cell stack could take over power

production during times with low power demand.

Average efficiency

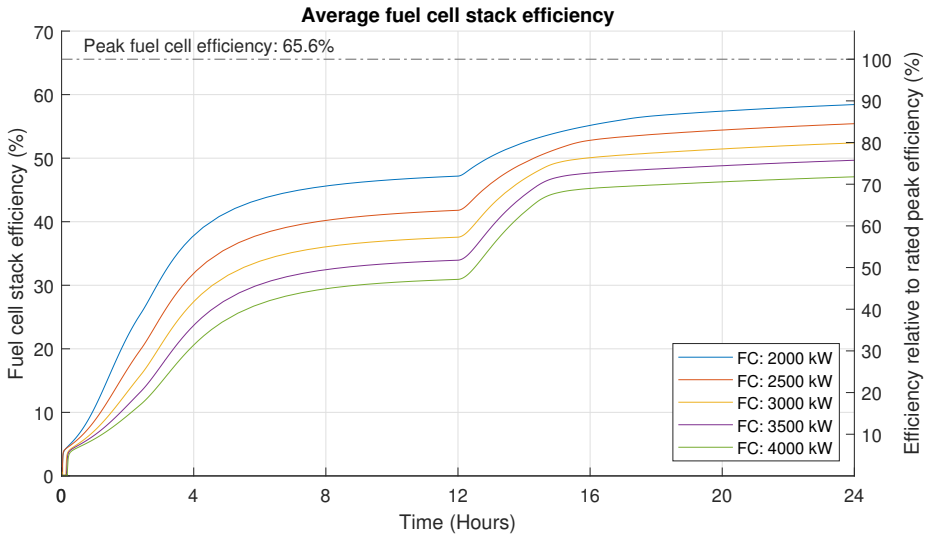

Figure 77: Average efficiency for fuel cell stacks with different maximum power capacities. The left y-axis indicates the average efficiency; while the right y-axis indicates the average efficiency relative to the rated peak efficiency of the fuel cells.

Another perspective of fuel cell stack efficiency is presented in fig. 77, and focuses on the average efficiency as it develops over time. To arrive at an average stack efficiency, the amount of electric energy produced by the fuel cells is divided by the amount of fuel energy consumed, in terms of Lower Heating Value, for all the power production up until the given point in time. In this way, a simple input–output relationship is established for efficiency calculations. The fuel consumption will be discussed further in section 7.4.4.

Figure 77 shows perhaps even clearer than fig. 76 that the smaller fuel cell stacks have an advantage in terms of efficiency.

For rated fuel cell stack power in increasing order (from 2000 to 4000 kW), the respective average production efficiencies are 58.4%, 55.4%, 52.4%, 49.7% and 47.1%. In other words, the two smallest fuel cell systems have an efficiency advantage of 11.5% and 5.8% relative to the base case with 3000 kW power capacity, and 24.0% and 17.6% compared to the 4000 kW rated fuel cell system.

Average efficiency relative to peak efficiency

By doing a readout of the plots in fig. 77 based on the right y-axis, it is also possible to determine how close the average production efficiencies of the fuel

cells are to the rated peak efficiency of 65.6%. By performing this scaling, it can be determined that the 24 hour production efficiencies of the fuel cell stacks for the load profile are: 89.1% (2000 kW); 84.5% (2500 kW); 79.9% (3000 kW); 75.7% (3500 kW); and 71.8% (4000 kW), relative to the peak efficiency. Based on these numbers it is fair to assert that the 24 hour production efficiencies of the fuel cell systems are in the range of approximately 70% to 90% of peak efficiency, with an average of circa 80%.

7.4.4 Fuel consumption

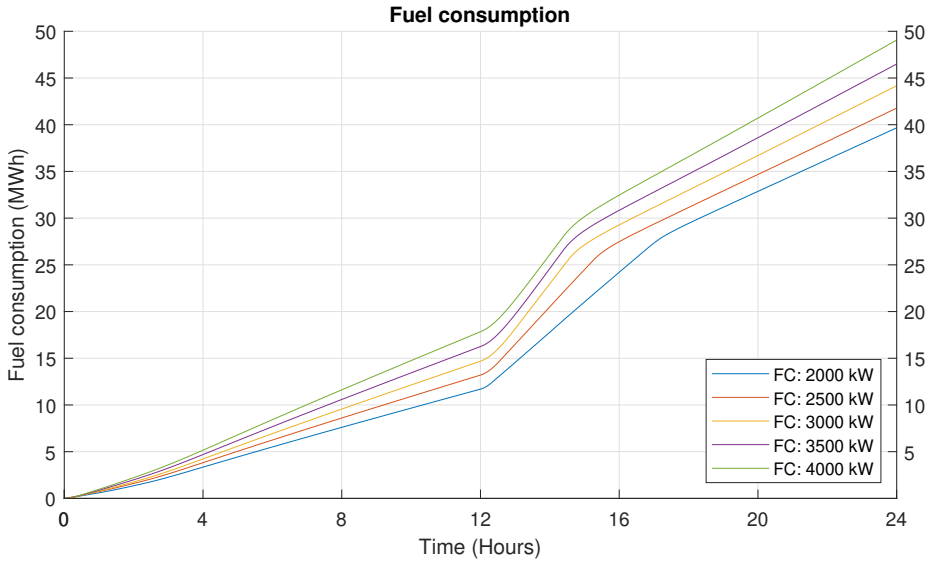

Figure 78: Fuel consumption in MWh of lower heating value based on fuel cell stacks with different maximum power capacities.

The fuel consumption for the different fuel cell stacks is plotted in fig. 78.

Again, a clear picture emerges: stacks with less rated power perform at higher efficiencies and therefore consume less fuel than the alternatives. For reference, the Operational load demand profile requires close to 23.1 MWh of electric energy for the 24 hour period, while the fuel cell stacks consume fuel energy (in terms of LHV) amounting to 39.7 MWh to 49.1 MWh, with the 3000 kW system at 44.2 MWh.

Compared to the base case of 3000 kW, scaling up to a 4000 kW fuel cell stack increases the theoretical fuel consumption with 11.1% and scaling down from 3000 kW to 2000 kW decreases the fuel consumption with 10.2%.

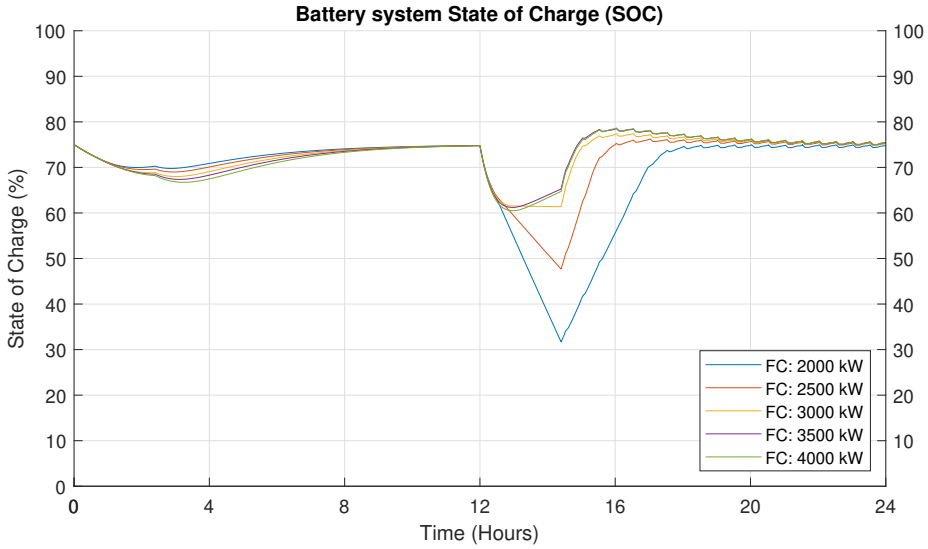

Figure 79: State of Charge of the battery system for different maximum power capacities of the fuel cell stack.

7.4.5 Battery system State of Charge (SOC)

Figure 79 shows the SOC for the battery pack as a function of time and rated power of the fuel cell stacks. For the fuel cell stacks rated 3000 kW and above, the battery SOC stays between 61.4% and 78.7%. For the fuel cell stacks rated below 3000 kW, the battery SOC drops far below 60% as the battery systems not only provides transient power buffering, but effectively also peak shaving. The peak shaving occurs when the load consumption stays above the rated capacities of the fuel cell stacks. The battery SOC for the systems with 2000 kW and 2500 kW rated fuel cell system power has a minimum at 31.7% and 47.7%, respectively. This has great effect on the recommended minimum battery scaling as proposed in section 7.4.6. The low SOC achieved in the systems with small fuel cell stacks also means that a long recharging period of several hours follows the drop in load consumption, when power capacities of the fuel cell stacks are shifted from load covering to battery charging.

7.4.6 Battery system scaling

The impact of fuel cell stack sizing on battery capacity sizing is presented in fig. 80. The development of the minimum recommended battery capacity is quite similar for all the different fuel cell stack configurations up until 12 hours of simulation time. This is because the load demand changes are relatively small during the first half of the load profile and little battery capacity is in active use to buffer during load transients. Additionally, no peak shaving is needed

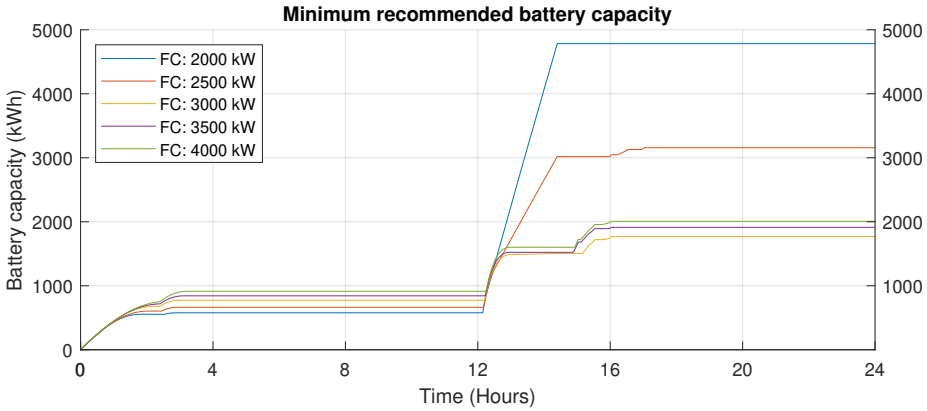

Figure 80: Battery scaling based on fuel cell stacks with different maximum power capacities.

during this time.

After the load increase to peak load demand at 12 hours, the different fuel cell stacks give vastly different results for utilised battery capacity. For the fuel cell stacks rated 3000 kW or above, the battery capacity requirements culminate in the range of 1777.9 kWh to 2005.3 kWh. For the smaller performing fuel cell stacks, the minimum recommended battery capacity is markedly higher and reaches 3160.9 kWh for the 2500 kW fuel cell system and 4846.9 kWh for the 2000 kW system, which is 77.8% and 172.6% higher than the for base case 3000 kW fuel cell system. Consequently, an inverse relationship exists between fuel cell stack size and fuel consumption on one side, and required battery system size on the other side.

8 Conclusion

In this master's thesis, an expansive technological overview and assessment of fuel cells and hydrogen-based energy carriers have been presented for both general and maritime applications. If fuel cells are combined with energy carriers produced with renewable energy and supported with an electric battery in a hybrid production environment, then fuel cell technology has a high potential for efficient, dynamic and carbon-neutral electric power generation.

The various fuel cell technologies and fuel cell compatible energy carriers all have different sets of characteristics and performances, with resulting technology selection complexity. As mentioned in the abstract, hydrogen is a popular energy carrier for fuel cells, however Ammonia (NH_3) and Methanol (CH_3OH), and the Proton Exchange Membrane Fuel Cell (PEMFC) and the Solid Oxide Fuel Cell (SOFC) have qualities, like high energy density and efficiency, that make them especially promising candidates for present and emerging electric power production systems. This applies in particular to applications with high energy demand between scarce refueling opportunities and where the fuel tank volume or placement is a limiting factor. Similarly, ammonia and the Direct Ammonia Fuel Cell (DAFC), Metal hydrides or Liquid Organic Hydrogen Carriers (LOHCs) with the LT-PEMFC, and metal hydrides or methanol with the Phosphoric Acid Fuel Cell (PAFC/HT-PEMFC) can also provide good solutions. In addition, it should be considered whether or not a system design makes it feasible to handle the complexity associated with fuel reforming and hydrogen purification, the high temperature operation of a SOFC system or if the system has the capacity to implement Combined Heat and Power for maximum power conversion efficiency. Regardless of the decided upon solution, care most be taken to ensure compatibility between fuel cells and energy carriers, so that the fuel cell performance is not degraded due to limited fuel cell catalyst tolerance of ammonia and carbon containing compounds.

Other applications, with less energy consumption between expected refuelling intervals and less strict fuel storage requirements, may benefit from using compressed hydrogen in a low-temperature PEMFC, even though the energy density of hydrogen is much lower compared to other energy carriers such as ammonia and methanol.

It can therefore be concluded that the optimal combination of fuel cell and energy carrier depends to a great extent on the system design requirements and limitations of a particular application, and is recommended to be evaluated on a case-by-case basis.

An analysis of commercially available fuel cell solutions, their features, and capital and operational costs have not been evaluated in this master's thesis and would be a natural supplement for decision makers and system designers.

In the case study of a Service Operation Vessel, the performance and feasibil-

ity of a hybrid fuel cell microgrid power production system was investigated and demonstrated with a simulation model. The electric power production was handled by the fuel cells, while the battery system provided effective peak shaving and transient load buffering to ensure that the fuel cells operated within their dynamic response limitations, and thus ensure long cell lifetime. The voltage level in the DC bus deviated only with 0.80% from the target level of 1200 V when the load consumption was stepped up from 500 kW to a peak of 3000 kW. The implementation of a power electronics converter between the DC bus and the battery system could further improve the voltage stability.

The simulations in the case study sensitivity analysis revealed that decreasing the power rating of the fuel cell stack from 3000 kW to 2500 and 2000 kW improved the average production efficiency from 52.4% to 55.4% and 58.4%, respectively. For the 2000 kW fuel cell stack, the fuel consumption was reduced with 10.2% compared to the 3000 kW system. The improved fuel efficiency did, however, come at the cost of an increase in the recommended battery size in the order of 77.8% and 172.6%, respectively, for the 2500 kW and 2000 kW fuel cell systems — mainly due to more peak load shaving by the battery. In contrast to these results, increasing the fuel cell stack from a rated power of 3000 kW to 3500 kW and 4000 kW decreased the fuel efficiency, while resulting in only minor changes in battery size requirements.

There exists a potential for improving the fuel cell efficiency by optimising the load sharing between the fuel cell and battery system. The SOFC system simulated in the case study has a very low efficiency for low power outputs and slightly reduced efficiency at power outputs near or at rated power. A more optimal fuel cell power production profile might therefore be obtain by, for instance, limiting the maximum power output of the fuel cells to below rated power or moving some of the battery recharging to off-peak hours where the fuel cell efficiency otherwise would be low.

While the case analysis can provide clear technical trends for system optimisation, economic and safety related aspects should also be considered before deciding on the power and energy capacity of the fuel cell and battery systems.

All in all, a diverse set of fuel cell and energy carrier combinations offer good and future-oriented solutions for environmentally friendly electrical power production, and already today fuel cell technology has proven efficient for demanding power production applications, as demonstrated in the case study of this thesis.

References

[1] Birger Nordvi. The future of hydrogen in marine applications. Technical report, NTNU, NO-7491 Trondheim, Norway, December 2018. The project thesis which this master's thesis builds and expands on.

[2] Proton-exchange membrane fuel cell. https://en.wikipedia.org/wiki/File:Pem.fuelcell2.gif. Original source: http://www1.eere.energy.gov/hydrogenandfuelcells/fc_animimation_process.html Creator: United States Department of Energy. As a work of the U.S. federal government, the image is in the public domain. Accessed: 2020-07-08.

[3] L. van Biert, M. Godjevac, K. Visser, and P.V. Aravind. A review of fuel cell systems for maritime applications. *Journal of Power Sources*, 327:345–364, 2016.

[4] R.E. Rosli, A.B. Sulong, W.R.W. Daud, M.A. Zulkifley, T. Husaini, M.I. Rosli, E.H. Majlan, and M.A. Haque. A review of high-temperature proton exchange membrane fuel cell (ht-pemfc) system. *International Journal of Hydrogen Energy*, 42(14):9293 – 9314, 2017. Special Issue on Sustainable Fuel Cell and Hydrogen Technologies: The 5th International Conference on Fuel Cell and Hydrogen Technology (ICFCHT 2015), 1-3 September 2015, Kuala Lumpur, Malaysia.

[5] N. Laosiripojana and S. Assabumrungrat. Catalytic steam reforming of methane, methanol, and ethanol over ni/ysz: The possible use of these fuels in internal reforming sofc. *Journal of Power Sources*, 163(2):943 – 951, 2007. Selected Papers presented at the Fuel Processing For Hydrogen Production Symposium at the 230th American Chemical SocietyNational Meeting Washington, DC, USA, 28 August – 1 September 2005.

[6] M. Boaventura, H. Sander, K.A. Friedrich, and A. Mendes. The influence of co on the current density distribution of high temperature polymer electrolyte membrane fuel cells. *Electrochimica Acta*, 56(25):9467 – 9475, 2011.

[7] Chao Pan, Ronghuan He, Qingfeng Li, Jens Oluf Jensen, Niels J. Bjerrum, Henrik Andersen Hjulmand, and Anders Børsting Jensen. Integration of high temperature pem fuel cells with a methanol reformer. *Journal of Power Sources*, 145(2):392 – 398, 2005. Selected papers presented at the Fuel Cells Science and Technology Meeting.

[8] Søren Juhl Andreasen, Søren Knudsen Kær, and Simon Sahlin. Control and experimental characterization of a methanol reformer for a 350 w

high temperature polymer electrolyte membrane fuel cell system. *International Journal of Hydrogen Energy*, 38(3):1676 – 1684, 2013. 2011 Zing International Hydrogen and Fuel Cells Conference: from Nanomaterials to Demonstrators.

[9] Ulrich Eberle, Bernd Müller, and Rittmar Helmolt. Fuel cell electric vehicles and hydrogen infrastructure: Status 2012. *Energy Environmental Science*, 5:8790–8798, 07 2012.

[10] Product data sheet, fcmove-hd. https://www.ballard.com/docs/default-source/motive-modules-documents/fcmovetm.pdf?sfvrsn=6a83c380_6. Accessed: 2020-04-29.

[11] Ms-100 datasheet. https://www.powercell.se/wordpress/wp-content/uploads/2019/11/MS-100-datasheet-2019.pdf. Accessed: 2020-05-25.

[12] Feng Xie, Zhigang Shao, Ming Hou, Hongmei Yu, Wei Song, Shucheng Sun, Li Zhou, and Baolian Yi. Recent progresses in h2-pemfc at dicp. *Journal of Energy Chemistry*, 36:129 – 140, 2019. Special Issue: In celebration of the 70th anniversary of Dalian Institute of Chemical Physics, Chinese Academy of Sciences.

[13] Osamah Siddiqui and Ibrahim Dincer. A review and comparative assessment of direct ammonia fuel cells. *Thermal Science and Engineering Progress*, 5:568 – 578, 2018.

[14] Pucheng Pei and Huicui Chen. Main factors affecting the lifetime of proton exchange membrane fuel cells in vehicle applications: A review. *Applied Energy*, 125:60–75, 2014.

[15] A.M.F.R. Pinto, V.S. Oliveira, and D.S.C. Falcao. *Direct Alcohol Fuel Cells for Portable Applications: Fundamentals, Engineering and Advances*. Elsevier Science, 2018.

[16] Vector diagram of pem and pafc operation. https://en.wikipedia.org/wiki/File:Proton_Exchange_Fuel_Cell_Diagram.svg. Public domain. Accessed: 2020-07-08.

[17] Fuel Cell Technologies Office. Fuel cell technologies office - multi-year research, development, and demonstration plan. Technical report, U.S. Department of Energy, Forrestal Building, 1000 Independence Avenue, SW, Washington, DC 20585, 2012.

[18] Phosphoric acid h3po4. https://pubchem.ncbi.nlm.nih.gov/compound/Phosphoric-acid. Accessed: 2020-04-24.

[19] S. Mekhilef, R. Saidur, and A. Safari. Comparative study of different fuel cell technologies. *Renewable and Sustainable Energy Reviews*, 16(1):981 – 989, 2012.

[20] Y. Oka. Fuel cells – phosphoric acid fuel cells — performance and operational conditions. In Jürgen Garche, editor, *Encyclopedia of Electrochemical Power Sources*, pages 589 – 596. Elsevier, Amsterdam, 2009.

[21] Editors: Jurgen Garche, Chris K. Dyer, Patrick T. Moseley, Zempachi Ogumi, David A. J. Rand, and Bruno Scrosa. *Encyclopedia of Electrochemical Power Sources*. Elsevier Science, 2013.

[22] Types of fuel cells — department of energy. https://https://www.energy.gov/eere/fuelcells/types-fuel-cells. Accessed: 2020-03-24.

[23] Chia-Lien Lu, Cheng-Ping Chang, Yi-Hsuan Guo, Tsung-Kuang Yeh, Yu-Chuan Su, Pen-Cheng Wang, Kan-Lin Hsueh, and Fan-Gang Tseng. High-performance and low-leakage phosphoric acid fuel cell with synergic composite membrane stacking of micro glass microfiber and nano ptfe. *Renewable Energy*, 134:982 – 988, 2019.

[24] Harikishan R. Ellamla, Iain Staffell, Piotr Bujlo, Bruno G. Pollet, and Sivakumar Pasupathi. Current status of fuel cell based combined heat and power systems for residential sector. *Journal of Power Sources*, 293:312 – 328, 2015.

[25] M Neergat and A.K Shukla. A high-performance phosphoric acid fuel cell. *Journal of Power Sources*, 102(1):317 – 321, 2001.

[26] John R. Varcoe, Plamen Atanassov, Dario R. Dekel, Andrew M. Herring, Michael A. Hickner, Paul. A. Kohl, Anthony R. Kucernak, William E. Mustain, Kitty Nijmeijer, Keith Scott, Tongwen Xu, and Lin Zhuang. Anion-exchange membranes in electrochemical energy systems. *Energy Environ. Sci.*, 7:3135–3191, 2014.

[27] Dario R. Dekel. Review of cell performance in anion exchange membrane fuel cells. *Journal of Power Sources*, 375:158 – 169, 2018.

[28] Alexey Serov, Iryna V. Zenyuk, Christopher G. Arges, and Marian Chatenet. Hot topics in alkaline exchange membrane fuel cells. *Journal of Power Sources*, 375:149 – 157, 2018.

[29] Kenneth A. Burke. Fuel cells for space science applications. Technical Report 2, The institution that published, Glenn Research Center, Cleveland, Ohio, 11 2003. NASA/TM—2003-212730.

[30] Lianqin Wang, Emanuele Magliocca, Emma Cunningham, William Mustain, Simon Poynton, Ricardo Escudero-Cid, Mohamed Nasef, Julia Ponce-Gonzalez, Rachida Bance-Soualhi, Robert Slade, Daniel Whelligan, and John Varcoe. An optimised synthesis of high performance radiation-grafted anion-exchange membranes. *Green Chem.*, 19:831–843, 11 2016.

[31] Yun Zhao, Brian P. Setzler, Junhua Wang, Jared Nash, Teng Wang, Bingjun Xu, and Yushan Yan. An efficient direct ammonia fuel cell for affordable carbon-neutral transportation. *Joule*, 3(10):2472 – 2484, 2019.

[32] C. Zamfirescu and I. Dincer. Using ammonia as a sustainable fuel. *Journal of Power Sources*, 185:4569–465, 2008.

[33] O. Siddiqui and I. Dincer. Development and performance evaluation of a direct ammonia fuel cell stack. *Chemical Engineering Science*, 200:285 – 293, 2019.

[34] Reza Abbasi, Brian P. Setzler, Junhua Wang, Yun Zhao, Teng Wang, Shimshon Gottesfeld, and Yushan Yan. Low-temperature direct ammonia fuel cells: Recent developments and remaining challenges. *Current Opinion in Electrochemistry*, 2020.

[35] Direct methanol fuel cell. https://freesvg.org/direct-methanol-fuel-cell. The figure is in public domain. Accessed: 2020-07-08.

[36] José J. de Troya, Carlos Álvarez, and Carlos Fernández-Garrido. Analysing the possibilities of using fuel cells in ships. *International Journal of Hydrogen Energy*, 41:2853–2866, 2015.

[37] S.S. Siwal, S. Thakur, Q.B. Zhang, and V.K. Thakur. Electrocatalysts for electrooxidation of direct alcohol fuel cell: chemistry and applications. *Materials Today Chemistry*, 14:100182, 2019.

[38] Julian Massing, Nadine [van der Schoot], Christian J. Kähler, and Christian Cierpka. A fast start up system for microfluidic direct methanol fuel cells. *International Journal of Hydrogen Energy*, 44(48):26517 – 26529, 2019.

[39] Yi Cheng, Jin Zhang, Shanfu Lu, and San Ping Jiang. Significantly enhanced performance of direct methanol fuel cells at elevated temperatures. *Journal of Power Sources*, 450:227620, 2020.

[40] Pulin Yeh, Chu Hsiang Chang, Naichien Shih, and Naichia Yeh. Durability and efficiency tests for direct methanol fuel cell's long-term performance assessment. *Energy*, 107:716 – 724, 2016.

[41] Asad Mehmood, M.Aulice Scibioh, Joghee Prabhuram, Myung-Gi An, and Heung Yong Ha. A review on durability issues and restoration techniques in long-term operations of direct methanol fuel cells. *Journal of Power Sources*, 297:224 – 241, 2015.

[42] A. A. Khuhro, Y. Ali, M. Najam-Uddin, and S. Khan. A technological, economical and efficiency review of direct methanol fuel cell. pages 1–4, March 2018.

[43] Nicky Bogolowski and Jean-Francois Drillet. Appropriate balance between methanol yield and power density in portable direct methanol fuel cell. *Chemical Engineering Journal*, 270:91 – 100, 2015.

[44] Guanbin Lu, Fandi Ning, Jun Wei, Yunbo Li, Chuang Bai, Yangbin Shen, Yali Li, and Xiaochun Zhou. All-solid-state passive direct methanol fuel cells with great orientation stability and high energy density based on solid methanol fuels. *Journal of Power Sources*, 450:227669, 2020.

[45] IEAGHG. Review of fuel cell technologies with co2 capture for the power sector. Technical report, International Energy Agency (IEA), Pure Offices, Cheltenham Office Park, Hatherley Lane, Cheltenham, GLOS, GL51 6SH, UK, April 2019.

[46] Andi Mehmeti, Francesca Santoni, Massimiliano [Della Pietra], and Stephen J. McPhail. Life cycle assessment of molten carbonate fuel cells: State of the art and strategies for the future. *Journal of Power Sources*, 308:97 – 108, 2016.

[47] H. Morita, M. Kawase, Y. Mugikura, and K. Asano. Degradation mechanism of molten carbonate fuel cell based on long-term performance: Long-term operation by using bench-scale cell and post-test analysis of the cell. *Journal of Power Sources*, 195(20):6988 – 6996, 2010.

[48] C. Wang and M. H. Nehrir. A physically based dynamic model for solid oxide fuel cells. *IEEE Transactions on Energy Conversion*, 22(4):887–897, Dec 2007.

[49] L. Blum, H. P. Buchkremer, S. M. Gross, L.G.J. de Haart, W. J. Quadakkers, U. Reisgen, R. Steinberger-Wilckens, R. W. Steinbrech, and F. Tietz. Overview of the Development of Solid Oxide Fuel Cells at Forschungszentrum Jülich. In *Solid Oxide Fuel Cells (SOFC IX) / ed.: S. C. Singhal, J. Mizusaki. - Pennington, NJ, 2005. - (Proceedings of the Electrochemical Society ; 2005-07). - 1-56677-465-9. - S. 39 - 47*, 2005. Record converted from VDB: 12.11.2012.

[50] N. D. Tuyen, G. Fujita, R. Yokoyama, K. Koyanagi, T. Funabashi, and M. Nomura. Load following characteristics and operating temperature control of sofc simulation. pages 1–4, 2009.

[51] Caisheng Wang and M. Hashem Nehrir. Load transient mitigation for stand-alone fuel cell power generation systems. *Energy Conversion, IEEE Transactions on*, 22:864 – 872, 01 2008.

[52] Francesco Baldi, Stefano Moret, Kari Tammi, and François Maréchal. The role of solid oxide fuel cells in future ship energy systems. *Energy*, 194:116811, 03 2020.

[53] Anke Hagen, Hendrik Langnickel, and Xiufu Sun. Operation of solid oxide fuel cells with alternative hydrogen carriers. *International Journal of Hydrogen Energy*, 44(33):18382 – 18392, 2019.

[54] Arnab Choudhury, H. Chandra, and A. Arora. Application of solid oxide fuel cell technology for power generation—a review. *Renewable and Sustainable Energy Reviews*, 20:430 – 442, 2013.

[55] Martin Andersson and Jan Froitzheim. Technology review – solid oxide cells 2019 energiforskrapport 2019-601. Technical Report 2019:601, Energiforsk, Olof palmes Gata 31, Stockholm, Sweden, 2019.

[56] Elcogen - solid oxide cells and stacks. https://elcogen.com. Accessed: 2020-05-25.

[57] Elcogen - solid oxide cells and stacks. https://elcogen.com/wp-content/uploads/2019/04/elcogen-sofc-white-paper-2019.pdf. Accessed: 2020-05-25.

[58] G. Cinti, G. Discepoli, E. Sisani, and U. Desideri. Sofc operating with ammonia: Stack test and system analysis. *International Journal of Hydrogen Energy*, 41(31):13583 – 13590, 2016.

[59] Yiming Lyu, Jintao Xie, Wang Dingbiao, and Jiarao Wang. Review of cell performance in solid oxide fuel cells. *Journal of Materials Science*, 55, 06 2020.

[60] F. Ramadhani, M.A. Hussain, H. Mokhlis, and S. Hajimolana. Optimization strategies for solid oxide fuel cell (sofc) application: A literature survey. *Renewable and Sustainable Energy Reviews*, 76:460 – 484, 2017.

[61] Reforming — chemistry — britannica. https://www.britannica.com/technology/reforming. Accessed: 2020-03-31.

[62] Autothermal. https://www.merriam-webster.com/dictionary/autothermal. Accessed: 2020-03-31.

[63] C. Bourne, T. Tietsch, Dave Griffiths, and Jon Morley. Application of fuel cells in surface ships. 2001.

[64] Jay Benziger, E. Chia, J.F. Moxley, and I.G. Kevrekidis. The dynamic response of pem fuel cells to changes in load. *Chemical Engineering Science*, 60:1743–1759, 2004.

[65] Nigel Sammes (Editor). *Fuel Cell Technology*. Springer, 2006.

[66] Stavros Lazarou, Eleftheria Pyrgioti, and Antonio T. Alexandridis. A simple electric circuit model for proton exchange membrane fuel cells. *Journal of Power Sources*, 190:380–386, 2009.

[67] Helge Weydahl, Steffen Møller-Holst, Georg Hagen, and Børre Børresen. Transient response of a proton exchange membrane fuel cell. *Journal of Power Sources*, 171(2):321 – 330, 2007.

[68] Chung-Hsing Chao and Tien-Chien Jen. Transient behavior experiments for hybrid fuel cell-battery systems. *International Symposium on Information Technology in Medicine And Education*, 2012:985–990, 2012.

[69] K.H. Loo, K.H. Wong, S.C. Tan, Y.M. Lai, and Chi K. Tse. Characterization of the dynamic response of proton exchange membrane fuel cells – a numerical study. *International Journal of Hydrogen Energy*, 35:11861–11877, 2010.

[70] Hydrogen. https://snl.no/hydrogen. Accessed: 2020-02-21.

[71] Heating values of hydrogen and fuels. https://chemeng.queensu.ca/courses/CHEE332/files/ethanol_heating-values.pdf. Accessed: 2020-03-18.

[72] Absolutt nullpunkt. https://snl.no/absolutt_nullpunkt. Accessed: 2020-03-18.

[73] J.O. Abe, A.P.I. Popoola, E. Ajenifuja, and O.M. Popoola. Hydrogen energy, economy and storage: Review and recommendation. *International Journal of Hydrogen Energy*, 44(29):15072 – 15086, 2019.

[74] S. Shiva Kumar and V. Himabindu. Hydrogen production by pem water electrolysis – a review. *Materials Science for Energy Technologies*, 2(3):442 – 454, 2019.

[75] Magnus Runnerstrøm. A feasibility study of wind powered hydrogen production at fosen. Master's thesis, NTNU, Trondheim, Norway, June 2019.

[76] Monterey Gardiner. *DOE Hydrogen and Fuel Cells Program Record*. US Department of Energy, 21000 Brookpark Road Cleveland, OH, USA, July 7th 2009.

[77] Odne Stokke Burheim. *Engineering Energy Storage*. Academic Press, 2017.

[78] United States of America Department of Energy. Energy requirements for hydrogen gas compression and liquefaction as related to vehicle storage needs. *DOE Hydrogen and Fuel Cells Program Record*, 9013:345–364, 2009.

[79] Sebastian Verhelst, James WG Turner, Louis Sileghem, and Jeroen Vancoillie. Methanol as a fuel for internal combustion engines. *Progress in Energy and Combustion Science*, 70:43 – 88, 2019.

[80] Päivi T. Aakko-Saksa, Chris Cook, Jari Kiviaho, and Timo Repo. Liquid organic hydrogen carriers for transportation and storing of renewable energy – review and discussion. *Journal of Power Sources*, 396:803 – 823, 2018.

[81] NASA Glenn Research Center. *NASA Glenn Safety Manual*. NASA Glenn Research Center, 21000 Brookpark Road Cleveland, OH, USA, September 2003.

[82] Hydrogenering. https://snl.no/hydrogenering. Accessed: 2020-03-26.

[83] Benzen. https://snl.no/benzen. Accessed: 2020-03-27.

[84] Metanol ch3oh. https://pubchem.ncbi.nlm.nih.gov/compound/Benzene. Accessed: 2020-03-27.

[85] Cyclohexane c6h12. https://pubchem.ncbi.nlm.nih.gov/compound/Cyclohexane. Accessed: 2020-03-27.

[86] Toluene c6h5ch3. https://pubchem.ncbi.nlm.nih.gov/compound/Toluene. Accessed: 2020-03-27.

[87] Methylcyclohexane c6h11ch3. https://pubchem.ncbi.nlm.nih.gov/compound/Methylcyclohexane. Accessed: 2020-03-27.

[88] Naphthalene c10h8. https://pubchem.ncbi.nlm.nih.gov/compound/Naphthalene. Accessed: 2020-03-28.

[89] Decahydronaphthalene c10h8. https://pubchem.ncbi.nlm.nih.gov/compound/Decahydronaphthalene. Accessed: 2020-03-28.

[90] Mass density of bicyclo[4.4.0]decane (pure). https://materials.springer.com/interactive?systemId=20102&propertyId=Mass%20Density. Accessed: 2020-03-29.

[91] Biphenyl c6h5c6h5. https://pubchem.ncbi.nlm.nih.gov/compound/Biphenyl. Accessed: 2020-03-29.

[92] Mass density of biphenyl (pure). https://materials.springer.com/interactive?systemId=20713&propertyId=Mass%20Density. Accessed: 2020-03-29.

[93] Bicyclohexyl c12h22. https://pubchem.ncbi.nlm.nih.gov/compound/Bicyclohexyl. Accessed: 2020-03-29.

[94] Mass density of bicyclohexyl (pure). https://materials.springer.com/interactive?systemId=20991&propertyId=Mass%20Density. Accessed: 2020-03-29.

[95] Robert Schlögl. Heterogeneous catalysis. *Angewandte Chemie International Edition*, 54(11):3465–3520, 2015.

[96] Katalysator. https://snl.no/katalysator. Accessed: 2020-03-26.

[97] Martin Johannes Schneider. Hydrogen storage and distribution via liquid organic carriers. In *Bridging Renewable Electricity with Transportation Fuels Workshop, Brown Palace Hotel, Denver, CO, August*, 2015.

[98] Jose [Bellosta von Colbe], Jose-Ramón Ares, Jussara Barale, Marcello Baricco, Craig Buckley, Giovanni Capurso, Noris Gallandat, David M. Grant, Matylda N. Guzik, Isaac Jacob, Emil H. Jensen, Torben Jensen, Julian Jepsen, Thomas Klassen, Mykhaylol V. Lototskyy, Kandavel Manickam, Amelia Montone, Julian Puszkiel, Sabrina Sartori, Drew A. Sheppard, Alastair Stuart, Gavin Walker, Colin J. Webb, Heena Yang, Volodymyr Yartys, Andreas Züttel, and Martin Dornheim. Application of hydrides in hydrogen storage and compression: Achievements, outlook and perspectives. *International Journal of Hydrogen Energy*, 44(15):7780 – 7808, 2019. A special issue on hydrogen-based Energy storage.

[99] Magnesium hydride h2mg. https://pubchem.ncbi.nlm.nih.gov/compound/Magnesium-hydride. Accessed: 2020-06-06.

[100] H. Zhong, H. Wang, J.W. Liu, D.L. Sun, F. Fang, Q.A. Zhang, L.Z. Ouyang, and M. Zhu. Enhanced hydrolysis properties and energy efficiency of mgh2-base hydrides. *Journal of Alloys and Compounds*, 680:419 – 426, 2016.

[101] Ammoniakk. https://snl.no/ammoniakk. Accessed: 2020-03-14.

[102] Yusuf Bicer. *Investigation of novel ammonia production options using photoelectrochemical hydrogen*. PhD thesis, 04 2017.

[103] Arda Yapicioglu and Ibrahim Dincer. A review on clean ammonia as a potential fuel for power generators. *Renewable and Sustainable Energy Reviews*, 103:96 – 108, 2019.

[104] C. Zamfirescu and I. Dincer. Using ammonia as a sustainable fuel. *Journal of Power Sources*, 185(1):459 – 465, 2008.

[105] J. J. MacKenzie and W. H. Avery. Ammonia fuel: the key to hydrogen-based transportation. 3:1761–1766 vol.3, Aug 1996.

[106] S. Giddey, S.P.S. Badwal, and A. Kulkarni. Review of electrochemical ammonia production technologies and materials. *International Journal of Hydrogen Energy*, 38(34):14576 – 14594, 2013.

[107] Ammonia nh3. https://pubchem.ncbi.nlm.nih.gov/compound/Ammonia. Accessed: 2020-04-14.

[108] Joshua W. Makepeace, Teng He, Claudia Weidenthaler, Torben R. Jensen, Fei Chang, Tejs Vegge, Peter Ngene, Yoshitsugu Kojima, Petra E. [de Jongh], Ping Chen, and William I.F. David. Reversible ammonia-based and liquid organic hydrogen carriers for high-density hydrogen storage: Recent progress. *International Journal of Hydrogen Energy*, 44(15):7746 – 7767, 2019. A special issue on hydrogen-based Energy storage.

[109] J.H. Kim, D.H. Um, and O.C. Kwon. Hydrogen production from burning and reforming of ammonia in a microreforming system. *Energy Conversion and Management*, 56:184 – 191, 2012.

[110] A Valera-Medina, H Xiao, M Owen-Jones, W.I.F. David, and P.J. Bowen. Ammonia for power. *Progress in Energy and Combustion Science*, 69:63 – 102, 2018.

[111] Hiroki Miyaoka, Hikaru Miyaoka, Tomoyuki Ichikawa, Takayuki Ichikawa, and Yoshitsugu Kojima. Highly purified hydrogen production from ammonia for pem fuel cell. *International Journal of Hydrogen Energy*, 43(31):14486 – 14492, 2018.

[112] M.E.E. Abashar. Ultra-clean hydrogen production by ammonia decomposition. *Journal of King Saud University - Engineering Sciences*, 30(1):2 – 11, 2018.

[113] Rong Lan, John T.S. Irvine, and Shanwen Tao. Ammonia and related chemicals as potential indirect hydrogen storage materials. *International Journal of Hydrogen Energy*, 37(2):1482 – 1494, 2012. 10th International Conference on Clean Energy 2010.

[114] Metanol. https://snl.no/metanol. Accessed: 2020-02-28.

[115] Lower and higher heating values of fuels. https://h2tools.org/hyarc/calculator-tools/lower-and-higher-heating-values-fuels. Accessed: 2020-03-18.

[116] K. Moirangthem and D. Baxter. Alternative fuels for marine and inland waterways. Technical Report EUR 27770 EN, European Comission, 2016.

[117] Severin Hänggi, Philipp Elbert, Thomas Bütler, Urs Cabalzar, Sinan Teske, Christian Bach, and Christopher Onder. A review of synthetic fuels for passenger vehicles. *Energy Reports*, 5:555 – 569, 2019.

[118] Maria Annesini, Vincenzo Piemonte, and Luca Turchetti. Carbon formation in the steam reforming process: A thermodynamic analysis based on the elemental composition. *Chem. Eng. Trans.*, 11:21–26, 01 2007.

[119] Gasoline gallon equivalent. https://https://en.wikipedia.org/wiki/Gasoline_gallon_equivalent. Accessed: 2020-04-17.

[120] What does gasoline gallon equivalent mean? https://www.definitions.net/definition/gasoline+gallon+equivalent. Accessed: 2020-04-17.

[121] 114000 btu to kwh. https://www.wolframalpha.com/input/?i=114000+BTU+to+kWh. Accessed: 2020-04-17.

[122] Fuel economy impact analysis of rfg. http://nepis.epa.gov/Exe/ZyPURL.cgi?Dockey=P100B3FL.txt. Accessed: 2020-04-17.

[123] Dominik Bongartz, Larissa Doré, Katharina Eichler, Thomas Grube, Benedikt Heuser, Laura E. Hombach, Martin Robinius, Stefan Pischinger, Detlef Stolten, Grit Walther, and Alexander Mitsos. Comparison of light-duty transportation fuels produced from renewable hydrogen and green carbon dioxide. *Applied Energy*, 231:757 – 767, 2018.

[124] Mårten Larsson, Stefan Grönkvist, and Per Alvfors. Synthetic fuels from electricity for the swedish transport sector: Comparison of well to wheel energy efficiencies and costs. *Energy Procedia*, 75:1875 – 1880, 2015. Clean, Efficient and Affordable Energy for a Sustainable Future: The 7th International Conference on Applied Energy (ICAE2015).

[125] Introduction to dp systems - what is a dynamic positioning. https://www.offshoreengineering.com/education/dynamic-positioning-dp/what-is-dynamic-positioning. Accessed: 2020-05-11.

[126] G. Abad. *Power Electronics and Electric Drives for Traction Applications*. Wiley, 2016.

[127] H. R. Esmaeilian, R. Fadaeinedjad, and G. Moschopoulos. Dynamic operation and control of a stand-alone pem fuel cell system. *IEEE Applied Power Electronics Conference and Exposition*, 2014:3378–3384, 2014.

[128] Maxwell Woody, Maryam Arbabzadeh, Geoffrey M. Lewis, Gregory A. Keoleian, and Anna Stefanopoulou. Strategies to limit degradation and maximize li-ion battery service lifetime - critical review and guidance for stakeholders. *Journal of Energy Storage*, 28:101231, 2020.

[129] Omar Z. Sharaf and Mehmet F. Orhan. An overview of fuel cell technology: Fundamentals and applications. *Renewable and Sustainable Energy Reviews*, 32:810–853, 2014.

[130] Joakim Frimann-Dahl. Kartlegging av energibehov og infrastruktursituasjon for fergesamband i nord trøndelag. May 2016.

[131] W.R.W. Daud, R.E. Rosli, E.H. Majlan, S.A.A. Hamid, R. Mohamed, and T. Husaini. Pem fuel cell system control: A review. *Renewable Energy*, 113:620–638, 2017.

[132] Yousri M. A. Welaya, M. Morsy El Gohary, and Nader R. Ammar. A comparison between fuel cells and other alternatives for marine electric power generation. *International Journal of Naval Architecture and Ocean Engineering*, 3:141–149, 2011.

[133] Andrew Dicks and D. A. J. Rand. *Fuel Cell Systems Explained.*, volume Third edition. Wiley, 2018.

[134] Louis Schlapbach and Andreas Züttel. Hydrogen-storage materials for mobile applications. *Nature*, 414:353–358, 2001.

[135] Shimshon Gottesfeld. The direct ammonia fuel cell and a common pattern of electrocatalytic processes. *Journal of The Electrochemical Society*, 165:J3405–J3412, 01 2018.

[136] Powercell fuel cell stacks and systems. http://www.scandinavianhydrogen.org/wp-content/uploads/2016/11/PowerCell-presentation-HFC2016-v2.pdf. Accessed: 2020-04-29.

[137] Turan Gönen. *Electrical Machines with MATLAB®*. CRC press, Boca Raton, Florida, 2012.

[138] Rauli Partanen, Harri Paloheimo, and Heikki Waris. *The World After Cheap Oil*. Routledge, 2014.

[139] T. Adefarati and R.C. Bansal. *Chapter 2 - Energizing Renewable Energy Systems and Distribution Generation*. Academic Press, 2019.

[140] Iupac - catalyst. http://goldbook.iupac.org/terms/view/C00876. Accessed: 2020-03-26.

[141] Powercell ms-100 datasheet (pdf). https://www.powercell.se/media/1280/powercell-ms100-datasheet-pdf.pdf. Accessed: 2018-10-09.

[142] Metanol ch3oh. https://pubchem.ncbi.nlm.nih.gov/compound/Methanol. Accessed: 2020-03-18.

[143] mp-23710: MgH2. https://materialsproject.org/materials/mp-23710/. Accessed: 2020-06-07.

[144] Gallon. https://snl.no/gallon. Accessed: 2020-04-17.

A Energy Carrier Density

Compund	Density [kg/m^3]	H2 mass fraction [%]	H2 storage [kg/m^3]	H2 storage [GJ/m³]	H2 storage [MJ/kg]	H2 storage [MWh/m³]	Comp. to H2 (690 bar)	Comp. To H2 (liquid)
H2 (690 bar)	37,5	100	37,5	4,5 GJ/m³	120,0 MJ/kg	1,25 MWh/m³	0 %	-47 %
H2 (liquid)	70,8	100	70,8	8,5 GJ/m³	120,0 MJ/kg	2,36 MWh/m³	89 %	0 %
Cyclohexane	778	7,2	56,0	6,7 GJ/m³	8,6 MJ/kg	1,87 MWh/m³	49 %	-21 %
Methylcyclohexane	769	6,2	47,7	5,7 GJ/m³	7,4 MJ/kg	1,59 MWh/m³	27 %	-33 %
Decalin	883	7,3	64,5	7,7 GJ/m³	8,8 MJ/kg	2,15 MWh/m³	72 %	-9 %
Bicyclohexyl	887	7,1	63,0	7,6 GJ/m³	8,5 MJ/kg	2,10 MWh/m³	68 %	-11 %
Ammonia	696	17,6	122,8	14,7 GJ/m³	21,2 MJ/kg	4,09 MWh/m³	228 %	73 %
Methanol (H2 only)	796	12,5	99,5	11,9 GJ/m³	15,0 MJ/kg	3,32 MWh/m³	165 %	41 %
Methanol (purified H2)	796	12,5	99,5	10,9 GJ/m³	13,7 MJ/kg	3,02 MWh/m³	141 %	28 %
Methanol (full combustion)	796			16,0 GJ/m³	20,1 MJ/kg	4,44 MWh/m³	255 %	88 %
Metal hydrides (MgH2)	1420	7,6	107,9	13,0 GJ/m³	9,1 MJ/kg	3,60 MWh/m³	188 %	52 %

Figure 81: Overview of data and calculations used to determine the gravimetric and volumetric energy density of various energy carriers.

B Energy Carrier Efficiency

	Efficiency								Electric energy storage capacity	
		Power-to-tank			Tank-to-power					
Energy carrier	H2-production	Synthesis	Storage	Reforming	H2-purification	Fuel Cell	Total	Relative	Peak efficiency	80% of peak efficiency
Hydrogen (690 bar, LT-PEMFC)	60 %	100 %	91 %	100 %	100 %	60 %	32,8 %	0 %	0,75 MWh/m³	0,60 MWh/m³
Hydrogen (690 bar, SOFC)	60 %	100 %	91 %	100 %	100 %	65 %	35,5 %	8 %	0,81 MWh/m³	0,65 MWh/m³
Hydrogen (liquid, LT-PEMFC)	60 %	100 %	70 %	100 %	100 %	60 %	25,2 %	-23 %	1,42 MWh/m³	1,13 MWh/m³
Hydrogen (liquid, SOFC)	60 %	100 %	70 %	100 %	100 %	65 %	27,3 %	-17 %	1,53 MWh/m³	1,23 MWh/m³
LOHC (LT-PEMFC)	60 %	98 %	100 %	98 %	94 %	60 %	32,5 %	-1 %	1,03 MWh/m³	0,83 MWh/m³
LOHC (SOFC)	60 %	98 %	100 %	98 %	100 %	65 %	37,5 %	14 %	1,19 MWh/m³	0,95 MWh/m³
Ammonia (LT-PEMFC)	60 %	84 %	95 %	97 %	91 %	60 %	25,4 %	-23 %	2,17 MWh/m³	1,73 MWh/m³
Ammonia (DAFC)	60 %	84 %	95 %	100 %	100 %	67 %	32,1 %	-2 %	2,74 MWh/m³	2,19 MWh/m³
Methanol (LT-PEMFC)	60 %	79 %	100 %	95 %	91 %	60 %	24,6 %	-25 %	1,72 MWh/m³	1,38 MWh/m³
Methanol (HT-PEMFC)	60 %	79 %	100 %	95 %	100 %	50 %	22,5 %	-31 %	1,58 MWh/m³	1,26 MWh/m³
Methanol (DMFC)	60 %	79 %	100 %	100 %	100 %	35 %	16,6 %	-49 %	1,56 MWh/m³	1,24 MWh/m³
Methanol (SOFC)	60 %	79 %	100 %	100 %	100 %	65 %	30,8 %	-6 %	2,89 MWh/m³	2,31 MWh/m³
Metal hydrides (MgH2, LT-PEMFC)	60 %	67 %	100 %	67 %	100 %	60 %	16,3 %	-50 %	1,45 MWh/m³	1,16 MWh/m³
Metal hydrides (MgH2, SOFC)	60 %	67 %	100 %	67 %	100 %	65 %	17,7 %	-46 %	1,57 MWh/m³	1,26 MWh/m³

Grey fields: estimations/low data quality

Figure 82: Overview of the efficiencies for the power-to-power processing steps of various fuel cell and energy carrier combinations. The electric energy storage capacity–columns are based on the energy density of the fuels (calculated in Appendix A) multiplied with the reformation, H_2-purification and fuel cell efficiencies — in other words the tank-to-power efficiencies. The *Relative*-column compares the respective total efficiencies with the total efficiency of compressed hydrogen fed to a LT-PEMFC.

Birger Nordvi

The Future of Fuel Cell Technology in Maritime Applications

NTNU
Norwegian University of
Science and Technology

KONGSBERG